Dissolution rates and mechanisms

-

experiments on alteration and reactivity of glasses and carbonates.

Julien Declercq

Department of Geosciences
University of Oslo

Series of dissertations submitted to the
Faculty of Mathematics and Natural Sciences, University of Oslo
No. 943

ISSN 1501-7710

Cover: Inger Sandved Anfinsen.
Printed in Norway: AiT e-dit AS.

Produced in co-operation with Unipub.
The thesis is produced by Unipub merely in connection with the
thesis defence. Kindly direct all inquiries regarding the thesis to the copyright
holder or the unit which grants the doctorate.

Preface

This thesis has been submitted to the Department of Geosciences at the University of Oslo in accordance with the requirements for the degree of Philosophiae Doctor (Ph.D) in geology. The work herein was completed as part of a three year project. This project was completed both at the Department of Geosciences in Oslo and at the Laboratoire des Matériaux et Transfert en Géologie (LMTG) in Toulouse through an exchange grant from the Research Concil.

This project was made possible through financial support made by the Research Council of Norway through project #165697 and SSE-Ramore project

The introduction to this thesis includes a brief description of the scopes and objectives, some background information on CO_2 sequestration and dissolution theory followed by a summary of papers and finally some concluding remarks. The individual papers are included as enclosure 1 trough 5. In addition one supplemental report is included as additional contribution (Appendix I). The results of this geochemical study of the dissolution mechanism of glass and carbonate mineral will be used in geochemical models.

Acknowledgements

I would like to thank everyone who has helped me along the way. I am forever grateful! First and foremost I would like to thank my advisors Professor Per Aagaard, Dr Eric Oelkers and Dr Jens Jahren for the opportunity and for their support, advice and contributions. Thank you to my colleagues Helge Hellevang and Binyam Lema Alemu in Oslo and Therese K. Flaathen and Giuseppe Saldi in Toulouse for their help and the countless discussion on both academic and non-academic subjects. And a big cheer up for the guys from the MIR-EST and Min-Gro networks, our meetings and short courses were one of the key to go forward through this project. I hope we will continue our *networking* in the future!

I would like to acknowledge the following persons: the technical staff at the department of Geosciences, University of Oslo: Mufak Naoroz (the person without whom nothing could be accomplished in the lab), Berit L. Berg and Turid Winje; the technical staff at the LMTG in Toulouse, for their support and unnatural skill for fixing the equipment.

I am forever grateful to my parents for their support throughout the years. And a (nice) thought to all the people who listened to my complaints along those years.

Contents

Scope and Objectives.

The aim of this study was to improve our understanding of water-rock interaction. In particular the dissolution/precipitation of minerals and glasses in aqueous media and their respective mechanisms. These kinetic studies yielded results applicable in several different fields. The most important is the updating of kinetic databases used in geochemical software like PHREEQC. But the knowledge gained can also be used, together with a careful application of geochemical models to address issues related to carbon storage and remediation, such as defining the phases forming when CO_2 is injected into the aquifer and reservoirs and the timeframe of such reactions.

The updated kinetic models can also be used outside of CO_2 sequestration, for example the alteration of glass and the secondary products generated during these processes. The dissolution of volcanic glass has a major role in natural processes. There is about one cubic kilometer of volcanic glass produced every year, mostly along volcanic ridges (Morgan and Spera, 2001). The weathering of the new ocean floor, mostly formed of basalts, influences the global amount of CO_2 in the atmosphere and thus the climate on the long term (Urey, 1952; Riley and Chester, 1971; Holland, 1978; Thompson, 1983; Berner, 1992; Spivack and Staudigel, 1994; Brady and Gíslason, 1997; Chester, 2000; Kump et al., 2000). The dissolution mechanism of volcanic glasses as been studied extensively (Kharkansis et al., 1980; Dickin, 1981; Petit, 1992 - White and Claassen, 1980; White et al., 1980; White, 1983; Allnatt et al., 1983; Dran et al., 1986, 1988; Magonthier et al., 1992; Mungall and Martin, 1994; Mazer and Walther, 1994; Fiore et al., 1999) but until now a unique dissolution mechanism has not been defined, for those different processes. Being able to generate one reaction mechanism, represented by one equation for all natural glasses extend the models to all glasses. We were then able to use that equation in the case of the alteration of impact glasses. In the case of impact craters most of the deposits are heavily weathered and are now composed of clay deposits. Being able to define and quantify the alteration production and rates allows us to define several key parameters of the impact.

Background

CO_2 storage and remediation

As stated in the latest IPCC report (February 2007), the increased atmospheric concentrations of greenhouse gases, which is caused by anthropogenic activities, is leading to global climate changes. To meet the requirements of international treaties, like the Kyoto protocol, and to mitigate those changes, the amount of CO_2 released into the atmosphere has to be reduced. Alternatively, or to further reduce the amount of greenhouse gases in the atmosphere, the CO_2 may be directly removed from the atmosphere or captured from the exhaust of powerplants (e.g. Lackner et al., 2009).

In any case, these capture techniques capture pure CO_2 which needs to be stored safely. A safely storage site of CO_2 is a formation where the CO_2 will be The gas will be transported toward the disposal area, this site will need to be safe for storage of CO_2 for thousands of years. Figure 1 illustrate a variety of storage sites like coal seams, depleted oil reservoir and saline aquifers, the general consensus points to store the carbon dioxide in saline aquifers. These formations are nearly ubiquitous,

therefore close to the production sites and can integrate enormous amounts of CO_2. The only drawback seems to be the relative poor knowledge of those formations, when compared to oil and gas fields.

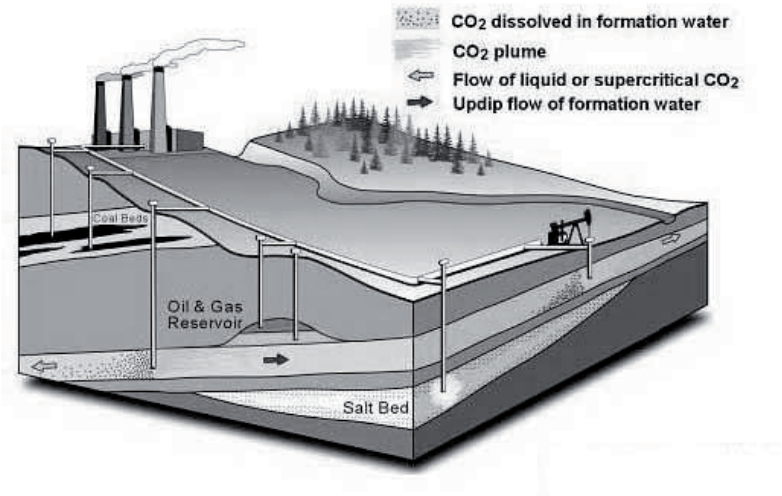

Fig. 1: The different ways to store CO_2 onshore, CO_2 might be injected into deep layers of porous and permeable rocks, which commonly form deep aquifers saturated with brine, oil and gas reservoirs, salt beds and coal beds. The presence of overlaying impermeable layers prevent any CO_2 from escaping to the surface (modified from ERCB – AGS).

Once the storage site is assessed and deemed valuable the injection of CO_2 will proceed and the processes described in figure 2 will occur. The CO_2 is first hydrodynamically trapped as fluid bubbles before it dissolves in water as $HCO_3^-/CO_3^{2-}/H_2CO_3$ (aqueous trapping, see Hitchen, 1996). Hydrodynamic trapping involves the storage of CO_2 as a supercritical fluid beneath a low permeability layer. This affects the pH of the solution, increasing the acidity and leading to the dissolution of the surrounding minerals. The subsequent neutralization may lead to the precipitation of secondary minerals, including carbonates. Such minerals (ankerite, calcite and dawsonite among others) are commonly viewed as sinks for CO_2 (Johnson et al., 2004, Ketzer et al., 2005, Soong et al., 2004, Xu et al., 2003, Xu et al., 2004, Xu et al., 2005 and Zerai et al., 2006) and in demonstration scale projects (Gale et al., 2001).

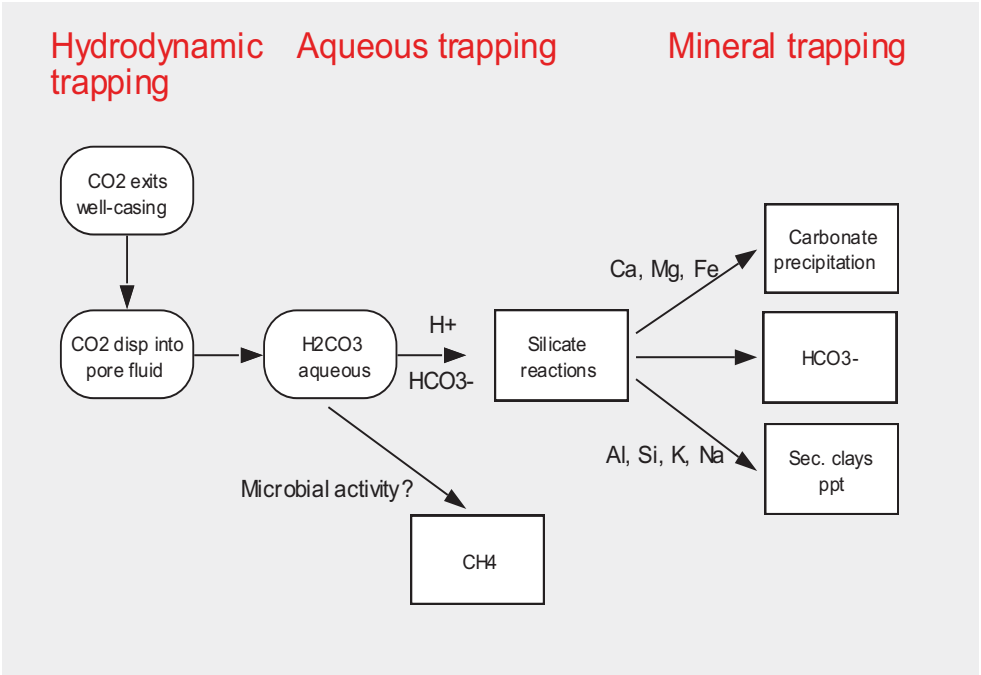

Fig. 2: the different phases of CO_2 trapping, from the injection where it is trapped in bubbles, dissolves into the pore fluid and reacts with the surrounding minerals, to the stable mineralogical form (Wawersik et al., 2001).

These reactions will affect the surrounding rocks and major changes will happen to the reservoir and caprock structure and chemical composition (Knauss et al., 2005). As part of the assessment of the geological storage site it is critical to evaluate the transformation of the reservoir and caprock following the injection of CO_2 as it can lead to a compromisation of its integrity and thus leakage of CO_2 back to the surface. This changes are based on which phases are dissolved and which ones are precipitated, it's effect on the porosity and permeability of the reservoir i.e. the chances to clog the system or compromise the caprock. It is equally possible to precipitate clay minerals or coatings in general which will prevent the dissolution of the primary minerals, inhibiting the release of metals and therefore hindering the precipitation of carbonates. The ability to estimate the timeframe of these reactions is essential for the success of storage operations.

This whole assessment is normally based on geochemical models, like PHREEQC (Parkhust and Appelo, 1999), and it is widely known that the databases used for these calculations are a collection of good data, but also involves a lot of assumptions, presumption and guesswork (e.g. Oelkers and Schott, 2009). The calculations therefore predict precipitation of minerals during CO_2 storage scenarios that rarely forms in natural analogues or in laboratory experiments. Dawsonite is a very good example, and it is the major focus of our work on carbonates, to provide better data and also improve the theory underlying those modeling codes.

Effect of organics on the habitus of dawsonite.

A wide range of organics are present in most reservoirs for example the coating of coccolithes. It is a poorly known domain. During injection the dissolution of the surrounding minerals will release these chemicals in the pore space. Considering the effect of fruit acids on carbonate like calcite and magnesite (Mao and Huang, 2006) it is highly probable that these organics will affect the precipitation and growth of the secondary minerals and mineralogical hosts for CO_2. We tested the effect of various organic compounds during dawsonite synthesis experiments.

Dawsonite has also industrial applications as it is a widely used fire retardant in paints and plastics. One aspect of our experimentation with organics was an attempt to make an ideal powder by controlling its growth.

Theoretical context on dissolution

Numerous studies of mineral dissolution kinetics have demonstrated that water rock interactions are controlled by chemical reactions occurring at the surface of the minerals. The observations of etched pits developing at the surface of solids being the proof (Berner and Schott, 1982; Brantley et al, 1986; Gautier et al, 2001). Moreover the knowledge of chemical reactions occurring at the surface of the mineral is not enough to predict the reaction rates in natural geochemical processes.

Dissolution mechanisms

The dissolution of minerals is a multistep process and during the water rock interaction there are three main steps occurring at the interface between the fluid and the liquid:

First, the aqueous transport of the reactant towards the reaction site, by convection, diffusion or migration along the surface. Secondly the reaction at the surface include the adsorption of reactant on the active sites from the mineral surface, the solubilization of the reaction products and their desorption. And third, the aqueous transport of the reaction products away from the liquid/solid interface (Berner, 1978 ; Lasaga, 1981, Schott et Petit, 1987 ; Guy et Schott, 1989).

In the case of dissolution reaction, the solubilization of the constitutive elements of the mineral is the result of physical processes (diffusion, adsorption) and chemical processes characteristic of heterogeneous reactions.

Depending on the relative speed of the transport in solution of the different species in the media and the chemical reaction on the surface of the mineral three different controls are observed.

Reaction and Transition state theory.

In the transition state theory (TST – Eyring 1935) during every chemical reaction occurring on the surface of a solid, the reactants are in equilibrium with a higher energy specie called activated complex. The adsorption rate of the reactants on the solid's surface being faster than the decomposition of the activated complex. This last step being the slowest it is also the limiting step of the reaction. This theory was developed to study simple chemical reactions and it is based on statistical mechanic.

Activated complex formation (*Lasaga, 1998).*

In elementary chemical reactions, products are formed by the colliding reactant at a molecular scale. These products are in a stable or metastable state at a lower level of free energy and they have to overstep an activation barrier, the activation energy (Ea) for the reaction to occur. They are then transformed into stable products. The reactional species corresponding to the maximal energy level through which the reactants have to pass is called activated complex. This specie appears only as a transitional state during the reaction. By convention the activated complex is in equilibrium with the reactant and it decomposes into the products. This decomposition is the limiting step in the dissolution processes.

The rate of the elementary reaction (A+B-> C+D) is defined by the following product:

$$r_+ = \frac{K_B T}{h}[P_+^{\#}] \quad (1)$$

Where K_B is the Boltzman constant, h, the Planck constant, T the temperature in Kelvin and $[P_+^{\#}]$ is the concentration of the activated complex.

Defining *upsilon* as:

$$\upsilon = \frac{k_B T}{h} \quad (2)$$

Upsilon represent the frequency of passing the potential barrier (Lasaga, 1981), therefore the dissolution rate becomes:

$$r_+ = \upsilon[P_+^{\#}] \quad (3)$$

And the law of mass action for the formation of the activated complex is written as follow :

$$K_+^{\#} = \frac{\gamma_+^{\#}[P_+^{\#}]}{\Pi_i a_i^{ni}} \quad (4)$$

Where $\gamma_+^{\#}$ defines the activity coefficient of the activated complex, n_i and a_i designate respectively the stoichiometric coefficient and the activity of the specie i during its reaction of formation, and $K_+^{\#}$ represent the equilibrium constant of the reaction of forming of the activated complex from the reactant.

The concentration of the activated complex is given by:

$$[P_+^{\#}] = \frac{K_+^{\#}}{\gamma_+^{\#}} \Pi_i a_i^{ni} \quad (5)$$

While inserting the expression of [$P^{\#}$] (5) is r+ as stated in Eqn. 3 we obtain:

$$r+= v\frac{K_{+}^{\#}}{\gamma_{+}^{\#}} \times \Pi i a_{i}^{n_j} \quad (6)$$

Where r+ is the forward dissolution rate, ν is the frequency, K represents the equilibrium constant of the reaction, γ_{+} denotes the activity coefficient of the activated complex and a_i represents the activity of the subscripted species. The rate r- of the inverse reaction (C+D->A+B) is written in the same fashion but with the hypothesis that the activated complex $P^{\#}_{-}$, different from $P^{\#}_{+}$, is in equilibrium with the products j of the reaction.

$$t-= v\frac{K^{\#}}{\gamma_{-}^{\#}} \times \Pi j a_{j}^{n_j} \quad (7)$$

Where $\gamma^{\#}_{-}$ represent the activity coefficient of the activated complex formed from the reaction products, n_j and a_j designate respectively the stoichiometric coefficient and the activity of j(aqueous) and $K^{\#}_{-}$ is the equilibrium constant of the reaction (formation of the activated complex).

The net reaction rate, r_{net} is then written:

$$r_{net} = r_{+} - r_{-} = r_{+}\left(1 - \frac{r_{-}}{r_{+}}\right) \quad (8)$$

The ratio r_{-}/r_{+} being given by:

$$\frac{r_{-}}{r_{+}} = \frac{K_{-}^{*}\gamma_{+}^{*}}{K_{+}^{*}\gamma_{-}^{*}} \frac{\Pi_j a_j^{n_j}}{\Pi_j a_i^{n_i}} \quad (9)$$

The activity product Q can be recognized in this expression (9):

$$Q = \frac{\Pi_j a_j^{n_j}}{\Pi_j a_i^{n_i}} \quad (10)$$

If the activated complex is the same for both forward and backward reaction it can be simplified into

$$\frac{r_{-}}{r_{+}} = \frac{Q}{K} \quad (11)$$

Where $K = \frac{K_{+}^{*}}{K_{-}^{*}}$ is the equilibrium constant of the reaction.

From equation 8 and 11 we can define the global rate:

$$r_{net} = r_{+}\left(1 - \frac{Q}{K}\right) = r_{+} \times \left(1 - exp\left(-\frac{A}{RT}\right)\right) \quad (12)$$

With A being the chemical affinity defined by:

$$A = -RTln\left(\frac{Q}{K}\right) \quad (13)$$

Combining eqn 6 and 12:

$$r_{net} = v\frac{K_+^{\#}}{\gamma_+^{\#}} \times \Pi i a_i^{n_i} \times \left(1 - exp\left(-\frac{A}{RT}\right)\right) = k_+ \times \Pi i a_i^{n_i} \times \left(1 - exp\left(-\frac{A}{RT}\right)\right) \quad (14)$$

where k_+ stands for the reaction rate constant.

One particular case is when protons and hydroxyls are the only species intervening in the reaction of formation of the activated complex. Equation 14 is then limited to the following (from Aagaard and Helgeson, 1982, Murphy and Helgeson, 1989a):

$$r_{net} = k_+ \left(a_{H^+}^{n_{H^+}}\right) \times \left(1 - exp\left(-\frac{A}{RT}\right)\right) \quad (15)$$

Where $a_{H}+$ and $n_{H}+$ are respectively the proton activity and the number of protons necessary to form the activated complex.

The Transition State Theory explicitly bounds the dissolution rate to the chemical affinity and links the thermodynamics and kinetics.

Application of the TST to the dissolution of minerals.

Dissolution reactions are generally not simple reactions, so the TST should not be applicable in that case. But the work of Aagaard and Helgeson (1977, 1982) on the dissolution of silicates allowed extending the TST to heterogeneous reactions. They demonstrated that the TST was applicable to dissolution reactions if they were considered as a chain of isolated simple reactions with one being responsible for the formation of the activated complex (Temkin, 1963, Boudart, 1976, Aagaard and Helgeson, 1977, 1982, Nagy et al., 1991). The decomposition of the activated complex in products controls the reaction rate.

The dissolution of oxides and hydroxides is possible due to the adsorption of proton, hydroxyls or ligands already in the solution. They polarize and weaken the metal-oxygen bound (Furrer and Stumm, 1986; Stumm, 1992). This explains why oxides and hydroxides dissolution rate is dependant on the pH and the species in solution. The dissolution mechanism of complex oxides differs from the simple ones in that they require the destruction of several metal-oxygen bounds. Similarly to the dissolution of simple oxides and hydroxides, the dissolution of complex oxides can be explained by a succession of metal-proton exchange reactions (Oelkers, 2001). It is also possible that other ions participate in these ion-exchange reactions if they are in high enough concentration and if their radius and charge correspond to the would be replaced cation.

Without such ions, protons are the major ions in ionic exchange reactions; this is due to the small radius of protons versus other cations. The number of protons involved in the reactions is hypothesized to be the same as the valence of the metal (Casey and Ludwig, 1996).

As with the dissolution rates of the different simple oxides and hydroxides may be different, the breaking rate of the different metal-oxygen bounds present in a complex oxide might vary significantly. The slower metal-proton reaction leads to the destruction of the crystalline structure

Summary of Paper

The five papers make the body of this thesis

Paper 1: ***Reactivity of Rhyolitic glass, Declercq J. and Oelkers E.H., to be submitted to GCA.***

Over the course of this paper we have determined the dissolution rate of rhyolitic glass over a large range of temperature and pH. In a similar way as Wolff-Boenisch et al. (2004a and b) the purpose of that study was to determine the dissolution mechanism of the rhyolitic glass and to compare it with the basaltic glass dissolution mechanism. The results show a very good agreement between the two mechanisms. Therefore it is share between the two compositional endmembers of the natural volcanic glass. To achieve our goal we have used a glass originating from the 1362 eruption of Öraefajökull, Iceland, powdered and free of minerals. In order to determine the reactivity of the glass we dissolved it in mixed-flow reactor (Parr^{TM}) and used the steady state $Si_{(aq)}$ and $Al_{(aq)}$ concentration in the output solution as proxies for the dissolution rate. The experience was conducted between 40 and 200°C and a pH range varying from 2 to 10. The solution was analyzed by colorimetry (Korolef, 1976) and ICP-AES at the ENSAT (Ecole Nationale Supérieure d'Agronomie de Toulouse) while the solid material was observed for surface changes and secondary precipitations with a SEM coupled to an EDS.

The main findings of this paper may be summarized as:

1) The dissolution of rhyolite is stoichiometric
2) The dissolution behaviour of rhyolitic glass is consistent with silicates, the shape of the curve of the rate when plotted against pH is controlled by the aluminium hydroxide complex
3) The dissolution behaviour of the glass is consistent with that of basaltic glass; both are apparently proportional to the activity ratio $[a^3_{H+}/a_{Al}{}^{3+}]$. This proportionality allows prediction of the effect of aqueous solution composition and rhyolitic glass dissolution rate
4) Confirming the results form Wolff-Boenisch et al. (2004a and b) the same dissolution mechanism applies for the two of the most extreme types of natural volcanic glass (basalt and rhyolite). Therefore it is conceivable to develop a general rate equation for the dissolution of natural glasses.

Paper 2: ***Experimental alteration of artificial and natural impact melt rock from the Chesapeake Bay impact structure*** **DECLERCQ, Julien, DYPVIK, Henning, AAGAARD, Per, JAHREN, Jens, FERRELL, Ray E., Jr., HORTON, J. Wright, Jr.** ***in*** **SPE458: The ICDP-USGS Deep Drilling Project** ***in*** **the Chesapeake Bay Impact Structure: Results from the Eyreville Core Holes edited by Gregory S. Gohn, Christian Koeberl, Kenneth G. Miller, and Wolf Uwe Reimold**

This article follows naturally as an application of the dissolution mechanism of the natural glass described in the previous study. We report the mineralogical changes observed during the laboratory alteration of two natural impact melt rocks from drill cores at different localities in the Chesapeake Bay impact structure and two artificially prepared glasses. The results are compared to equilibrium mineral assemblages calculated with PHREEQC and to mineral assemblages in the Chesapeake Bay impact structure drill cores in order to improve our understanding of impact melt alteration processes.

The natural samples were collected from clasts in the suevites from the CBIS and the artificial glasses made at the Center for Materials, Oslo, by fusing two finely grounded powders of known mineralogical and chemical composition in a furnace at 1045°C for 45 minutes. Those samples were subsequently used in alteration experiments with alteration solution being an artificial and simplified seawater. The third part of the study, the modelling was performed using seawater as defined by Nordstrom et al. in 1978, adding the solid with the composition defined from the analysis of the natural samples. The starting material macroscopic features was also described from the observation of thin sections while it's chemical and mineralogical composition was determined by respectively XRF and XRD. After the experiment the resulting powder was analyzed by XRD to determine the mineralogical assemblage.

The main findings of this study are the partial but incomplete agreement among actual, experimental, and theoretical ways to assess melt-rock alteration processes. A general model for prediction of alteration processes and products cannot be developed because of the compositional complexity of the melt rocks, including glasses, generated by impact. The presence of albite and analcime in a core and treated artificial glass samples, and their disappearance in the natural sample during laboratory experiments, suggest that alteration may have occurred at temperatures near 265^{o}C. However, the stability limit is affected by original melt rock or glass composition. In our experiments, 13 wt% of the melt glass or melt rock was dissolved and reprecipitated as mainly analcime, clinochlore, illite, montmorillonite, and saponite. During the alteration a complex and diverse mineralogical assemblage is precipitated, this assemblage will depend on the altered glass and on the weathering fluid composition. The system is complex and therefore it is difficult to use the mineral abundance as a proxy for the volume of glass produced during an impact event. Being aware of these limitations we attempted such a back calculation. Our results are within the margin of other results obtained with different calculation method, using the size and depth of the crater.

The formation of melt during impact is an important factor in crater formation on the Earth and in our planetary system, i.e. on the surface of Mars. There, comparable clay minerals may be present. Consequently, the preservation and alteration of impact melts, including glasses, may significantly influence the surface properties of planetary bodies within the Solar System.

Paper 3: ***The reactivity of hydrothermally synthesized dawsonite*** **H. Hellevang, J. Declercq, B. Kvamme, P. Aagaard, submitted to *Applied Geochemistry*.**

The main objective of this paper is to report the dissolution rate of dawsonite at acidic conditions and to compare the apparent pH dependency of dawsonite with those of the common carbonate. As there is not enough natural chemically homogeneous dawsonite available we synthesized it. The synthesis process is described in the paper.
Dawsonite synthesis was performed in Teflon liners put into a rotating stage oven at a selected temperature following the procedure described by Zhang et al (2004). The degree of conversion form the reactant to dawsonite was estimated through an XRD analysis of the resulting powder. Its surface area was also measured by BET using a Strohlein area meter. The synthetic dawsonite powder was then subjected to dissolution experiments in free drift batch reactors at 77°C. The dissolution rate was estimated from the difference in element concentration in solution overtime.

The main results of this paper can be summarized by the following.

1) Dawsonite synthesis revealed that the formation rate of dawsonite is dependent on the dissolution rate of the aluminium source.
2) The faster-dissolving crystalline gibbsite resulted in a higher degree of conversion to dawsonite than the amorphous hydrous aluminohydroxide.
3) Dissolution experiments on the synthetic dawsonite showed that the dissolution rate at pH 4 and 22°C is comparable with that of magnesite. At pH < 4 the rates are first-order dependent on the proton activity, whereas at higher pH the rate approach a pH-independent region which is strongly supported by the earlier reported rate data by Hellevang et al. (2005).
4) Based on the similarity in activation energies between dawsonite, calcite and magnesite over the proton promoted rate region we propose that a similar mechanism is responsible for the dissolution rate at acidic conditions for all three.
5) As natural occurrences of dawsonite as well as thermodynamics indicate that dawsonite is only likely to form at circumneutral to basic conditions, the high apparent activation energy of dissolution of 80.58 ± 8.1 kJ/mol may indicate that growth is constrained by an activation barrier at low temperatures.
6) Based on the crystal structure of dawsonite we suggest that dawsonite growth mainly occur along the crystallographic c-axis by the adhesion of $Al(OH)_2^+$ to a chain of octahedral coordinated Al stabilized by carbonate groups. This carboaluminate chain forms the backbone of the dawsonite structure bond together by hydrogen bonds and the interstitial sodium ions.

Paper 4: ***Dawsonite dissolution rate and mechanism at neutral and basic pH ; implication for CO_2 storage*** **Declercq J., Hellevang H., Aagaard P., submitted to Oil and Gas Research and Technology (IFP Review).**

The main objective of this article is to understand the dissolution mechanism of dawsonite above pH 4.

The dawsonite used in the experiment was synthesized based on Zang et al., 2005, the synthetic dawsonite powder was then subjected to dissolution experiments in free drift batch reactors at 25°C and 80C. The dissolution rate was estimated from the difference in element concentration in solution overtime. Experiments were carried out in 500ml batch reactors, the pH of the solution was adjusted to the desired value by using analytical grade HCl and $Mg(OH)_2$ saturated solution. The solution was sampled regularly and $[Al]_{aq}$ and $[Na]_{aq}$ were analysed by ICP-AES and atomic absorption at the University of Oslo.
The main results of this article are summarized below:

1) The dawsonite formation requires the formation of Al-OH bounds and is hindered by the high activation energy. Thus it will be very difficult to form.

2) Even if dawsonite forms, as soon as it becomes undersaturated it will dissolve at once due to its high dissolution rate. Releasing the mineralized CO_2 in the process.

3) Dissolution experiments on dawsonite showed that the dissolution rate at pH 4 and 22°C is comparable with that of magnesite. At pH < 4 the rates are first-order dependent on the proton activity.

4) Based on the similarities between the activation energies of dawsonite, calcite and magnesite over the whole pH range we propose that the dissolution mechanism of dawsonite is limited by only one step, the removal of sodium from the crystal structure.

5) Around neutrality the rate approach a pH-independent region which is strongly supported by the earlier reported rate data by Hellevang et al. (2005), at pH above 8 the rate decrease.

6) For pH > 4 we suggest that the rates are dominated by surface hydration

7) At pH > 8 the dawsonite saturation index indicates its supersaturation; the reduction of the rates can be attributed to backward precipitation of dawsonite.

Paper 5: ***Why is dawsonite absent in CO_2 charged reservoirs?*** **H. Hellevang, J. Declercq and P. Aagaard. Submitted to Oil and Gas Research and Technology (*IFP review)*.**

The main objective of this article is to provide a basis to understand the stability of dawsonite in various CO_2 storage settings based on the stability of dawsonite relative to aluminosilicate minerals and sodium carbonate. Earlier studies have shown that dawsonite is highly stable at low temperature (<80°C) up to quartz saturation.

The main results of this study can be summarized as follow:

1. The stability field of dawsonite is reduced when the solution is undersaturated with respect to quartz, typically at low temperature (below 60 to 80°C).

2. The stability of dawsonite is limited by the solubility of nahcolite at a given CO_2 pressure which dictates the upper Na activity limit.

3. Comparison between natural quartz precipitation rates and laboratory derived rates suggests that the quartz rates obtained in the laboratory might be overestimated by several orders of magnitude compared to the natural process.

Concluding remarks

The results from this study provide an insight on the reactivity of aluminosilicates glass and carbonates. The kinetic values extracted from the experiments will provide a mean to calibrate or update existing databases.

The emphasis of this study was on the dissolution mechanism and required a large number of experiments and analysis. In the case of the dawsonite, managing to get the experiments working was quite time consuming and the number of valid data obtained was rather limited. More work should be carried out with respect to the precipitation kinetics of the mineral. The precipitation mechanism, especially the breaking of the Al-OH bonds and the behavior of the water shell around the metals is poorly understood.

The main findings of this study may be summarized as follows:

- The same dissolution mechanism applies to rhyolitic and basaltic glass, and can be extended to all natural glasses.

- Alteration of impact glasses yield a specific clay assemblage. This assemblage can be used to determine the original glass content in the sediment.

- Dawsonite behaves like a monocomponent carbonate, exhibiting similar activation energy as magnesite and calcite; therefore the dissolution mechanisms require only one step, the removal of Na from the structure.

- Dawsonite dissolution rates exhibit three domains with respect to pH, these are linked to different mechanisms occurring on the surface of the mineral. At pH below 4, the rates show a first order dependence on pH, the dissolution mechanism is linked to the protonation of the surface and exchange with sodium. At pH neutral (between 4 and 8) the rates are pH independent and dominated by the hydration of the surface. The same mechanism prevails at pH above 8, but the rates forward slowed down due to the backward precipitation of dawsonite.

- Dawsonite dissolution mechanism can be described by the removal of the Na from the structure which then collapses and disintegrate the carboaluminate chains.

Additional contributions

Report on dawsonite synthesis: ***Dawsonite Synthesis*****, Y. Jia, H. Hellevang, J. Declercq, P. Aagaard**

The present study presents detailed procedures for synthesis of dawsonite. The results suggest that the method used is reproducible and reliable. Dawsonite with crystal habit that resembles natural samples is easily produced. The presence of additives such as citric acid will change the morphology of dawsonite as it inhibits growth in the crystallographic z-direction. The present work is the basis for the next stage of experiments which comprise: (1) to achieve the reaction rate of dawsonite at different chemical conditions; and (2) further studies on the precipitation of dawsonite at various chemical conditions.

Posters

Goldschmidt 2007, August 2007, Cologne – Germany Reactivity of Rhyolitic Glass. J.Declercq, E.H.Oelkers

CMS, June 2007, Santa Fe – New Mexico – USA Alteration of synthetic impact crater glass. J.Declercq, H.Dypvick, J.Jahren

GSA, November 2007, Denver – Colorado – USA EXPERIMENTAL ALTERATION OF IMPACT GLASSES FROM THE CHESAPEAKE BAY IMPACT — EYREVILLE AND CAPE CHARLES CORES. J.Declercq, H.Dypvik, P.Aagaard, J.Jahren, R.E.Ferrel, J.W.Horton

EGU, April 2008, Vienna – Austria Dawsonite Dissolution Rates. J.Declercq, H.Hellevang, P.Aagaard

Rencontres Scientifiques de l'IFP, May 2009, Rueil-Malmaison – France Dawsonite dissolution rate and mechanism at neutral and basic pH ; implication for CO_2 storage. J.Declercq, H.Hellevang, P.Aagaard.

Reykjavik – Iceland Dawsonite Dissolution Mechanism. J.Declercq, H.Hellevang, P.Aagaard

References

Aagaard, P., Helgeson, H.C., Thermodynamic and kinetic constraints on the dissolution of feldspars. *GSA Abstr. Prog.* **9** (1977), pp. 873.

Aagaard, P., Helgeson, H.C. Thermodynamic and kinetic constraints on reaction rates among minerals and aqueous solutions; I, Theoretical considerations *American Journal of Science* 1982, **282**: 237-285

Allnatt, A.R., Bancroft, G.M., Fyfe, W.S., Jacobs, P.W.M., Karkhanis, S.N., Melling, P.J., Nishijima, A., Vempati, C.S., Tait, J., Leaching behavior and electrical conductivity of natural rhyolite and modified synthetic rhyolites, *Chemical Geology*. **38** (1983), pp. 329–357

Berner, R.A., Schott, J., Mechanism of pyroxene and amphibole weathering. II. Observations of soil grains. *American Journal of Science* **282** (1982), pp. 1214–1231.

Berner, R.A., Weathering, plants, and the long-term carbon cycle, *Geochimica et Cosmochimica Acta* **56** (1992), pp. 3225-3231.

Boudart, M., Consistency between kinetics and thermodynamics. *J. Phys. Chem.* **80** (1976), pp. 2869-2870.

Brady, P.V. and Gíslason, S.R., Seafloor weathering controls on atmospheric CO2 and global climate. *Geochimica et Cosmochimica Acta*, **61** (1997) pp.965-973.

Brantley, S.L., Crane, S.R., Crerar, D.A., Hellmann, R., Stallard, R., Dissolution at dislocation etch pits in quartz, *Geochimica et Cosmochimica Acta*, **50** (1986) pp. 2349-2361,

Casey, W.H., Ludwig, C., The mechanism of dissolution of oxide minerals. *Nature* **381** (1996), pp. 506–509.

Chester, R., Marine Geochemistry. (2nd ed.), Blackwell, Oxford (2000), pp. 506.

Dickin, A.P., Hydrothermal leaching of rhyolite glass in the environment has implications for nuclear waste disposal, *Nature* **294** (1981), pp. 342–347.

Dran, J.-C., Petit, J.-C., Brousse, C., Mechanism of aqueous dissolution of silicate glasses yielded by fission tracks, *Nature* **319** (1986), pp. 485–487

Dran, J.-C., Della Mea, G., Paccagnella, A., Petit, J.-C., Trotignon, L., The aqueous dissolution of alkali silicate glasses: reappraisal of mechanisms by H and Na depth profiling with high energy ion beams, *Phys. Chem. Glasses* **29** (1988), pp. 249–255.

Eyring,L., The activated complex in chemical reactions. *J. Chem. Phys.* **3** (1935), pp. 107-115.

Fiore, S., Huertas, F.J., Tazaki, K., Huertas, F., Linares, J., A low temperature experimental alteration of a rhyolitic obsidian, *European Journal of Mineralogy* **11** (1999), pp. 455–469.

Furrer, G., Stumm, W., The coordination chemistry of weathering: I. Dissolution kinetics of δ-Al_2O_3 and BeO, *Geochimica et Cosmochimica Acta* **50** (1986), pp. 1847–1860.

Gale, J., Christensen, N.P., Cutler, A., Torp, T.A., Demonstrating the potential for geological storage of CO_2: the Sleipner and GESTCO projects, *Environ. Geosci.* **8** (2001), pp. 160–165.

Gautier, J.-M., Oelkers, E.H., Schott, J., Are quartz dissolution rates proportional to BET surface areas?, *Geochimica et Cosmochimica Acta* **65** (2001), pp. 1059–1070.

Guy, C., Schott, J., Multisite surface reaction versus transport control during the hydrolysis of a complex oxide, *Chemical Geology* **78** (1989), pp. 181-204

Harrison, W.J., Wendlandt, R.F., Geochemical interactions resulting from carbon dioxide disposal on the seafloor. *Applied Geochemistry* **10** (1995), pp. 461-475.

Hellevang, H., Aagaard, P., Oelkers, E.H., Kvamme, B., Can dawsonite permanently trap CO_2? *Environ. Sci. Technol.* **21** (2005), pp.8281-7

Hendriks, V., Blok, K., Underground storage of carbon dioxide, *Energ. Conver. Manage.* **36** (1995), pp. 539–542

Hitchen, B., Aquifer disposal of carbon dioxide, hydrologic and mineral trapping, Geoscience Publishing Sherwood Park, Alberta, Canada (1996).

Holland, H.D., *The Chemistry of the Atmosphere and Oceans*, Wiley (1978).

Holloway, B., An overview of the underground disposal of carbon dioxide, *Energy Convers. Manage.* **38** (1997), pp. S193–S198.

Houghton, J.T., Meira Filho, L.G., Griggs, D.J., Maskell, K., Stabilization of atmospheric greenhouse gases: physical, biological and socio–economic implications. International Panel for Climate Change Technical Paper III (1997).

IPCC : *The Physical Science Basis. Contributions of the Working Group I to The Fourth Assessment Report of the Intergovernmental Panel on Climate Change*. Solomon et al. Eds. Cambridge University Press, United Kingdom and New York, NY, USA (2007).

Johnson, J.W., Nitao, J.J., Steefel, C.I., Knauss, K., Reactive transport modeling of geologic CO_2 sequestration in saline aquifers: the influence of intra-aquifer shales and the relative effectiveness of structural, solubility, and mineral trapping during prograde and retrograde sequestration. Proceeding, First National Conference on Carbon Sequestration, Washington (2001).

Ketzer, J.M., Carpentier, B., LeGallo, Y., Le Thiez, P. Geological sequestration of CO_2 in mature hydrocarbon fields – basin and reservoir numerical modeling of the Forties Field, North Sea, *Oil Gas Sci. Technol.* **60** (2005), pp. 259–273.

Karkhansis, S.N., Bancroft, G.M., Fyfe, W.S., Brown, J.D., Leaching behaviour of rhyolite glass, *Nature* **284** (1980), pp. 435–437.

Knauss, K.G., Johnson, J.W., Steefel, C.I., Evaluation of the impact of CO_2, co-contaminant gas, aqueous fluid and reservoir rock interactions on the geologic sequestration of CO_2. *Chemical Geology* **217** (2005), pp.339-350.

Koroleff F. Determination of silicon. In *Methods of Seawater Analysis* (ed. K. Grassnoff). Springer-Verlag (1976).

Kump, L.R., Brantley, S.L. Arthur, M.A., Chemical weathering, atmospheric CO_2, and Climate, *Ann. Rev. Earth Planet. Sci.* **28** (2000), pp. 611–667.

Lackner, K.S., Park, A.-H.A., Miller, B.G., Eliminating CO_2 Emissions from Coal-Fired Power Plants, Generating Electricity in a Carbon-Constrained World, Academic Press, Boston (2010).

Lasaga, A.C., Chemical kinetics of water–rock interaction, *J. Geophys. Res.* **89** (1984), pp. 4009–4025

Lasaga, A.C., Berner, R.A., Fundamental aspects of quantitative models for geochemical cycles, *Chemical Geology*, **145,** 3-4, 15 (1998), pp. 161-175.

Magonthier, M.-C., Petit, J.-C., Dran, J.-C., Rhyolitic glasses as natural analogues of nuclear waste glasses: behaviour of an Icelandic glass upon natural aqueous corrosion, *Applied Geochemistry*, **7** (1992), pp. 83-93,

Mazer, J.J. and Walther, J.V. Dissolution kinetics of silica glass as a function of pH between 40 and 85°C. *J. Non-Cryst. Solids* **170** (1994), pp. 32–45.

Morgan, N.A., Spera, F.J., A molecular dynamics study of the glass transition in CaAl 2 Si 2 O 8 ; thermodynamics and tracer diffusion *American Mineralogist* **86** (2001), pp. 915-926.

Mao, Z., Huang, J., Habit modification of calcium carbonate in the presence of malic acid, *Journal of Solid State Chemistry*, **180**, 2 (2007), pp. 453-460.

Mungall, J.E. and Martin, R.F., Severe leaching alteration of trachytic glass without devitrification, Terceira, Azores. *Geochimica et Cosmochimica Acta* **58** (1994), pp. 75–83.

Murphy, W.M., Helgeson, H.C., Thermodynamic and kinetic constraints on reaction rates among minerals and aqueous solutions. III. Activated complexes and the pH-dependence of the rates of feldspar, pyroxene, wollastonite, and olivine hydrolysis, *Geochimica et Cosmochimica Acta* **51** (1987), pp. 3137-3153.

Nagy, K.L., Blum, A.E., Lasaga, K., Dissolution and precipitation kinetics of kaolinite at 80C and pH 3: the dependence on saturation state. *Amer. J. Sci.* **291** (1991), pp. 649-686.

Nordstrom, D.K., Plummer, L.N., Wigley, T. M. L., Wolery, T.J., Ball, J.W., Jenne, E.A., Basset, R. L., Crerar, D.A., Florence, T.M., Fritz, B., Hoffman, M., Holden Jr, G.R., JR.12 ,Laffon, G.M., Mattigod, S.V., McDuff, R. E., Morell, F., Reddy, M.M., Sposito, G., Thrailkill, J., A comparison of computerized chemical models for equilibrium calculations in aqueous systems, Chemical Modeling *in* Aqueous Systems; *ACS Symposium Series* **93** (1979), pp. 857–892.

Oelkers, E.H., A general kinetic description of multi-oxide silicate mineral and glass dissolution, *Geochimica et Cosmochimica Acta* **65** (2001), pp. 3703–3719

Oelkers, E.H., Schott, J. Thermodynamics and kinetics of water-rock interaction *in* Reviews in Mineralogy and Geochemistry, **70** (2009).

Petit, J.C., Natural analogues for the design and performance assessment of radioactive waste forms: A review, *Journal of Geochemical Exploration*, **46**, 1, The Pocos de Caldas Project: Natural Analogues of Processes in a Radioactive Waste Repository, Part II, (1992), pp. 1-33,

Pokrovsky, O.S., Schott, J., Processes at the magnesium-bearing carbonates/solution interface. II. kinetics and mechanism of magnesite dissolution., *Geochimica et Cosmochimica Acta* **63** (1999), pp. 881-897.

Pokrovsky, O.S., Schott, J., Thomas, F., Processes at the magnesium-bearing carbonates/solution interface. I. a surface speciation model for magnesite, *Geochimica et Cosmochimica Acta*, **63** (1999), pp. 863-880.

Riley, J.P. and Chester, R., *Introduction to Marine Chemistry* Academic Press (1971).

Schott et Petit, 1987 ;

Soong, Y., Goodman, A. L., McCarthy-Jones, J. R., Baltrus, J. P., Experimental and simulation studies on mineral trapping of CO_2 with brine, *Energy Conversion and Management*, **45** (2004), pp. 1845-1859.

Spivack A.J., Staudigel, H., Low-temperature alteration of the upper oceanic crust and the alkalinity budget of seawater, *Chemical Geology,* **115** (1994), pp. 239–247.

Stumm, W. Chemistry of the Solid Water Interface; John Wiley and Sons: New York (1992).

Temkin, M.I., The kinetics os stationary reactions. *Akad. Nauk. SSR Doklady* **152** (1963), pp. 782-785.

Thompson, D.W. and Pownall, P.G., Surface electrical properties of calcite. *J. Colloid Interface Sci.* **131** (1989), pp. 74–82.

Urey, 1952; The Planets: Their Origin and Development: New Haven, Yale University Press, p. 245.

Van Cappellen, P., Charlet, L., Stumm, W. and Wersin, P., A surface complexation model of the carbonate mineral-aqueous solution interface. *Geochim. Cosmochim. Acta* **57** (1993), pp. 3505–3518.

Wawersik, W.R., Rudnicki, J.W., Dove, P., Harris, J., Logan, J.M, Pyrak-Nolte, L., Orr F.M.Jr., Ortoleva, P.J., Richter, F., Warpinski, N.R., Wilson, J.L., Wong, T.-F., Terrestrial sequestration of CO2: An assessment of research needs, In: Renata Dmowska and Barry Saltzman, Editor(s), Advances *in Geophysics*, **43** (2001), pp. 97-177.

White, A.F., Claassen, H.C., Kinetic model for the short-term dissolution of a rhyolitic glass, *Chem. Geol.* **28** (1980), pp. 91–109

White, A.F., Surface chemistry and dissolution kinetics of glassy rocks at 25°C, *Geochim. Cosmochim. Acta* **47** (1983), pp. 805–815.

Wolff-Boenisch, D., Gíslason, S.R., Oelkers, E.H., The effect of fluoride on the dissolution rate of natural glasses at pH 4 and 25°C. *Geochim. Cosmochim. Acta* **68** (2004), pp. 4571-4582

Wolff-Boenisch, D., Gíslason, S.R., Oelkers, E.H., Putnis, C.V., The dissolution rates of natural glasses as a function of their composition at pH 4 and 10,6, and temperatures from 25 to 74°C. *Geochim. Cosmochim. Acta* **68** (2004), pp.4843-4858.

Xu, T., Apps J.A., Pruess, K., Reactive geochemical transport simulation to study mineral trapping for CO_2 disposal in deep arenaceous formations, *J. Geophys. Res.* **108** (2003), pp. 2071.

Xu, T., Apps J.A., Pruess, K., Numerical simulation of CO_2 disposal by mineral trapping in deep aquifers, *Applied Geochemistry* **19** (2004), pp. 917–936.

Xu, T., Apps J.A., Pruess, K., Mineral sequestration of carbon dioxide in a sandstone-shale system, *Chemical Geology* **217** (2005), pp. 295–318.

Xu, T., Apps, J.A., Pruess, K., Yamamoto, H., Numerical modeling of injection and mineral trapping of CO_2 with H_2S and SO_2 in a sandstone formation. *Chemical Geology* **242** (2007), pp. 319-346.

Zerai, B., Saylor, B.Z., Matisoff, G., Computer simulation of CO_2 trapped through mineral precipitation in the Rose Run Sandstone, *Ohio Applied Geochemistry* **21** (2006), pp. 223–240.

Zhang, X., Wen, Z., Gu, Z., Xu, X., Lin, Z., Hydrothermal synthesis and thermodynamic analysis of dawsonite-type compounds, *Journal of Solid State Chemistry* **177** (2004), pp. 849-855

Paper 1: An experimental study of the dissolution rates of rhyolitic glass at temperatures from 40 to 200°C and 2<pH<10.4.

Julien Declercq[1], Eric Oelkers[2]

(1) Department of geosciences, University of Oslo, P.O.Box 1047, Oslo, NO 316, Norway, julien.declercq@geo.uio.no

(2) LMTG - UMR 5563 UR 154 CNRS Université Paul-Sabatier IRD, 14, avenue Edouard Belin, 31400 Toulouse, France

Abstract - The steady-state dissolution rates of Öraefajökull rhyolitic glass were measured as a function of aqueous Si and Al concentration at temperatures from 40°C to 200°C and for pH from 2 to 10.4. Constant temperature and pH dissolution rates are independent of aqueous Si concentration but increase with decreasing aqueous aluminium concentration. All measured dissolution rates were found to be consistent with:

$$r_+ = k_+ . \exp\left(\frac{-E_A}{RT}\right).\left[\frac{a_{H^+}^3}{a_{Al}^{3+}}\right]^{0.18}$$

where r_+ refers to the dissolution rate, k_+ represents a rate constant equal to 0.031 mol.cm^{-2}.s^{-1}, E_A denotes an Activation Energy equal to 77.3 kJ mol^{-1}, R designates the gas constant, T correspond to the absolute temperature and a_i defines the activity of the subscripted aqueous species. This rate behaviour is similar to that previously proposed for basaltic glass. This similarity suggests similar dissolution mechanism of all natural volcanic glasses consisting of the sequential removal of metals from the glass structure via proton exchange reaction. The overall dissolution rate, however, is controlled by the detachment of Si tetrahedral that have been partially liberated from the glass structure through the removal of adjoining Al.

1. INTRODUCTION

Volcanic glass dissolution plays a major role in a variety of natural processes. Nearly 1km^3 of glass is produced every year, mostly along the oceanic ridges (Morgan and Spera, 2001). Dispersal of airborne volcanic glass primarily of silica-rich tephra, originating from explosive volcanic eruptions has a large role in the sedimentary processes in the North Atlantic (Haflidason et al., 2000; Larsen et al., 2001; Lacasse and Bogaard, 2002). Glass shards fall on land and on the seafloor within a few hours or days after an explosive eruption (Carey, 1997). Volcanic glass release divalent cations during its dissolution which can influence the long-term atmospheric CO_2 content (Urey, 1952; Riley and Chester, 1971; Holland, 1978; Thompson, 1983; Berner, 1992; Spivack and Staudigel, 1994; Brady and Gíslason, 1997; Chester, 2000; Kump et al., 2000). Because of their high reactivity, chemical weathering of natural glass plays a significant role in the global cycle of numerous elements (Gíslason et al., 1996; Brady and Gíslason, 1997; Louvat, 1997; Moulton et al., 2000; Dessert et al., 2001; Stefansson and Gíslason, 2001).

In contrast to the plethora of studies focussed on the dissolution rates of basaltic and borosilicate glasses, relatively few corresponding studies have focussed on acidic volcanic glasses. Studies of acid volcanic glass dissolution behaviour include work aimed at their potential utility as nuclear waste hosts (Kharkansis et al., 1980; Dickin, 1981; Petit, 1992*), as well as* on the leaching behaviour of silica rich glasses in an effort to better understand their dissolution mechanism (White and Claassen, 1980; White et al., 1980; White, 1983; Allnatt et al., 1983; Dran et al., 1986, 1988; Magonthier et al., 1992; Mungall and Martin, 1994; Mazer and Walther, 1994; Fiore et al., 1999).

Building on these studies, the dissolution rates of Öraefajökull rhyolitic glass has been measured as a function of temperature and aqueous solution composition. The goal of this paper is to present the results of this experimental study, to use these results to illuminate the dissolution mechanism of natural glass, and generate a quantitative expression describing acid glass dissolution in natural solution.

2. THEORETICAL CONSIDERATION

All aqueous activities in the present study were generated using the PHREEQC 2.6 computer code (Parkhurst and Appelo, 1999). The only significant Al-bearing aqueous species considered in the thermodynamic model are Al_3^+, $Al(OH)_2^+$, $Al(OH)_2^+$, $Al(OH)_3$, and $Al(OH)_4^-$. Equilibrium constants were taken from the PHREEQC database for all aqueous species and minerals. Dissolution is controlled by processes occurring on the mineral or glass surface. A number of studies have successfully modelled mineral dissolution rates by assuming these rates are proportional to the concentration of adsorbed surface species (Stumm et al., 1983; Wieland et al., 1988; Chaïrat, 2005). Such adsorbed species are presumed to weaken metal-oxygen bonds surrounding a metallic center (Furrer and Stumm, 1986). These concepts have been incorporated within the framework of Transition State Theory (TST) (Eyring, 1935) yielding (Helgeson, 1971, 1972; Helgeson et al., 1984; Lasaga, 1981; Wieland et al., 1988).

$$r+ = k\left[P_+^{\#}\right] \tag{1}$$

where r_+ is the dissolution rate, k the rate constant and $[P_+\#]$ is the concentration of the precursor complex. Due to their similar composition and structure it seems likely that the dissolution mechanism of rhyolitic glass is similar to that of basaltic glass. The dissolution mechanism of the basaltic glass was reported by Oelkers and Gíslason (2001) and the activated complex is represented by the silica tetrahedral linked to one of the aluminium sites replaced by hydrogen. Therefore the concentration of the activated complex can be determined with a law of mass action of the forming reaction given by:

$$n{>}Si\text{-}O\text{-}Al + 3H+ = n{>}Si\text{-}O\text{-}H3 \tag{2}$$

so the law of mass action implies:

$$K = \frac{a_{Al^{3+}}[> Si - O - H_3]^n}{a_{H^+}^3[> Si - O - Al]^n} \tag{3}$$

where K represents the equilibrium constant of reaction 2 and a_i is the activity of the i aqueous species. If the concentration of the activated complex is low equations 1 and 3 can be combined to:

$$r+ = kK^{1/n}\left(\frac{a_{H+}^3}{a_{Al^{3+}}}\right)^{1/n} = k'\left(\frac{a_{H+}^3}{a_{Al^{3+}}}\right)^{1/n} \quad (4)$$

The Eq. 4 describes the dissolution rates of the basaltic glass as a function of the composition of aqueous solutions at a constant temperature (Oelkers and Gíslason, 2001, Gíslason and Oelkers, 2003). The variation of rate constant can be described by an Arrhenius equation (Arrhenius, 1889):

$$k' = Ae^{-\left(\frac{E_A}{RT}\right)} \quad (5)$$

where A represent a constant, E_A stand for the activation energy, R refers to the gas constant and T signifies the absolute temperature. A combination of Eq. 4 and 5 gives an equation describing the dissolution of the basaltic glasses with respect to the temperature and aqueous solution composition:

$$r_+ = Ae^{-\left(\frac{E_A}{RT}\right)}\left(\frac{a_{H+}^3}{a_{Al^{3+}}}\right)^{1/n} \quad (6)$$

We will use the same formalism and equation to interpret the dissolution rate data of the rhyolitic glass. To apply the Eq. 6 we will determine the following parameters A, E_A and $1/n$. the degree to which Eq. 6 can describe accurately the dissolution rates of rhyolitic glass will be explicated below.

3. SAMPLE PREPARATION AND EXPERIMENTAL METHODS

The rhyolitic glass used in the experiments is volcanic ash collected from the 1362 eruption of the Öraefajökull, in south-eastern Iceland. The glass contains less than 1% quenched crystals. The chemical composition of the sample is given in table 1. It is close to the composition of mean rhyolite. The ash was dried, first at ambient temperature in the laboratory and then at 110°C overnight. The

specific surface area of the initial glass powder was measured using the BET method with nitrogen gas, the BET surface area of the glass powder being $0.43 cm^2.g^{-1}.10^{-4}$and the geometrical surface area being $324 cm^2.g^{-1}$. Glass powders were analyzed before and after dissolution experiments using a LEO 435 VP Scanning Electron Microscope (SEM) at the LMTG in Toulouse, France. SEM images of the glass powder before experiments are shown in Figure1. It can be seen in this figure that the initial rhyolitic glass grains are free of fine particles, and appear to have sharp edges on a micron scale.

All dissolution experiments were performed in titanium mixed-flow reactor systems (figure 2). Application of mixed-flow reactors to measure mineral dissolution rates have been described in detail by Dove and Crerar (1990), Berger et al. (1994a), and Oelkers and Schott (1995, 1999). A High Precision/High Pressure Liquid Chromatography Pump provided continuous fluid flow ranging from 0.9 to 10 g/min during the experiments. The precision of the fluid flow rates was ±4%. The volume of the titanium reactor was 300 mL. The solution within the reactor was stirred by a Parr magnetically driven stirrer, the temperature controlled by a Parr controlled furnace, and elevated pressure was maintained using a back pressure regulator. The temperature of individual experiments ranged from 25°C to 250°C, and pressure for experiments performed in excess of 100°C was kept slightly above the liquid-vapour curve of H_2O. The fluid left the reactor through a 1 µm titanium filter, quenched, and passed through the back pressure regulator to the outlet, where it was sampled. The pH of the outlet solutions was then measured with a 713 Metrohm pH meter coupled to a Mettler Toledo Inlab® 422.

Each experimental series consisted of several different experiments performed on a single rhyolitic glass powder. A list of the sequence of conditions performed during each series is listed in Table 2. At the beginning of each experimental series the reactor was dismantled at ambient conditions. A specific mass of dry glass powder was placed in the reactor. The reactor was filled with the starting solution, closed, and placed in the furnace. The temperature, pressure, flow and stirring rate were adjusted to desired settings. Fluid flow rate and outlet solution composition were measured regularly. When steady-state conditions were confirmed for any experimental condition, the inlet solution composition, temperature, pressure, and/or fluid flow rate were changed to the next desired setting.

The inlet solutions used in this study were comprised of demineralised H_2O plus sufficient quantities of reagent grade HCl, NH_4Cl, and/or NH_3 to obtain a 0.01 mol/kg ionic strength solution of the desired pH at 25°C. Compositions of all inlet solutions are listed in Table 2. The aqueous silica concentration of all inlet and outlet solutions were measured using the molybdate blue method of Fishman and Friedman (1989) with Varyan Spectrophotometer using 1 and 5cm flow cells. All standards and blanks were obtained using the experimental inlet solutions as diluents. The precision of the aqueous Si concentration measurements was within 3% for concentrations above 50 g/kg Si, but close to 10% for the 50–10 µg/kg Si concentration. These subsamples were acidified with concentrated suprapure HNO_3 before analysis. The aluminium concentration was determined by atomic absorption at the Lara-Europe Analyses laboratory in Toulouse, and by the catechol violet (Dougan and Wilson, 1974).

4. EXPERIMENTAL RESULTS AND DISCUSSION

For each input fluid composition and flow rate, the reaction was allowed to proceed until the output fluid composition attained a steady-state. These steady-state fluid compositions were used to calculate rhyolitic glass dissolution rates using:

$$r_+ = \left(\frac{q([i]_o - [i]_i)}{Sm\nu_i} \right) \tag{8}$$

where q designates the flow rate, $[i]_i$ and $[i]_o$ refer to the concentration of the element i in the outlet and inlet solution respectively, S denotes the specific surface of the glass, m represents the mass of glass in the reactor and ν_i signifies the stoichiometric coefficient of i in the glass normalised to one mole of silica. Input and output fluid compositions, flow rates, computed steady state dissolution rates and chemical affinities with respect to diaspore for all experiments are listed in Table 2.

The stoichiometry of these dissolution experiments at steady-state can be assessed with the aid of Fig.3, where the outlet Al concentration is plotted as a function of the corresponding outlet Si concentration. The line in this figure has a slope of 0.16, which represent the Al to Si ratio in the dissolving rhyolitic glass. Glass dissolution is close to stoichiometric for those experiments that were undersaturated with respect to diaspore. In contrast outlet solutions that were supersaturated with respect to diaspore were relatively depleted in Al suggesting diaspore precipitation. To assess the degree to which rhyolite dissolution is consistent with Eqn.4 and the mechanism described above the logarithm of measured 80°C rates have been plotted as a function of (a^3_{H+}/a_{Al}^{3+}). The data points in this figure exhibit a linear trend consistent with Eqn.4. The slope of this linear trend is consistent with n= 0.18. This value is similar to that proposed by Wolff-Boenisch et al. (2004b) based on the variation of rhyolite dissolution rates as a function of aqueous fluoride concentration a t pH 4.

The variation of 80°C rates as a function of pH is illustrated in Fig.5. Rates exhibit a characteristic synclinal form, decreasing with increasing pH at acid conditions and increasing with increasing pH at basic conditions. This behaviour as been observed for the dissolution of numerous aluminosilicate minerals and glasses (Wolff-Boenish et al., 2003) and can be attributed, within the dissolution mechanism described above, to the effect of pH on the aqueous activity ratio (a^3_{H+}/a_{Al}^{3+}). (Oelkers and Gíslason, 2001).

An Arrhenius plot of rates measured at pH 2 is shown on Fig.6. The linear fit shown in the figure is consistent with EA= 73.3 kJ.mol^{-1}. This activation energy is similar to that found for other aluminosilicates glasses and minerals (Crovisier, 1985; Crovisier et al., 1990 ; Gíslason and Eugster, 1987; Guy, 1989; Guy and Schott, 1989; Berger et al. 1994 ; Grambow et al., 1985 ; Daux et al., 1997 ; Guy et al.,1997) suggesting a similar dissolution mechanism for these phases.

Taking account of the distribution of points shown in Fig.4. and 6. it seems likely that rhyolite steady state dissolution rates can be described as a function of temperature and solution composition using Eqn.6. A regression of the rate data in Table 2 with Eqn.6. yields:

$$r_+ = 0{,}031.\exp\left(\frac{-73{,}3}{RT}\right).\left[\frac{a_{H^+}^3}{a_{Al}^{3+}}\right]^{0.18} \quad (9)$$

The degree to which Eqn.9. describes the rate data obtained in the present study can be assessed with Fig.7. 32 of the 40 measured rates are within ±1 log units of those calculated using Eqn.9.

The evolution of the weathering rate for basaltic and rhyolitic glass as well as obsidian with the inverse of temperature is shown in Fig. 8. The rates obtained on this study are demonstrated to be consistent with the literature data as the points aligns for all experiments with rhyolitic glass. The logarithm of the rate for the three types of glass decreases with temperature. This decrease is not constant for the whole scale for obsidian, around 100°C a break of the slope show a variation in the dissolution mechanism. Our data consistently with the rhyolitic rates in the literature do not show such behaviour. Rhyolitic glass and basaltic glass dissolution behaviour are similar and demonstrate that the same dissolution mechanism applies for both glasses.

5. Experimental uncertainties.

Uncertainties associated with the rates generated in this study arise from a variety of sources, including the measurement of aqueous solution concentrations, fluid flow rates, and glass surface areas. The uncertainties in the measured values of the total aqueous silica and aluminium concentration are on the order of ±10% or less. Computational and experimental uncertainties on the pH measured are on the order of ±0.1 pH units. Uncertainties in fluid flow rate measurements are not more than 4%. In contrast, uncertainties associated with the measurement of the surface area of the initial rhyolitic glass powder are ±10%. If uncertainties were estimated exclusively from the sum of these contributions, an overall uncertainty of the dissolution rates reported in this would be on the order of 20%. Although this estimate appears to be consistent with the rates obtained from a single

steady state, it is substantially less than the apparent scatter among the rates obtained from different steady-state conditions as depicted in Fig. 8. This discrepancy possibly stems from an evolution of basaltic glass reactive surface area during the course of the experiments. As emphasized by Gautier et al. (2001), the degree to which reactive surface area varies in response to BET surface area changes is currently impossible to define unambiguously. Consequently, overall uncertainties associated with the rates reported in the present study are unclear. Consideration of the scatter in the Fig. 7 suggests that the overall uncertainty on the rhyolitic glass dissolution rates measured in the present study to be on the order of ±0.4 log units.

6. CONCLUSION

The results presented above allow estimates of the role of rhyolitic glass dissolution in a variety of natural processes including chemical weathering and hydrothermal alteration. The major conclusions of this study include.

1) The dissolution of rhyolite is stoichiometric.

2) A general equation can be used to predict the dissolution rate of rhyolitic glass:

$$r_+ = 0{,}031.\exp\left(\frac{-73{,}3}{RT}\right).\left[\frac{a_{H^+}^3}{a_{Al}^{3+}}\right]^{0.18}$$

3) The dissolution behaviour of rhyolitic glass is consistent with that of basaltic glass; both are apparently proportional to the activity ratio $[a_{3H+}/a_{Al}^{3+}]$. This proportionality allows prediction of the effect of aqueous solution composition and rhyolitic glass dissolution rate.

4) The same dissolution mechanism applies for the two most extreme types of natural volcanic glass. Therefore it is conceivable to develop a general rate equation for the dissolution of natural glasses.

Figure list and caption:

Figure1: SEM of the glass, figures 1a and c represent the glass shards before experiment, 1b and 1d denotes the shards after 1 week at pH3 and 80°C, 1b in particular shows detail of the roundness of the edges of the shards as well as secondary precipitation.

Figure2: Scheme of a Parr^{TM} reactor after Gautier et al. (1994).

Figure3: Outlet concentration of Al plotted against the respective Si concentration, the data point supersaturated with respect to diaspore are marked by hollow diamonds.

Figure4: Plot of the dissolution rate versus the logarithm of the ration of Al^{3+} and H^{+} activities at 80°C and pH2.

Figure5: Arrhenius plot of rates measured at pH 2.

Figure6: logarithm of the dissolution rate plotted against the pH at 80°C.

Figure7: Comparison of the dissolution rate calculated using Eqn. 6 and the rates determined from the experiment.

Figure8: Dissolution rate of natural glasses, square symbols represents basaltic glass while the diamonds represents the rhyolitic glass.

References:

Allnatt, A.R., Bancroft, G.M., Fyfe, W.S, Jacobs, P.W.M, Karkhanis, S.N., Melling, P.J., Nishijima, A., Vempati, C.S., Tait, J., 1983. Leaching behaviour and electrical conductivity of natural rhyolite and modified synthetic rhyolites. Chemical Geology, Vol.38, Issues 3-4, pp.329-357

Arrhenius, S., 1889. Über die Reaktionsgeschwindigkeit bei der Inversion von Rohzucker durch Säuren, *Zeitschrift für physikalische Chemie* 4, pp. 226–248.

Berger, G., Schott, J., Guy, C., 1994. Dissolution rate of basaltic glass in silica-rich solutions: implications fort he long-term alteration. Geochimica et Cosmochimica Acta, 22, pp. 4875-4886.

Berner, U.R., 1992. Evolution of pore water chemistry during degradation of cement in a radioactive waste repository environment, Waste Management, Vol.12, Issues 2-3, pp. 201-219.

Bourcier, W.L., 1989. Improvements in the solid solution modelling capabilities of the EQ3/6 geochemical code. , Lawrence Livermore National Laboratory, Livermore, California UCID-20587 .

Brady, Gíslason, S.R., 1997. Seafloor weathering controls on atmospheric CO2 and global climate. Geochimica et Cosmochimica Acta, 61, pp.965-973.

Carey, S. N., 1997. Influence of convective sedimentation on the formation of widespread tephra layers in deep sea. Geology, 25, pp. 839-842.

Chaïrat, C., 2005. (Thèse) Etude expérimentale de la cinétique et des mécanismes d'altération des minéraux apatitiques.

Chester, D.K., Degg, M., Duncan, A.M., Guest, J.E., 2000. The increasing exposure of cities to the effects of volcanic eruptions: a global survey Global Environmental Change Part B: Environmental Hazards, Vol.2, Issue 3, pp. 89-103.

Crovisier, J.L., Dissolution du verre basaltique dans l'eau de mer: approche expérimentale et thermodynamique, Doctorat d'Université, Université Louis Pasteur, Strasbourg, 1985, p. 178

Crovisier, J.L., Atassi, H., Daux, V., Eberhart, J.P., 1990. Hydrolyse d'un verre basaltique tholéitique à 60 °C, Dissolution sélective puis congruente par élévation du pH, Comptes Rendus-Académie des Sciences, Série II: sciences de la Terre et des Planètes, vol. 310, p. 941

Daux, V., Guy, C., Advocat, T., Crovisier J.L., Stille P., 1997. Kinetic aspect of basaltic glass dissolution at 90°C : role of aqueous silicon and aluminium. *Chemical Geology*, 142, pp. 109-126.

Dessert, C., Dupré, B., François, L.M, Schott, J., Gaillardet, J., Chakrapani, G., Bajpai, S., 2001. Erosion of Deccan Traps determined by river geochemistry. Impact on global climate and 87Sr/86Sr ratio of seawater, Earth Planet. Sci. Lett. 188, pp. 459–474

Dickin, A.P., 1981. Hydrothermal leaching of rhyolite glass in the environment has implication for nuclear waste disposal. Nature, 294, pp. 342-347.

Dougan, WK and Wilson, AC, 1974. The absorptiometric determination of aluminium in water. A comparison of some chromogenic reagents and the development of an improved method. Analyst, 99, pp. 413–430

Dove, P.M., Crerar, D.A., 1990. Kinetics of quartz dissolution in electrolyte solutions using a hydrothermal mixed flow reactor. *Geochimica et Cosmochimica Acta*, 54, pp. 955969.

Dran, J.-C., Petit, J.-C., Brousse, C., 1986. Mechanism of aqueous dissolution of silicate glasses yielded by fission tracks, *Nature* **319**, pp. 485–487.

Dran, J.-C., Della Mea, G., Paccagnella, A., Petit, J.-C., Trotignon, L., 1988. The aqueous dissolution of alkali silicate glasses: reappraisal of mechanisms by H and Na depth profiling with high energy ion beams, *Phys. Chem. Glasses* **29**, pp. 249–255.

Dran, J.C., Mea, G.D., Paccagnella, A. and Petit, J.C., 1988. Aqueous dissolution of alkali-silicate glasses: reappraisal of mechanisms by H and Na depth profiling with high energy ion beams. Phys. Chem. Glasses 29,249-255.

Eyring, H., 1935. The activated complex in chemical reactions *, J. Chem. Phys*., 3, pp. 107-115.

Fiore, S., Huertas, F.J., Tazaki, K., Huertas, F., Linares, J., A low temperature experimental alteration of a rhyolitic obsidian, *European Journal of Mineralogy* 11 (1999), pp. 455–469.

Fishman, M.J. and L.C. Friedman. 1989. Methods for determination of inorganic substances in water and fluvial sediments. U.S. Geological Survey Techniques of Water-Resources Investigations, Book 5, chap. A1, 545 p.

Furrer, G., Stumm, W., The coordination chemistry of weathering: I. Dissolution kinetics of δ-Al_2O_3 and BeO, *Geochimica et Cosmochimica Acta* **50** (1986), pp. 1847–1860.

Gauthier, J.M., Oelkers, E.H., and Schott, J., 1994; Experimental study of K-Feldspar dissolution rate as a function of chemical affinity at 150°C and pH9. Geochimica et Cosmochimica Acta. 58, 4549-4560.

Gíslason and H.P. Eugster. Geochim. Cosmochim. Acta **51** 10 (1987), p. 2827

Gíslason, S. R., Arnórsson, S., Armannsson, H., 1996. Chemical weathering of basalt in SW Iceland: Effects of runoff, age of rocks, and vegetative/glacial cover. American Journal of Science, 296, pp. 837-907.

Gíslason, S. R., Oelkers, E. H., 2003. The mechanism, rate and consequence of basaltic glass dissolution: II. An experimental study of the dissolution rates of basalts as a function of pH at temperatures from 6°C to 150°C. Geochimica and Cosmochimica Acta, 67, pp. 3817-3832.

Grambow, B., Jercinovic, M.J., Ewing, R.C., Byers, C.D., Materials Research Society Conference Proceedings, Scientific Basis for Nuclear Waste Management, IX, vol. 50, 1985, p. 263

Guy, C., Mécanismes de dissolution des solides dans les solutions hydrothermales déduits du comportement de verres basaltiques et de calcites déformées, Thèse de Doctorat de l'Université Paul Sabatier, Toulouse, 1989, p. 188.

Guy, C., Schott, J., 1989. Multisite surface reaction versus transport control during the hydrolysis of a complex oxyde. *Chemical Geology* **78**, pp. 181-204.

Eiríksson, H., van Krefeld, S., van Krefeld, J., 2000. The tephrochronology of Iceland and the North Atlantic region during the Middle and Late Quaternary: a review. *Journal of Quaternary Science* **15**, pp. 3–22.

Helgeson, H.C., 1972. Kinetics of mass transfer among silicates and aqueous solutions, *Geochimica et Cosmochimica Acta* **35**, 5, pp. 421-469.

Helgeson, H.C., 1972. Kinetics of mass transfer among silicates and aqueous solutions: Correction and clarification, *Geochimica et Cosmochimica Acta* **36**, 9, pp. 1067-1070.

Helgeson, H.C., Murphy, W.M., Aagaard, P., 1984. Thermodynamic and kinetic constraints on reaction rates among minerals and aqueous solution. *Geochim. Cosmochim. Acta* **48**, pp. 2405–2432

Holland, H.D., 1978. *The Chemistry of the Atmosphere and Oceans*, Wiley.

Kharkansis, S.N., Bancroft, G.M., Fyfe, W.S. and Brown, J.D., 1980. Leaching behaviour of rhyolite glass. *Nature*, **284**, 435-437.

Kump, L. R., Brantley, S. L., Arthur, M. A., 2000. Chemical weathering, atmospheric CO2, and climate. *Annual Review Earth and Planetary Science* **28**, pp. 611-667.

Lacasse, C., van den Bogaard, P., 2002. Enhanced airborne dispersal of silicic tephras during the onset of northern hemisphere glaciation, from 6 to 0 Ma records of explosive volcanism and climate change in subpolar North Atlantic. Geology, 30, pp. 623-626

Larsen, G., Newton, A.J., Dugmore, A.J., Vilmundardottir, E.G., 2001. Geochemistry, dispersal, volumes and chronology of Holocene silicic tephra layers from the Katla volcanic system, Iceland, J. Quat. Sci. 16 (2001), pp. 119–132.

Lasaga, A.C., 1981; Transition state theory. In Lasaga A.C., Kirkpatrick R.J., (eds) Kinetics of Geochemical Processes. Rev. Mineral.

Louvat, P., 1997; Present denudation rates on the island of Réunion determined by river geochemistry: Basalt weathering and mass budget between chemical and mechanical erosions. *Geochimica et Cosmochimica Acta*, Volume 61, Issue 17, pp. 3645-3669

Magonthier, M.-C., Petit, J.-C., Dran, J.-C., Rhyolitic glasses as natural analogues of nuclear waste glasses: behaviour of an Icelandic glass upon natural aqueous corrosion, *Applied Geochemistry*, **7**, 1 (1992), pp. 83-93,

Mazer, J.J. and Walther, J.V., 1994. Dissolution kinetics of silica glass as a function of pH between 40 and 85°C. *J. Non-Cryst. Solids* **170**, pp. 32–45.

Metz, V., Ganor, J., 2001. Stirring effect on kaolinite dissolution rate. Geochimica and Cosmochimica Acta, Vol. 65, No 20, 3475-3490.

Morgan, N.A., Spera, F.J., 2001. Glass transition, structural relaxation, and theories of viscosity. A molecular dynamics study of amorphous CaAl2Si2O8, Geochim. Cosmochim. Acta 65, pp. 4019–4041.

Moulton, K.L., West J., Berner, R.A., 2000. Solute flux and mineral mass balance approaches to the quantification of plant effects on silicate weathering. *American Journal of Science* **300**, pp. 539–570.

Mungall, J.E., Martin, R.F., 1994. Severe leaching of trachytic glass without devitrification, Terceira, Azores Geochimica et Cosmochimica Acta, Vol. 58, Issue 1, pp. 75-83.

Murphy, W.M., Helgeson, H.C., 1987. Thermodynamic and kinetic constraints on reaction rates among minerals and aqueous solutions. III. Activated complexes and the pH-dependence of the rates of feldspar, pyroxene, wollastonite, and olivine hydrolysis Geochimica et Cosmochimica Acta, Volume 51, Issue 12, pp. 3137-3153.

Oelkers E. H. and Gíslason S. R., 2001. The mechanism, rates, and consequences of basaltic glass dissolution: I. An experimental study of the dissolution rates of basaltic glass as a function of aqueous Al, Si, and oxalic acid concentration at 25°C and pH = 3 and 11. Geochimica and Cosmochimica Acta, Vol. 65, No 21, pp. 3703-3719.

Oelkers, E.H., Schott, J., 1995. Experimental study of anorthite dissolution and the relative mechanism of feldspar hydrolysis. Geochimica et Cosmochimica Acta, Vol.59, Issue 24, pp.5039-5053

Oelkers, E.H., Schott, J., 1999. Experimental study of kyanite dissolution rates as a function of chemical affinity and solution composition. Geochimica et Cosmochimica Acta, Vol. 63, Issue 6, pp. 785-797.

Parkhurst, D.L., Appelo, C.A.J., 1999. User's guide to PHREEQC (Version 2) — A computer program for speciation, batch-reaction, one-dimensional transport, and inverse geochemical calculations, U. S. G. S. Wat. Res. Inv. Report, pp. 99-4259.

Petit, J. C., 1992. Natural analogues for the design and performance assessment of nuclear radioactive waste form: a review. Journal of chemical exploration, 46, pp. 1-33.

Riley, J.P. and Chester, R., *Introduction to Marine Chemistry* Academic Press (1971).

Spivack, A.J., Staudigel, H., 1994. Low-temperature alteration of the upper oceanic crust and the alkalinity budget of seawater, Chem. Geol. 115, pp. 239–247.

A. Stefansson and S.R. Gíslason, Chemical weathering of basalts, Southwest Iceland: Effect of rock crystallinity and secondary minerals on chemical fluxes to the ocean, *Am. J. Sci.* **301** (2001), pp. 513–556.

Stumm, W., 1992. Chemistry of the Solid Water Interface; John Wiley and Sons: New York.

Techer, I., 1999. (Thèse de doctorat, Montpellier II) Apports des analogues naturels vitreux à la validation des codes de prédiction du comportement à long terme des verres nucléaires.

Techer, I., Advocat, T., Lancelot, J., Liotard, J.M., 2001. Dissolution kinetics of basaltic glasses Control by solution chemistry and protective effect of the alteration film, Chem. Geol. 176, pp. 235–263.

Thompson, D.W. and Pownall, P.G., Surface electrical properties of calcite. *J. Colloid Interface Sci.* **131** (1989), pp. 74–82.

Urey, H.C., 1952. The origin and development of the earth and other terrestrial planets: A correction Geochimica et Cosmochimica Acta, Volume 2, Issues 5-6, 1952, Pp.263-268

White, A.F., Claassen, H.C., 1980. Kinetic model for the short-term dissolution of a rhyolitic glass Chemical Geology, Vol. 28, pp. 91-109.

White, A.F., 1983. Surface chemistry and dissolution kinetics of glassy rocks at 25°C. Geochimica et Cosmochimica Acta, Volume 47, Issue 4, pp. 805-815.

Wieland, E., Wehrli, B., Stumm, W., 1988. The coordination chemistry of weathering: III. A generalization on the dissolution rates of minerals. Geochimica et Cosmochimica Acta, Volume 52, Issue 8, pp. 1969-1981.

Wolff-Boenish, D., Gíslason, S. R., Oelkers, E. H., Putnis, C. V. 2003. The dissolution rates of natural glasses as a function of their composition at pH 4 and 10.6 and temperatures from 25 to 74°C. Geochimica and Cosmochimica Acta, Vol. 68, No 23, pp. 4843-4858.

Figures and tables.

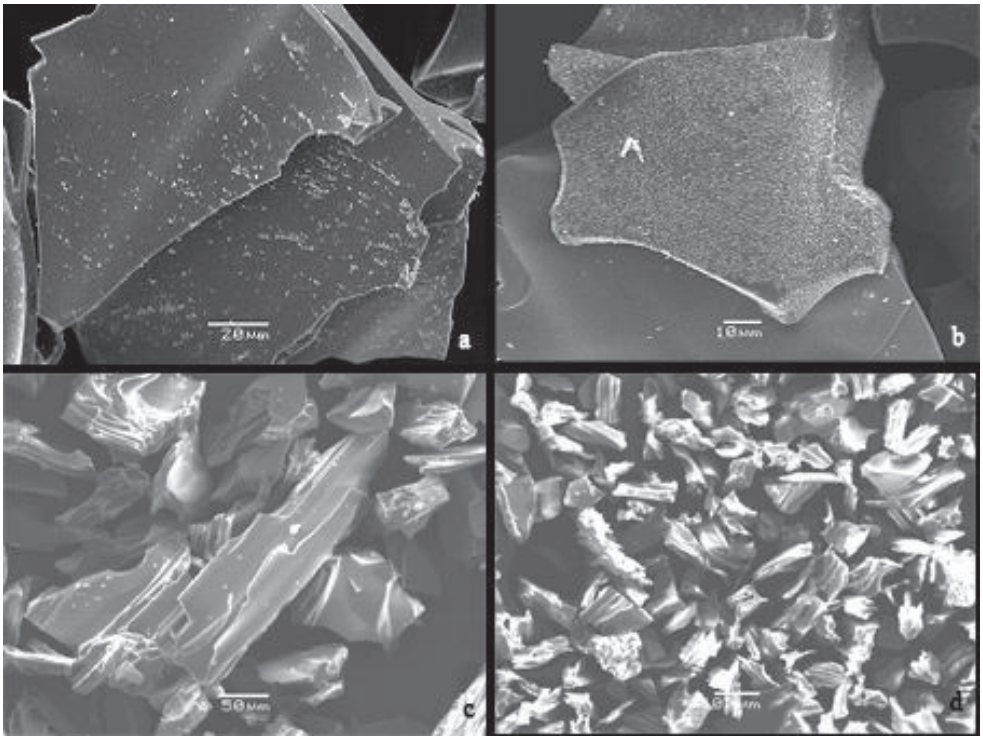

Figure 1: SEM of the glass, figures 1a and c represent the glass shards before experiment, 1b and 1d denotes the shards after 1 week at pH3 and 80°C, 1b in particular shows detail of the roundness of the edges of the shards as well as secondary precipitation.

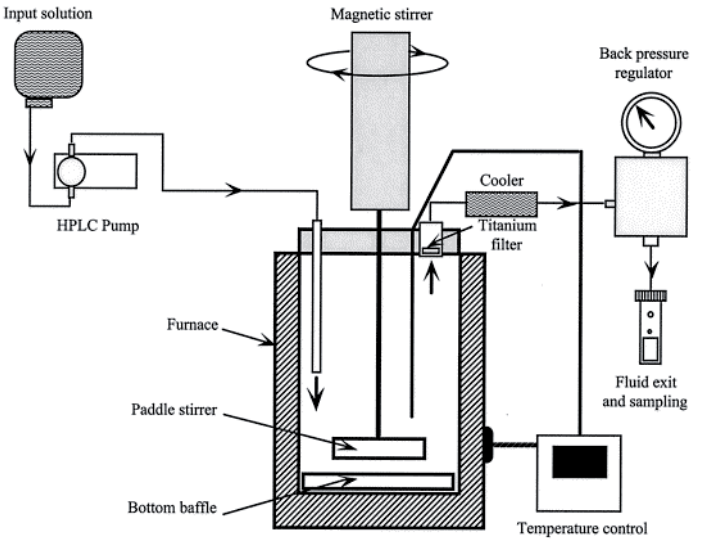

Figure2: Scheme of a Parr™ reactor after Gautier et al. (1994).

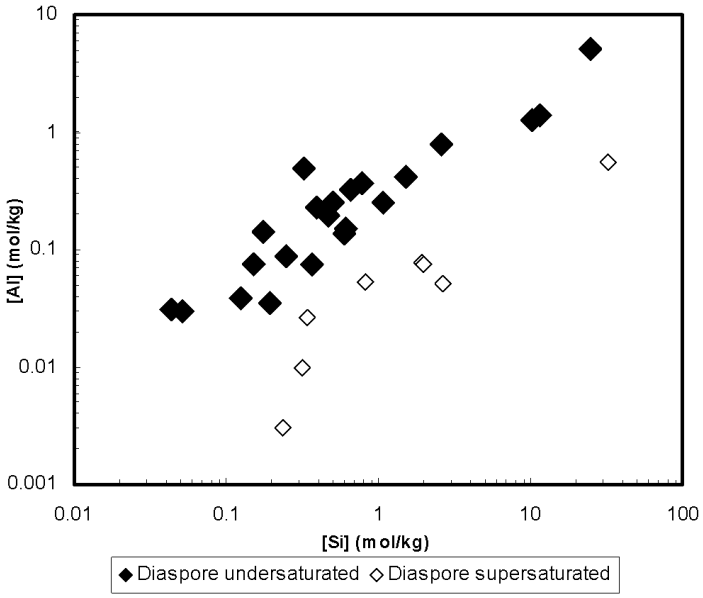

Figure3: Outlet concentration of Al plotted against the respective Si concentration, the data point supersaturated with respect to diaspore are marked by hollow diamonds.

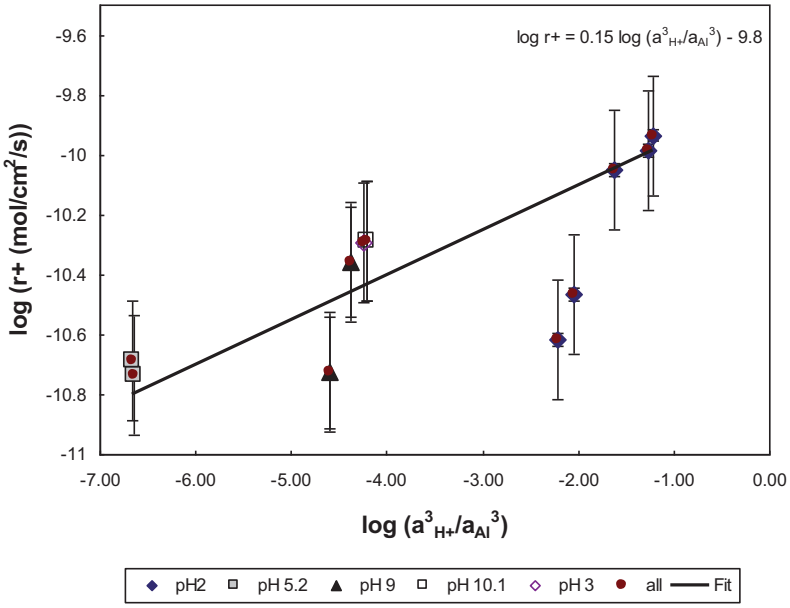

Figure4: Plot of the dissolution rate versus the logarithm of the ration of Al^{3+} and H^{+} activities at 80°C and pH2.

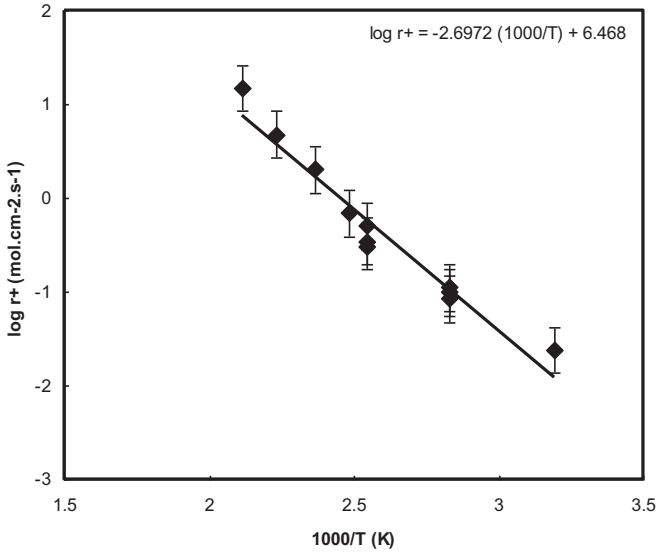

Figure5: Arrhenius plot of rates measured at pH 2

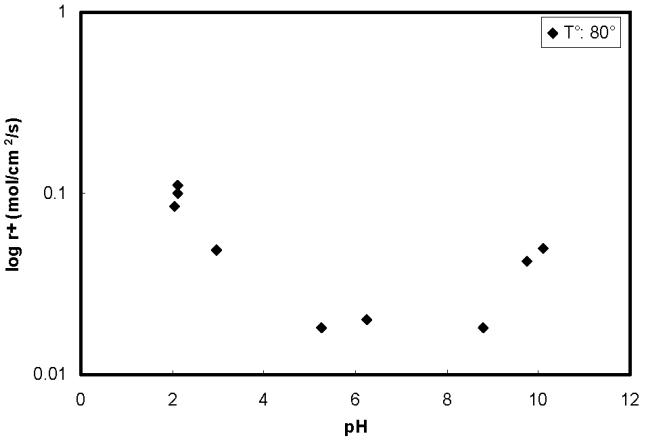

Figure6: logarithm of the dissolution rate plotted against the pH at 80°C.

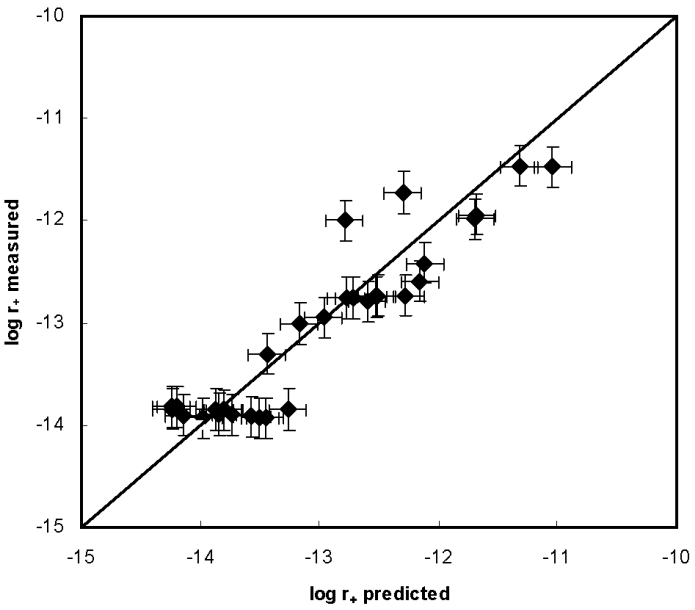

Figure7: Comparison of the dissolution rate calculated using Eqn. 6 and the rates determined from the experiment.

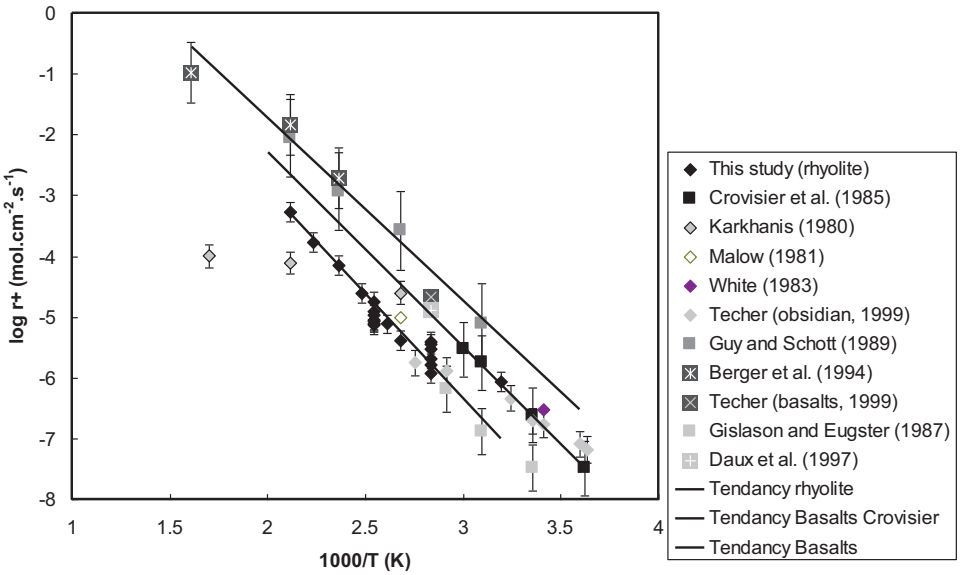

Figure8: dissolution rate of natural glasses, square symbols represents basaltic glass while the diamonds represents the rhyolitic glass.

Table 1: Composition of the rhyolitic glass measured by XRF.

SiO_2	TiO_2	Al_2O_3	Fe_2O_3	FeO	MnO	MgO	CaO	Na_2O	K_2O	P_2O_5
70,6	0,24	13	2,4	1,18	0,1	0,02	0,97	5,45	3,41	0,02

Table 2: dissolution rates obtained for every stable state achieved during the study.

Exp	**T°** (°C)	**pH**	**m** (g)	**Flux** (g/min)	**[Si]** in[a]	**[Al]** out[a]	**[Si]** inlet[a]	**[Al]** outlet[a]	**Δ**[Al]/ **Δ**[Si] [b]	**r_+** x 10^{12} [c]	**Affinity** **Diaspore**	**log** **(a^3_{H+}/a^3_{Al})**	**log r** predicted
G9	200	2.1	2	7.00	0	0	32.065	0.548	0.017	14.845	2.36	-6.00	-11.00
RG2-19	175	2.12	0.424	2.48	0	0	11.660	1.414	0.121	9.019	2.06	-1.90	-10.82
F8	175	2.11	2	7.00	0	0	10.359	1.280	0.124	4.796	1.89	-2.23	-10.87
A31	150	1.97	2	0.10	0	0	24.508	5.209	0.213	0.162	2.11	-2.20	-11.40
RG2-13	150	2.06	0.424	2.48	0	0	2.609	0.791	0.303	2.019	-14.09	-2.90	-11.51
K4	150	3.2	1.18	7.00	0	0	2.670	0.051	0.019	2.095	4.78	-5.27	-11.89
E7	130	2.03	2	7.00	0	0	1.506	0.416	0.276	0.697	-10.96	-0.37	-11.58
J6	130	3.18	0.986	7.00	0	0	0.821	0.053	0.065	0.771	-19.60	-5.14	-12.34
RG2-24	120	2.12	0.424	2.47	0	0	0.328	0.489	1.491	0.253	-35.97	-0.86	-11.91
RG1-26	120	2.1	0.431	2.48	0	0	0.661	0.325	0.492	0.503	-37.17	-2.24	-12.13
RG2-7	120	2.06	0.424	2.48	0	0	0.394	0.226	0.574	0.305	-38.30	-2.08	-12.11
RG4-8	120	2	0.505	2.50	0	5	0.340	6.325	18.603	0.223	-29.27	-	-
RG6-3	120	2.02	0.505	2.50	0	1	0.526	1.755	3.337	0.345	-10.69	-	-
RG3-9	120	2	0.454	2.60	0	1	0.312	1.555	4.984	0.236	-32.66	-	-
RG5-3	120	2.01	0.492	2.63	0	10	0.295	6.421	21.766	0.209	-29.27	-	-
E-06-10	120	3.62	0.68	0.50	0	0	1.926	0.078	0.040	0.187	-41.69	-1.48	-12.01
E-06-12	120	3.62	0.68	0.50	0	0	1.981	0.076	0.038	0.193	-41.76	-1.47	-12.01
E-06-2	120	1.9	0.68	0.50	0	0	1.083	0.248	0.229	0.527	-38.00	-1.97	-12.09
E-06-4	120	2.37	0.68	0.50	0	0	0.613	0.152	0.248	0.298	-39.58	-1.76	-12.06
E-06-6	120	2.35	0.68	0.50	0	0	0.603	0.137	0.227	0.293	-39.88	-1.72	-12.05
E-06-8	120	2.89	0.68	0.50	0	0	0.616	0.149	0.242	0.300	-39.58	-1.75	-12.06
C7	110	2.11	2	7.00	0	0	0.465	0.193	0.415	0.215	-37.84	-1.89	-12.35
I8	110	3	0.986	7.00	0	0	0.362	0.075	0.207	0.340	-17.60	-4.36	-12.74
RG1-18	100	2.04	0.431	2.48	0	0	0.152	0.076	0.502	0.115	-39.64	-1.52	-12.57
P II7	80	2.03	1.16	0.50	0	0	0.788	0.370	0.470	0.045	-33.05	-2.21	-13.29

PI4	80	1.98	1.16	1.00	0	0	0.509	0.248	0.487	0.058	-34.13	-2.05	-13.27
B6	80	2.1	2	2.00	0	0	0.175	0.142	0.811	0.023	-35.69	-1.82	-13.23
RG1-10	80	2.02	0.431	2.43	0	0	0.044	0.031	0.705	0.033	-40.15	-1.17	-13.13
P V 2	80	2.13	1.16	3.00	0	0	0.250	0.089	0.356	0.085	-37.04	-1.62	-13.20
P IV 6	80	2.12	1.16	5.00	0	0	0.195	0.035	0.179	0.111	-39.74	-1.22	-13.13
PIII4	80	2.05	1.16	7.00	0	0	0.124	0.039	0.314	0.099	-39.47	-1.27	-13.14
H8	80	2.97	0.986	7.00	0	0	0.052	0.030	0.577	0.049	-18.79	-4.25	-13.62
Q2	80	5.26	0.89	0.50	0	0	0.236	0.003	0.013	0.018	16.83	-6.64	-14.00
P7	80	6.24	1.06	0.50	0	0	0.315	0.010	0.032	0.020	22.44	-6.66	-14.00
O7	80	8.8	1.24	0.50	0	0	0.337	0.026	0.077	0.018	15.88	-4.60	-13.67
N7	80	9.75	1.02	0.50	0	0	0.648	0.146	0.225	0.042	14.53	-4.39	-13.64
M4	80	10.1	1.08	0.50	0	0	0.810	0.247	0.305	0.050	13.38	-4.22	-13.61
L7	80	10.4	1.18	0.50	0	0	3.045	0.908	0.298	0.171	15.61	-4.54	-13.67
D7	40	2.06	2	7.00	0	0	0.051	0.010	0.196	0.024	-38.48	-	-

Paper 3: The reactivity of hydrothermally synthesized dawsonite H. Hellevang, J. Declercq, B. Kvamme, P. Aagaard, submitted to Applied Geochemistry.

H. Hellevang[a,*], J. Declercq[a], B. Kvamme[b], P. Aagaard[a]

[a]Department of Geosciences, University of Oslo, Pb. 1047, Blindern, Oslo, Norway

[b]Department of Physics and Technology, University of Bergen, Allégaten 44, 5007 Bergen, Norway

Abstract

Occurrences of the mineral dawsonite ($NaAl(OH)_2CO_3$) after natural CO_2 accumulations support that the mineral may contribute to long-term storage of CO_2 in geological formations. Knowledge about the reactivity of dawsonite is crucial to better understand its role as a CO_2 storage host. We present free-drift batch dissolution rate experiments done at 22 and 77°C performed on synthesized dawsonite. The experiments suggest that the dissolution rates at pH 0.9 to 4.8 can be expressed by two parallel mechanisms according to $r_+ = k_1 \cdot \mathbf{a}_{H^+} + k_2$, where $\mathbf{a}_{H^+}$ denotes the proton activity. An overall rate equation expressing both the far-from-equilibrium proton promoted and hydration promoted dissolution rates from highly acidic to circumneutral conditions is given by:

$$r_+ = S\left\{10^{3.43}\mathbf{a}_{H^+}\exp\left(\frac{-44600}{RT}\right) + 10^{5.26}\exp\left(\frac{-80600}{RT}\right)\right\}$$

where S is reactive surface area, T is absolute temperature and R is the gas constant. Because the apparent activation energy for the proton promoted dawsonite dissolution rate is identical within experimental uncertainty to the calcite and magnesite activation energies, we propose that the $>CO_3H^0$ surface complex which is suggested responsible for the calcite and magnesite rates are also responsible for the dawsonite dissolution rates. The high apparent activation energy for the hydration-dominated pH region is however very different compared to the other carbonates.

Keywords: dawsonite, CO_2 storage, hydrothermal synthesis, surface complex, dissolution mechanism, reaction rate

*Corresponding author.

E-mail address: helge.hellevang@geo.uio.no (H. Hellevang)

Telephone: +47 228 57026

Fax: +47 228 54215

1. Introduction

Increasing rates of CO_2 emissions to the atmosphere may contribute to a global temperature rise of our planet. One way to reduce emission rates is to capture CO_2 from large anthropogenic point sources and inject the carbon into underground geological aquifers (Holloway, 1997; Bouchard and Delaytermoz, 2004; Gale, 2004). To understand the temporal and spatial behaviour of CO_2 as it is stored underground for hundreds to thousands of years, it is important to gain knowledge on the interactions between CO_2 and reservoir rocks. The mineral dawsonite ($NaAl(OH)_2CO_3$) has been suggested to play a significant role as a CO_2 storage host in saline alkaline aqueous solutions with a moderate to high CO_2 pressure (Worden, 2006). Dawsonite is reported to be abundant in natural reservoirs that are currently at a high CO_2 pressure, or that have previously experienced an influx of CO_2 (Smith and Milton, 1966; Baker et al., 1995; Moore et al., 2005; Worden, 2006; Golab et al., 2006; 2007). In such settings feldspars are typically replaced by dawsonite and/or kaolinite and silica (e.g., Moore et al., 2005; Worden, 2006). Numerical simulations of a variety of reservoir mineralogies over hundreds to thousands of years suggest that dawsonite may form either an intermediate phase stable only in a narrow chemical window, or a phase that is stable throughout the simulated time (e.g., Harrison and Wendlandt, 1995; Johnson et al., 2004; Zerai et al., 2005; Knauss et al., 2005; Xu et al., 2007). The scarcity of dawsonite observed in natural CO_2 accumulations may however indicate that numerical simulations overrate the formation of dawsonite. As the thermodynamic stability of dawsonite is well known through the data reported by Ferrante et al. (1976) and recently confirmed by Benezeth et al. (2007), it may be that dawsonite formation is prevented by constraints on the reaction rates. Although

some data on the reaction rate of dawsonite has been reported by Hellevang et al. (2005), calculations up to present on the potential of carbonate storage during CO_2 sequestration have employed reaction rates of dawsonite based on proxy minerals like siderite (Xu et al., 2005; Gherardi et al., 2007; Zhang et al., 2009), calcite (White et al., 2005), or rates that are intermediate between calcite and magnesite (Johnson et al., 2001; 2004; Gaus et al., 2003; Knauss et al., 2005; André et al., 2007; Cantucci et al., 2009). This includes using proxy values for reaction rate coefficients, apparent activation energies, and pH dependencies. The rates reported in Hellevang et al. (2005) cover only a limited range of chemical and physical conditions as the experiments were constrained by the small amount of natural dawsonite available. The report suggests that the dissolution rates are pH-independent from pH 3.5 to 8.6 and places dawsonite among the slower-reacting carbonates with a 80°C rate of 1.58×10^{-9} moles/m^2s (Hellevang et al., 2005). No activation energy or suggestions of reaction mechanisms were reported. The limited reaction rate data available today thus call for more comprehensive studies. As carbonates commonly show apparent dependencies on pH outside the circumneutral pH region (e.g., Pokrovsky et al., 2009; Golubev et al., 2009) we chose to expand the experiments down to strongly acidic conditions at pH 0.9 and up to 4.8 to overlap with the previously reported data. The goal was to compare the apparent pH dependency of dawsonite with those of the common carbonates. We also chose to run experiments at two different temperatures to estimate the apparent activation energies for dawsonite dissolution in the acidic region. The size of the apparent activation energy and possible variations over the pH region may provide valuable information to understand the mechanisms responsible for the reactivity. The dawsonite we used for the experiments was made synthetically because pure natural dawsonite in sufficient amount to run the dissolution rate experiments was not available. Procedures for making synthetic dawsonite are easily available and we based our procedure on descriptions by Zhang et al., (2004) and the detailed recipes provided by US patent #4.221.771. As we made synthetic material for the dissolution rate experiments we gained the additional opportunity to look into some of the parameters that constraints dawsonite growth. We tried with different aluminium sources, crystalline gibbsite and amorphous hydrous aluminohydroxide, to see if possible differences in the aluminium source reactivity would affect the dawsonite growth rate. If so it would indicate that the overall growth reaction is limited by the reactivity of the aluminium source. We also tried to vary the sources of sodium by mixing sodium carbonate, sodium bicarbonate and sodium hydroxide in different proportions, and we varied the temperature and experimental durations. Because we wanted to use the synthetic material for dissolution rate experiments we mapped out the thermodynamic stability of dawsonite relative to boehmite (γ-AlO(OH)) and sodium bicarbonate and constructed equations to make sure that the initial mineral mixtures could theoretically be completely converted to dawsonite. The first part of this paper cover the theoretical considerations of the hydrothermal precipitation experiments whereas sections 3 to 5 present the methods, results of precipitation and dissolution experiments, and discuss the findings with an emphasize on the understanding of dawsonite stability in the context of previous knowledge about carbonate reactivity.

2. Theoretical background

The formation of dawsonite requires aluminium, sodium and carbonate and is favoured by high pH. The precipitation reaction can be described by:

$$Na^+ + Al(OH)_4^- + CO_{2,aq} \rightarrow NaAl(OH)_2CO_3 + H_2O\,, \tag{1}$$

At temperatures above 100°C, which is proper for the synthesis reactions (e.g. Zhang et al. 2004), and at the presence of carbonate, the upper limits for aqueous sodium and aluminium are controlled by the sodium carbonate nahcolite:

$$NaHCO_3 + H^+ \leftrightarrow Na^+ + CO_{2,aq} + H_2O, \tag{2}$$

and boehmite respectively:

$$\gamma - AlO(OH) + 2H_2O \leftrightarrow Al(OH)_4^- + H^+ \tag{3}$$

A significant surplus of sodium relative to aluminium has been suggested as a requisite to successfully synthesize dawsonite (e.g., Zhang et al., 2004; US patent #4,221.771). The maximum surplus of sodium over aluminium that can completely consume reactants and produce a pure dawsonite is given by the constraint that the excess sodium in the final reacted solution must not exceed the solubility limit for nahcolite. For a reactant mixture the surplus moles of sodium relative to aluminium in a reactor can be calculated by:

$$n_{Na}^e = \sum_i n_{i,Na}\upsilon_{i,Na} - \sum_j n_{j,Al}\upsilon_{j,Al}\,, \tag{4}$$

where n is moles of reactant minerals, υ is stoichiometric coefficient of the element in the mineral, and indices i and j indicate sodium and aluminium source minerals respectively. The maximum surplus of sodium is then given by adding the potential moles of aluminium that can be precipitated in the dawsonite to the moles of sodium at nahcolite saturation. The maximum surplus of sodium expressed by activity limits for sodium and aluminium is given by:

$$n_{Na}^{e,max} = V\left\{\frac{\mathbf{a}_{Na^+}^{sat}}{\gamma_{Na^+}} + \frac{\left(\mathbf{a}_{Al(OH)_4^-}^{B} - \mathbf{a}_{Al(OH)_4^-}^{DxN}\right)}{\gamma_{Al(OH)_4^-}}\right\} \tag{5}$$

where V is volume reacted solution, $\mathbf{a}$ and γ denote activity and activity coefficients respectively, and superscripts *sat*, *B* and *DxN* denotes the activity of sodium at nahcolite saturation, activity of aluminium at boehmite saturation and at the invariant point where the dawsonite saturation crosses the nahcolite saturation value. This is illustrated in Fig. 1 where the solubility limits of dawsonite, nahcolite, boehmite and gibbsite are plotted with respect to the aqueous activities of sodium and aluminium relative to protons at a given CO_2 fugacity at 100 and 175C°. The solubility limit of dawsonite is, after adding H^+ on both sides of reaction (1), expressed as:

$$\log\left(\frac{\mathbf{a}_{Na^+}}{\mathbf{a}_{H^+}}\right) = -\log\left(\mathbf{a}_{Al(OH)_4^-}\mathbf{a}_{H^+}\right) - \log\mathbf{a}_{CO_{2,aq}} - \log K_1 \tag{6}$$

where K_1 is the equilibrium constant for reaction (1).The saturation values of reaction (2) and (3) are similarly given by:

$$\log\left(\mathbf{a}_{Al(OH)_4^-}\mathbf{a}_{H^+}\right) = \log K_2 \tag{7}$$

and

$$\log\left(\frac{\mathbf{a}_{Na^+}}{\mathbf{a}_{H^+}}\right) = -\log \mathbf{a}_{CO_{2,aq}} + \log K_3 , \quad (8)$$

where K_2 and K_3 are the equilibrium constants for the reactions (2) and (3) respectively. The fugacity of CO_2 is constrained by the vapour pressure of water and given by the partial pressure of the gas assuming a unit fugacity coefficient. To construct the activity diagrams, thermodynamic integrations were performed using the computer code SUPCRT92 (Johnson et al., 1992) with the dprons96.dat database. In order to relate experiments to the activity diagrams, speciation of sodium, aluminium, and carbon was solved using the numerical code PHREEQC v2 (Parkhurst and Appelo, 1999) with the LLNL database that is in turn based on the thermo.com.V8.R6.230 database prepared at the Lawrence Livermore National Laboratory. To relate the experimental solutions to the activity diagram, the sodium and aluminium concentrations at nahcolite and boehmite saturations respectively were calculated at a CO_2 fugacity and pH that correspond to the vapour pressure of water (Table 1). The shaded area in Fig. 1 illustrates the chemical window where dawsonite is supersaturated and stable relative to nahcolite and boehmite. Because nahcolite is expected to dissolve fast compared to the dawsonite precipitation, sodium concentrations are likely to be close to the nahcolite saturation. The reaction rate of gibbsite and the hydrous aluminohydroxide relative to dawsonite is harder to predict and the aqueous aluminium may reside somewhere inside the dawsonite stability field. As the aluminium source is also unstable relative to boehmite at 100 and 175°C we also expect recrystallization to the stable phase during the conversion to dawsonite. The maximum supersaturation of dawsonite is at the crossing between nahcolite and boehmite saturations (Fig. 1). This value can only be achieved if the dawsonite precipitation rate given by reaction (1) is slower than the dissociation reactions (2) and (3) and thus controlling the rate for the overall reaction progress.

3. Materials and methods

3.1. Dawsonite synthesis

Dawsonite synthesis experiments were performed in 50 ml Teflon liners placed inside stainless steel autoclaves that were in turn placed within a heating oven on a vertical rotating stage. The capacity of the oven was four simultaneous autoclaves. The temperature of the oven was specified and

thermostatically controlled. All reactants were weighed with a precision of three digits and chemicals used were analytical grade. Sodium carbonate (Na_2CO_3), citric acid ($C_6H_8O_7$), malic acid ($C_4H_6O_5$), and amorphous, hydrous $Al(OH)_3xH_2O$ were purchased from Sigma Aldrich (99.5%+), sodium bicarbonate from BDH Prolabo, gibbsite ($Al(OH)_3$) from Riedel deHaen, and NaOH from Merck. Water used in the synthesis was of milliQ quality deionized/demineralized H_2O. To detect the degree of conversion of reactants to dawsonite or formation of other minerals than dawsonite in the reacted samples, X-ray diffraction (XRD) data of experiments obtained with an X'Pert MPD (Phillips, Netherlands), were compared to reference 2θ-angles of the reactant sodium carbonates, alumino hydroxides and dawsonite. The Brunauer-Emmet-Teller (BET) surface area (Brunauer et al., 1938) was measured using a Strohlein Area-Meter (Germany) using N_2 adsorption, whereas pH was measured using an ISFET IQ125 pH meter from IQ Scientific, USA. Data for the experimental solution pH at 25ºC of synthetic mixtures were calculated using the PHREEQC v2. code. Solubility calculations of the reactant phases suggested that the experimental solutions were undersaturated with respect to the sodium carbonates, whereas gibbsite or boehmite was supersaturated. The pH was thus calculated from a mixture of the carbonates and pure water equilibrated with gibbsite at 25ºC.

3.2. Reaction rates experimental procedure

Dissolution rates were obtained using free-drift batch reactors. Polypropylene reactors open to the atmosphere but with a cover to prevent evaporation, were placed in a shaker-bath with 460 ± 60 ml aqueous solution. When the solution reached the target temperature of 77°C approximately 0.1 to 0.3 grams of synthetic dawsonite was added. Sampling was done at progressively longer time intervals by withdrawing 10 ml reacted solution using syringes equipped with 0.45μm Millipore© filters. Initial aqueous solutions were prepared by mixing HCl with deionized water to a target initial pH. Reacted aqueous samples were analyzed for Na and Al using a Varian SpectrAA 300 atomic absorption spectrometer with detection limits of 0.05 and 1 ppm respectively for Na and Al. As a measure of the distance from equilibrium for dawsonite and alumino hydroxide relative to the reacted solutions we used PHREEQC to estimate the solubility indices $\log(\Omega)$, where $\Omega = \exp(\Delta G/RT)$.

Because the chemical composition continuously drifted the reaction rate *r* was estimated from the difference in element concentration over each time interval according to:

$$r_t = \frac{2V_{t-1}}{(m_t + m_{t-1})S_{BET}} \cdot \frac{\Delta C}{\Delta t} \tag{9}$$

where V is volume aqueous solution, C is concentration, m is mass and t is time. Subscripts t and $t-1$ denotes time of sampling and time at previous sampling respectively. In addition experiments were done to check if the element release from the synthetic dawsonite behaved stoichiometric. These experiments were done at 25°C with repeated additions of 0.3N HCl to ensure that the aqueous solutions stayed undersaturated with respect to the aluminous phases. pH was measured with an accuracy of two digits using a Metrohm combined flat membrane electrode.

Apparent activation energies for the dawsonite dissolution, following the assumption that the activation energies were constant within the selected temperature range, were calculated according to:

$$E_a = -\frac{\partial \ln r}{\partial (1/T)} \cdot R \tag{10}$$

where r is the dissolution rate, T is absolute temperature, and R is the gas constant. To avoid differences in calculated rates caused by preferential dissolution of fines, all rates and corresponding reaction affinities were calculated at the point when 50% of the material was dissolved. This was done by a linear interpolation over the calculated rates and affinity over the time interval passing 50% remaining dawsonite according to:

$$A_{x=0.5} = \left(\frac{A_{x_2} - A_{x_1}}{X_2 - X_1} \right) (0.5 - X_2) + A_{x_1} \tag{11}$$

where A is the interpolated property, X is the fraction of dawsonite left, and subscripts 1 and 2 refer to the samples passing $X = 0.5$.

4. Experimental results

4.1. Dawsonite synthesis

Synthetic dawsonite was made following the experiments done by Zhang et al. (2004) and recipes described in US patent #4.221.771. These reports suggest that reacting aluminohydroxides with sodium carbonate and bicarbonate and/or sodium hydroxid at high temperatures, typically 120-180°C, may produce a pure well-crystalline dawsonite. In our first experiment we reacted $NaHCO_3$, NaOH and amorphous $Al(OH)_3xH_2O$ at 135°C for 2 hours and 30 minutes (Table 2). The pH at 25°C measured after the experiment was 10. The result was an amorphous phase without traces of dawsonite. We thus increased the temperature to 165°C, increased the time to 48 hours, and switched aluminium source to the crystalline gibbsite for the second experiment. This time the experiments resulted in a high degree of conversion to dawsonite. Some sodium bicarbonate impurity was however present as the excess sodium in the system was higher than the maximum allowed for a 100% conversion estimated by using equation (5). The following experiments switched between the two aluminium sources at 165 and 175°C at experimental durations of 1 hour and 45 minutes to 13 hours and revealed that the aluminohydroxide source was a limiting factor in the conversion to dawsonite (Table 2). The maximum yield using the amorphous aluminium source was in excess of 90% after 12 hours at 165°C with SEM evidence of unreacted aluminium hydroxide. Using the crystalline gibbsite yielded close to 100% conversion to dawsonite after 1 hour and 45 minutes at 175°C (Table2; experiment 6). Although the yield of experiments 5-1 and 5-2 using the two different aluminium sources looks similar, the nature of the impurity was different. Experiment 5-1 using crystalline gibbsite had remains of sodium because of a surplus of sodium in the system in excess of what was allowed for a complete conversion. Experiment 5-2 had on the other hand remains of a significant fraction of aluminium hydroxide

After observing an apparent complete conversion to dawsonite by experiment 4-2, a series of identical experiments (not listed in Table 2) were done to produce dawsonite for the dissolution rate experiments. Fig. 2 shows a SEM image of the dawsonite synthesized during experiment 4 (Table 2). Swiping over the synthetic material by the SEM revealed a material that appeared to be pure dawsonite. Moreover, the XRD reflections of experiments 4 and 8 (Fig. 3a) compares well with the natural dawsonite used earlier by Hellevang et al. (2005) for their dissolution rate experiments (Fig. 3b). The subsequent batch dissolution rate experiments revealed however that minor amounts of both sodium carbonate and aluminohydroxide were present in the synthetic material. A closer inspection of the XRD patterns of the synthetic dawsonite revealed traces of boehmite ($2\theta = 37.3$), whereas sodium carbonate impurities were not detectable on the XRD data.

4.2. Element release stoichiometry from the synthetic material

Before starting the dissolution rate experiments, two 25°C batch dissolution experiments were done with repeated additions of 0.3N HCl to test if the element release performed stoichiometricaly, i.e. that the released molar Na to Al ratio corresponded to the compositional 1:1 ratio. The low temperature and additions of acid ensured that secondary phases like gibbsite did not form. The experimental solutions are listed in Table 3 whereas Fig. 4 shows the concentrations of Al versus Na and the line that corresponds to the ideal 1:1 ratio between Al and Na in the dawsonite structure. It is evident from the figure that the synthetic material releases sodium in excess of aluminium. However, after an initial rapid increase of the Na to Al ratio the experimental data progressed parallel to the stoichiometric line. This suggests that the synthetic material still contained remains of unreacted sodium carbonate and that this impurity completely dissolved within a few minutes. A line fitted through the datapoints suggests that the synthetic material gave rise to approximately 0.9 mmol of excess Na at zero Al for the 0.4 liters solution. From this value we estimated that the amount of sodium carbonate impurity in the material was 0.18 mmol or 19 mg Na_2CO_3. This is approximately 4% of the initial 0.5 grams of synthetic material used for the stoichiometry experiments.

4.3. The dissolution rate of dawsonite

The dissolution rate of dawsonite was calculated using equation (9) on the Na or Al concentrations measured after the batch reaction rate experiments. Tables 4 and 5 list a summary of results and the complete overview of the experiments respectively. Because of the rapid dissolution of the sodium carbonate impurity during the initial minute of the experiment the reaction rates were based on the Al release up to the first sample and on the changes in sodium concentration for the samples that followed. As preferential dissolution of fines resulted in reduced rates when normalized to a constant BET surface area, all dissolution rates with three exceptions were estimated at 50% dissolved material according to equation (11). Experiment 4 dissolved more than 50% material before the first sample was taken at 55 seconds (Table 5) and in this case the rate was estimated based on the sodium concentration at the first sample minus the estimated sodium released from the Na_2CO_3 impurity. Moreover, experiments 10 and 11 did not reach 50% dissolved dawsonite (Table 5) and the rates were in this case calculated based on the last samples.

The estimated dissolution rates at 22 and 77°C are shown in Fig. 5. After attempting aqueous solutions with initial pH from 0.8 (experiment 9; Table 5) to 2.7 (experiment 15; Table 5) we achieved a range of dissolution rates estimated at 50% dissolved material at pH ranges from 0.9 to 4.3 at 22°C and from 1.6 to 4.8 at 77°C. The figure shows that the rates increased steadily with decreasing pH. At 22°C pH 4.2 to 4.3 rates were approximately $10^{-8.5}$ moles/m^2s increasing to $10^{-5.3}$ at pH 0.9. The same is seen at 77°C with an increase from $10^{-6.8}$ moles/m^2s at pH 4.8 to $10^{-4.8}$ at pH 1.6. The increase in rates caused by increasing the temperature from 22 to 77°C is seen to be pH dependent. At pH 4 rates increased by approximately 2 orders of magnitude over the temperature interval, whereas at the more acidic conditions the increase was slightly larger than 1 order of magnitude. Table 4 shows that at 50% dissolution experiments 14 and 15 were the closest to dawsonite saturation with solubility index values of -1.37 and -0.46 respectively which corresponds roughly to a 23 and 3 times undersaturated solutions respectively. The saturation indices of boehmite (77°C experiments) and gibbsite (22°C experiments) were also estimated by PHREEQC, and most experiments reaching the higher pH were to various degrees supersaturated (Table 5). These experiments precipitated the aluminohydroxide as seen by Al reaching a close to constant concentration whereas the Na concentration increased steadily with the experimental progress.

5. Discussion

5.1. What controls the formation rate of dawsonite?

Earlier studies on the synthesis of dawsonite (e.g. Zhang et al., 2004; US patent #4,221.771) have shown that mixing sodium carbonate and aluminium hydroxide in basic conditions produces dawsonite. The yields in these studies have been attributed to experimental temperatures, and the mixing fractions of initial sodium carbonates and aluminium hydroxide. The synthesis experiments done in this study showed that different alumino hydroxide reactants, gibbsite or hydrous amorphous alumino hydroxide, strongly affected the yield. The gibbsite source generally produced a higher fraction of dawsonite than the hydrous amorphous source. Moreover, XRD spectra showed a complete consumption of gibbsite in the high-yield experiments, but indicate the presence of the high-temperature alumino hydroxy variety boehmite. In addition, batch dissolution experiments showed a surplus of sodium over aluminium compared to the expected 1:1 stoichiometric element ratio of dawsonite. The variation in yield observed by using different aluminium sources is in agreement with an overall conversion rate to dawsonite constrained by the dissolution rates of the aluminium sources.

This has previously been suggested based on theoretical considerations around aluminium supply rate from multi-mineral assemblages (Hellevang et al., 2004), and from experiments comparing dawsonite synthesis using gibbsite and kaolinite ($Al_2Si_2O_5(OH)_4$) or albite ($NaAlSi_3O_8$) as source minerals (Kaszuba et al., 2006). As we observed boehmite forming during the transformation reactions an additional constraint on the formation rate of dawsonite may be the recrystallization reactions from gibbsite or hydrous aluminohydroxide into boehmite. The aluminium reactivity in the system can be summarized by the dissolution/precipitation or recrystallization reactions (12) to (14):

$$Al(OH)_3 \times H_2O \xrightarrow{k_I} \gamma AlO(OH) + 2H_2O, \quad (12)$$

$$Al(OH)_{3,s} \xrightarrow{k_{II}} \gamma AlO(OH) + H_2O, \quad (13)$$

$$\gamma AlO(OH) + 2H_2O \xrightarrow{k_{III}} Al(OH)_4^- + H^+, \quad (14)$$

where k_I to k_{III} are reaction rate coefficients, and finally the consumption of aluminium by dawsonite precipitation given by reaction (1). Moreover, direct formation of dawsonite from dissolving gibbsite or hydrous alumino hydroxide and only partly conversion into boehmite is an additional possibility that can not be ruled out. The dissolution rates of gibbsite and boehmite have been extensively studied in the past (e.g., Bloom, 1983; Nagy and Lasaga, 1992; Ganor et al., 1999; Benezeth et al., 2008). By comparing these rates with dissolution rates of dawsonite (this study) we see that dawsonite reacts orders of magnitude faster at the same conditions. If we assume that the dawsonite precipitation rate is proportional to the product of the far-from-equilibrium dissolution rate coefficient for dawsonite and the thermodynamic driving force, we expect that the precipitation rate is correspondingly fast compared to the dissolution of the aluminous phases. The limiting steps for the overall synthetic reaction is hence, assuming that the sodium carbonates dissolve sufficiently fast, the transformation rates of solid alumino hydroxide into dissolved aluminium. Moreover, as the aluminium source mineral is seen to strongly affect the transformation rate, we speculate that the overall rate is likely controlled by the kinetics given by reactions (12) and (13), or the direct dissolution of these phases with only partly recrystallization to boehmite, rather than the dissolution rate of boehmite.

5.2. What are the mechanisms responsible for the dawsonite dissolution rates?

This study suggests that the dissolution rate of dawsonite increases as a function of proton activity at pH below 4 to 5 whereas the study by Hellevang et al. (2005) done at 80°C suggest that rates are independent of pH from 3.5 to 8.6. This may suggest that a proton promoted mechanism dominates at low pH whereas surface hydration dominates at higher pH. The reaction order v with respect to protons and the reaction rate coefficient k_1 can be found by fitting the rate data (Table 4) to:

$$\log r = \nu \log \mathbf{a}_{H^+} + \log k_1. \quad (15)$$

The coefficient for the hydration mechanism k_2 can then be found by fitting the calculated rates to the combined rate equation reading:

$$r = k_1 \mathbf{a}^{\nu}_{H^+} + k_2. \quad (16)$$

Fig. 6 shows the curves resulting from a fit of equations (15) and (16) to the calculated reaction rates. This suggests that the reaction order of dawsonite with respect to protons at pH < 4 is first order and that k_1 and k_2 respectively equal $10^{-4.46}$ and 10^{-9} moles/m^{2}s at 22°C and $10^{-3.22}$ and $10^{-6.74}$ moles/m^{2}s at 77°C. At pH 4 and 22°C this gives a rate of $10^{-8.35}$ moles/m^{2}s which is close to the rate of magnesite and 4 orders of magnitude slower than calcite (Pokrovsky et al., 2009). The mechanisms responsible for the dissolution rate may however differ from the other carbonates as the pH dependence of magnesite and dawsonite appear different at strongly acidic conditions. While dawsonite appears to have a continuous first order dependence on the proton activity (this study), the magnesite rate get pH independent on strongly acidic conditions (Pokrovsky and Schott, 1999; Pokrovsky et al., 2009).

The apparent activation energies were calculated using equation (10) on the 22°C and 77°C reaction rate coefficients. As the calculated rate coefficients represents a fit to all experimental points and because all data are using the same surface area normalization, the error on the activation energy is set to ± 10%. Following this the apparent activation energy for the protonation mechanism is 44.61 ± 4.5 kJ/mol and for the hydration mechanism is 80.58 ± 8.1 kJ/mol. By comparison the calcite and

magnesite apparent activation energies at pH 3 to 4 are 48.2 ± 4.6 and 44 ± 2 kJ/mol (Pokrovsky et al., 2009), which is similar to what was found for the proton-promoted dissolution rates at acidic conditions in the present study. The activation energy for the hydration mechanism of dawsonite is however much higher than the 16 and 34 kJ/mol measured at pH 5.5 and 5.4 for calcite and magnesite respectively. This may suggest that the dawsonite reactivity at pH > 4 is a result of different mechanisms than the other common carbonates like calcite and magnesite.

For carbonates the pH dependence is classically described by a series of parallel reactions with individual rates dominating within given pH ranges (Plummer et al., 1978; Chou et al., 1989). This normally results in a pH-independent region around neutral pH, and elevated rates at strongly acidic conditions (e.g. Chou et al., 1989). If we assume that dawsonite can also be described by similar parallel reactions as those described for the simple MCO_3-carbonates, we can divide the dissolution into the following two reactions giving first and zeroth order dependences on H^+ respectively:

$$NaAlCO_3(OH)_2 + H^+ + 2CO_{2,aq} \xrightarrow{k^*_1} Na^+ + Al^{3+} + 3HCO_3^-, \quad (17)$$

and

$$NaAlCO_3(OH)_2 \underset{k^*_{-2}}{\overset{k^*_2}{\leftrightarrow}} Na^+ + Al(OH)_2^+ + CO_3^{2-}, \quad (18)$$

where k^*_1 and k^*_2 are rate constants for the forward reactions (17) and (18), and k^*_{-2} is the rate constant for the dawsonite precipitation. As dawsonite is strongly favoured to form at basic conditions, we can assume that the dawsonite precipitation rate is dominated by reaction (18). By combining reactions (17) and (18) the net dissolution rate can then be expressed as:

$$k = k^*_1 \cdot \mathbf{a}_{H^+} \mathbf{a}^2_{CO_{2,aq}} + k^*_2 + k^*_{-2} \cdot \mathbf{a}_{Na^+} \mathbf{a}_{Al(OH)_2^+} \mathbf{a}_{CO_3^{2-}} \quad (19)$$

This equation predicts three different features of the reactivity of dawsonite: (1) The dissolution rate at acidic conditions shows a second-order dependence on aqueous CO_2 activity; (2) precipitation requires incorporation of $Al(OH)_2^+$; and (3) the very high activation energy for the second rate coefficient suggests that the formation of dawsonite is strongly favoured at higher temperatures. The effect of

CO_2 activity on carbonate dissolution rates of common carbonates like magnesite, calcite, siderite and dolomite has been showed to be very low or even inhibiting rather than catalyzing (Pokrovsky and Schott, 1999; Pokrovsky et al., 2009; Golubev et al., 2009). For magnesite, dolomite and calcite this has been explained within the framework of a surface complexation model where the rates at all pH are constraint solely by the activity of the surface complexes $>MeOH_2^+$ and $>CO_3H^0$, where Me is the divalent cation Ca^{2+} or Mg^{2+} (Van Cappelen et al., 1993; Pokrovsky et al., 1999a, b; Pokrovsky and Schott, 1999; Pokrovsky et al., 2005; Gautelier et al., 2007; Pokrovsky et al., 2009; Golubev et al., 2009). An increased CO_2 does not increase the $>CO_3H^0$ activity and lowers the activity of $>MeOH_2^+$ (Pokrovsky et al., 2009). As the activation energy and pH dependence of the dawsonite dissolution rate at pH < 4 is similar to magnesite and calcite (e.g., Pokrovsky et al., 2009), it is tempting to suggest that the dawsonite dissolution rate is also proportional to the activity of the $>CO_3H^0$ surface complex. However, any experimental verification of this is outside the scope of the present study. Some insight into the possible mechanisms responsible for the reactivity of dawsonite is available through considerations around the crystal structure of dawsonite.

The dawsonite structure can be described by a chain of $Al(O)_2(OH)_4$ octahedra bond together by common hydroxyl ions along the *c-axis* crystallographic direction. This chain is stabilized by carbonate groups forming the carboaluminate chain $[Al(OH)_2CO_3]_n^-$ (Frueh and Golightly, 1967; Fernández-Carrasco et al., 2005) which is the backbone of the dawsonite structure. These chains are bond together by hydrogen bonds and by sodium (Frueh and Golightly, 1967; Fernández-Carrasco et al., 2005). Fig. 7 illustrates the structure schematically by a projection parallel to the *c-axis*. Bond angles and atomic positions do not correspond with the real structure and is only meant for illustration. The internal bond lengths in the carboaluminate chain are 1.86 and 1.95Å for the Al-OH and Al-O bonds respectively (Frueh and Golightly, 1967; Fig. 7), whereas the octahedral coordinated sodium surrounded by four oxygens and two hydroxyl ions have Na-O and Na-OH bondlengths of 2.47 and 2.39Å respectively (Frueh and Golightly, 1967; Fig. 7). The O-OH and O-O bonds are generally 2.74Å or greater, but one oxygen of each carbonate group is 2.66Å from a hydroxyl ion suggesting hydrogen bonds (Frueh and Golightly, 1967; Fig. 7). By assuming that the shorter bonds observed within the carboaluminate chain are stronger than the Na-O and Na-OH bonds, we propose that the first-order dependence of the rates with respect to proton activity at pH < 4 can be explained by surface protonation of surface carbonate complexes where Na^+ is exchanged by H^+:

$$>CO_3Na^0 + H^+ \Leftrightarrow >CO_3H^0 + Na^+ \quad (20)$$

This is followed by a disintegration of the surface CO_3 group from the carboaluminate chain.

$$>CO_3H^0 + H^+ \Leftrightarrow H_2CO_3^* \quad (21)$$

this results in destabilization of the aluminate chain and a collapse of the dawsonite structure. One interesting point is that if this is the case then the rate-controlling step is the disintegration of the surface complex with a rate according to reaction (21) proportional to the H^+ activity and inversely proportional to the activity of carbonic acid:

$$r_{>CO_3H^0} = k_{>CO_3H^0} \frac{\mathbf{a}_{H^+}}{\mathbf{a}_{H_2CO_3^*}} \quad (22)$$

This agrees with the inhibiting effect caused by increasing CO_2 partial pressures as observed for magnesite, calcite and dolomite (e.g., Pokrovsky et al., 2009). It is however outside the scope of the present study to demonstrate the dependence of dawsonite reactivity on CO_2. Independent of the exact mechanism responsible for the rate dependence pattern observed in the experimental data, by combining equation (16) with the apparent activation energies and the broad pH independent region around circumneutral pH reported by Hellevang et al. (2005), the overall dissolution rate at strongly acidic to circumneutral conditions can be expressed as:

$$r_+ = S\left\{10^{3.43} \cdot \mathbf{a}_{H^+} \cdot \exp\left(\frac{-44600}{RT}\right) + 10^{5.26} \cdot \exp\left(\frac{-80600}{RT}\right)\right\} \quad (23)$$

where S is reactive surface area, **a** is activity, T is absolute temperature, and R is the gas constant.

6. Conclusions

Our dawsonite synthesis revealed that the formation rate of dawsonite is dependent on the dissolution rate of the aluminium source. The faster-dissolving crystalline gibbsite resulted in a higher degree of conversion to dawsonite than the amorphous hydrous aluminohydroxide. Dissolution experiments on the synthetic dawsonite showed that the dissolution rate at pH 4 and 22°C is comparable with that of magnesite. At pH < 4 the rates are first-order dependent on the proton activity, whereas at higher pH the rate approach a pH-independent region which is strongly supported by the earlier reported rate data by Hellevang et al. (2005). Based on the similarity in activation energies between dawsonite, calcite and magnesite over the proton-promoted rate region we propose that a similar mechanism is responsible for the dissolution rate at these conditions for all three. For calcite and magnesite the activity of the $>CO_3H^0$ surface complex has been suggested to constrain the rate at acidic conditions (e.g., Van Cappelen et al., 1993; Pokrovsky et al., 1999a, b; Pokrovsky and Schott 1999; Pokrovsky et al., 2009). Moreover, we propose that the rate may be controlled by a second protonation step releasing the surface complex and forming carbonic acid. This would lead to the first order dependence on proton, and in addition to rates that are inversely proportional to the activity of dissolved CO_2. The inhibiting effect by an increased CO_2 partial pressure has been demonstrated for carbonates like calcite, magnesite and dolomite (Pokrovsky et al., 2009). It was however outside the scope of the present study to demonstrate the effect of CO_2 on the dawsonite dissolution rates. For pH > 4 we suggest that the rates are dominated by surface hydration. Going from the proton-promoted region to the hydration-dominated region is followed by a large increase in the apparent activation energy. As natural occurrences of dawsonite as well as thermodynamics indicate that dawsonite is only likely to form at circumneutral to basic conditions, the high apparent activation energy of 80.58 ± 8.1 kJ/mol may indicate that growth is constrained by an activation barrier at low temperatures. This is supported by the ease of synthesizing dawsonite at hydrothermal conditions, whereas low temperature synthesis has not been reported efficient. Based on the crystal structure of dawsonite we suggest that dawsonite growth mainly occur along the crystallographic *c-axis* by the adhesion of $Al(OH)_2^+$ to a chain of octahedral coordinated Al stabilized by carbonate groups. This carboaluminate chain forms the backbone of the dawsonite structure bond together by hydrogen bonds and the interstitial sodium ions.

Acknowledgments

The authors strongly appreciate the work done by Aweewan Mangmeechai, Rune Wendelbo and Yu Jia during the synthesis experiments. We appreciate all the work done by Turid Winje and Berit Løken Berg on their SEM and XRD examinations of experimental powders. We also would like to thank Mufak Naoroz for preparing and tuning the atomic absorption spectrometer for our analyses. This project was made possible through financial support made by the Research Council of Norway through project #165697.

References

André, L., Audigane, P., Azaroual, M., Menjoz, A., 2007. Numerical modeling of fluid-rock chemical interactions at supercritical CO_2-liquid interface during CO_2 injection into a carbonate reservoir, the Dogger aquifer (Paris Basin, France). Energy Conversion and Management 48, 1782-1797.

Baker, J.C., Bai, G.P., Hamilton, P.J., Golding, S.D., Keene, J.B., 1995. Continental-scale magmatic carbon dioxide seepage recorded by dawsonite in the Bowen-Gunnedah-Sydney Basin system, eastern Australia. Journal of Sedimentary Research 65, 522-530.

Bénézeth, P., Palmer, D.A., Anovitz, L.M., Horita, J., 2007. Dawsonite synthesis and reevaluation of its thermodynamic properties from solubility measurements: Implications for mineral trapping of CO_2. Geochimica et Cosmochimica Acta 71, 4438-4455.

Bénézeth, P., Palmer, D.A., Wesolowski, D.J., 2008. Dissolution/precipitation kinetics of boehmite and gibbsite: Application of a pH-relaxation technique to study near-equilibrium rates.

Bloom, P.R., 1983. The kinetics of gibbsite dissolution in nitric acid. Soil Science Society of America Journal 47, 164-168.

Bouchard, R., Delaytermoz, A., 2004. Integrated path towards geological storage. Energy 29, 1339-1346.

Brunauer, S., Emmett, P.H., and Teller, E., 1938. Adsorption of gases in multimolecular layers. Journal of American Chemical Society 60, 309-319.

Cantucci, B., Montegrossi, G., Vaselli, O., Tassi, F., Quattrocchi, F., Perkins, E.H., 2009. Geochemical modeling of CO2 storage in deep reservoirs: The Weyburn Project (Canada) case study. Chemical Geology, in press.

Chou, L., Garrels, R.M., Wollast, R., 1989. Comparative study of the kinetics and mechanisms of dissolution of carbonate minerals. Chemical Geology 78, 269-282.

Ferrante, M.J., Stuve, J.M., Richardson, D.W., 1976. Thermodynamic data for synthetic dawsonite. U.S. Bureau of Miners Report Investigation 8129, Washington D.C., 13p.

Fernández-Carrasco, L., Puertas, F., Blanco-Varela, M.T., Vázquez, T., Rius, J., 2005. Synthesis and crystal structure solution of potassium dawsonite: An intermediate compound in the alkaline hydrolysis of calcium aluminate cements. Cement and Concrete Research 35, 641-646.

Frueh, A.J., Golightly, J.P., 1967. The crystal structure of dawsonite $NaAl(CO_3)OH_2$. Canadian Mineralogist 9, 51-56.

Gale, J., 2004. Geological storage of CO_2: What do we know, where are the gaps and what more needs to be done? Energy 29, 1329-1338.

Ganor, J., Mogollon, J.L., Lasaga, A.C, 1999. Kinetics of gibbsite dissolution under low ionic strength conditions. Geochimica et Cosmochimica Acta 63 (11-12), 1635-1651.

Gaus, I., Azaroual, M., Czernichowski-Lauriol, I., 2003. Reactive transport modeling of dissolved CO_2 in the Cap Rock Base during CO_2 sequestration (Sleipner Site, North Sea). Proceedings, Second Annual Conference on Carbon Sequestration, Alexandria, Virginia.

Gautelier, M., Schott, J., Oelkers, E.H., 2007. An experimental study of dolomite dissolution rates at 80°C as a function of chemical affinity and solution composition. Chemical Geology 242, 509-517.

Gherardi, F., Xu, T., Pruess, K., 2007. Numerical modeling of self-limiting and self-enhancing caprock alteration induced by CO_2 storage in a depleted gas reservoir. Chemical Geology 244, 103-129.

Golab, A.N., Carr, P.F., Palamara, D.R., 2006. Influence of localised igneous activity on cleat dawsonite formation in Late Permian coal measures, Upper Hunter Valley, Australia. International Journal of Coal Geology 66, 296-304.

Golab, A.N., Hutton, A.C., French, D., 2007. Petrography, carbonate mineralogy and geochemistry of thermally altered coal in Permian coal measures, Hunter Valley, Australia. International Journal of Coal Geology 70, 150-165.

Golubev, S.V., Bénézeth, P., Schott, J., Dandurand, J.L., Castillo, A., 2009. Siderite dissolution kinetics in acidic aqueous solutions from 25 to 100°C and 0 to 50 atm pCO2. Chemical Geology, in press.

Harrison, W.J., Wendlandt, R.F., 1995. Geochemical interactions resulting from carbon dioxide disposal on the seafloor. Applied Geochemistry 10, 461-475.

Hellevang, H., Kvamme, B., Aagaard, P., 2004. Long term interactions between minerals and reactive fluids - Stability of dawsonite. In Proceedings of the Third Annual Conference on Carbon Capture and Sequestration DOE/NETL, Alexandria, VA, May 3-6, 1-7

Hellevang, H., Aagaard, P., Oelkers, E.H., Kvamme, B., 2005. Can dawsonite permanently trap CO_2? Environmental Science and Technology 39, 8281-8287.

Holloway, S., 1997. An overview of the underground disposal of carbon dioxide. Energy Conversion And Management 38, 193-198.

Johnson, J.W., Oelkers, E.H., Helgeson, H.C., 1992. SUPCRT92: A software package for calculating the standard molal thermodynamic properties of minerals, gases, aqueous species, and reactions fro 1 to 5000 bar and 0 to 1000°C. Computers and Geosciences 18 (7), 899-947.

Johnson, J.W., Nitao, J.J., Steefel, C.I., Knauss, K., 2001. Reactive transport modeling of geologic CO2 sequestration in saline aquifers: the influence of intra-aquifer shales and the relative effectiveness of structural, solubility, and mineral trapping during prograde and retrograde sequestration. Proceeding, First National Conference on Carbon Sequestration, Washington.

Johnson, J.W., Nitao, J.J., Knauss, K.G., 2004. Reactive transport modeling of CO2 storage in saline aquifers to elucidate fundamental processes, trapping mechanisms and sequestration partitioning. In: Baines, S.J., and Worden, R.H. (eds), Geological Storage of Carbon Dioxide. Geological Society, London, Special Publications, 233, 107-128.

Kaszuba, J.P., Viswanathan, H.S., Carey, B., Carpenter, T.M., Counce, D. and Duan, R., 2006. On the reactivity of dawsonite in geological carbon sequestration. American Geophysical Union, Fall Meeting, 2006, abstract #V53D-1779.

Knauss, K.G., Johnson, J.W., Steefel, C.I., 2005. Evaluation of the impact of CO_2, co-contaminant gas, aqueous fluid and reservoir rock interactions on the geologic sequestration of CO_2. Chemical Geology 217, 339-350.

Moore, J., Adams, M., Allis, R., Lutz, S, Rauzi, S., 2005. Mineralogical and geochemical consequences of the long-term presence of CO2 in natural reservoirs: An example from the Springerville-St. Johns Field, Arizona, and New Mexico, U.S.A. Chemical Geology 217, 365-385.

Nagy, K.L., Lasaga, A.C., 1992. Dissolution and precipitation kinetics of gibbsite at 80°C and pH 3: The dependence on solution saturation state. Geochimica et Cosmochimica Acta 56, 3093-3111.

Parkhurst, D.L., and Appelo, C.A.J., 1999. User's guide to PHREEQC (version 2) – A computer program for speciation, batch-reaction, one-dimensional transport, and inverse geochemical calculations. U.S. Geological Survey Water-Resources Investigations Report 99-4259. 312p.

Plummer, L.N., Wigley, T.M.L., Parkhurst, D.L., 1978. The kinetics of calcite dissolution in CO_2-water system at 5° to 60°C and 0.0 to 1.0 atm CO_2. American Journal of Science 278, 179-216.

Pokrovsky, O.S., Schott, J., Thomas, F., 1999a. Processes at the magnesium-bearing carbonates/solution interface. I. A surface speciation model of magnesite. Geochimica et Cosmochimica Acta 63, 863-880.

Pokrovsky, O.S., Schott, J., Thomas, F., 1999b. Dolomite surface speciation and reactivity in aquatic systems. Geochimica et Cosmochimica Acta 63, 3133-3143.

Pokrovsky, O.S., Schott, J., 1999. Processes at the magnesium-bearing carbonates/solution interface. II. Kinetics and mechanism of magnesite dissolution. Geochimica et Cosmochimica Acta 63, 881-897.

Pokrovsky, O.S., Golubev, S.V., Schott, J., 2005. Dissolution kinetics of calcite, dolomite and magnesite at 25°C and 0 to 50 atm pCO2. Chemical Geology 217, 239-255.

Pokrovsky, O.S., Golubev, S.V., Schott, J., Castillo, A., 2009. Calcite, dolomite and magnesite dissolution kinetics in aqueous solutions at acid to circumneutral pH, 25 to 150°C and 1 to 55 atm pCO_2: New constraints on CO_2 sequestration in sedimentary basins. Chemical Geology, In Press,

Smith, J.W., Milton, C., 1966. Dawsonite in the Green River formation of Colorado. Economic Geology 61, 1029-1042.

White, S.P., Allis, R.G., Moore, J., Chidsey, T., Morgan, C., Gwynn, W., Adams, M., 2005. Simulation of reactive transport of injected CO_2 on the Colorado Plateau, Utah, USA. Chemical Geology 217, 387-405.

Van Cappelen, P., Charlet, L., Stumm, W., Wersin, P., 1993. A surface complexation model of the carbonate mineral-aqueous solution interface. Geochimica et Cosmochimica Acta 57, 3505-3518.

Worden, R.H., 2006. Dawsonite cement in the Triassic Lam Formation, Shabwa Basin, Yemen: A natural analogue for a potential mineral product of subsurface CO_2 storage for greenhouse gas reduction. Marine and Petroleum Geology 23, 61-77.

Xu, T., Apps, J.A., Pruess, K., 2005. Mineral sequestration of carbon dioxide in a sandstone-shale system. Chemical Geology 217, 295-318.

Xu, T., Apps, J.A., Pruess, K., Yamamoto, H., 2007. Numerical modeling of injection and mineral trapping of CO_2 with H_2S and SO_2 in a sandstone formation. Chemical Geology 242, 319-346.

Zerai, B., Saylor, B.Z., Matisoff, G., 2005. Computer simulation of CO2 trapped through mineral precipitation in the Rose Run Sandstone, Ohio. Applied Geochemistry 21, 223-240.

Zhang, W., Li, Y., Xu, T., Cheng, H., Zheng, Y., Xiong, P., 2009. Long-term variations of CO2 trapped in different mechanisms in deep saline formations: A case study of the Songliao Basin, China. International Journal of Greenhouse Gas Control 3, 161-180.

Zhang, X., Wen, Z., Gu, Z., Xu, X., Lin, Z., 2004. Hydrothermal synthesis and thermodynamic analysis of dawsonite-type compounds. Journal of Solid State Chemistry 177, 849-855.

Figure captions

Fig. 1. Activity-activity diagram depicting the solubility limit of dawsonite, gibbsite, boehmite and nahcolite. The shaded region is the window where dawsonite is expected to form. The points at 1 and 2 indicate the expected reaction chemistry during the synthesis and the final invariant point where the solution will reach if the final reaction mixtures have sodium carbonate in excess of what can be consumed by dawsonite.

Fig. 2. Synthetic dawsonite produced during experiment 4.

Fig. 3. XRD 2θ angles for dawsonite. Indicative peaks for dawsonite is is marked by their crystallographic indices. A) The synthetic materials produced during experiment 6; and B) natural dawsonite from Monticolo, Italy, used by Hellevang et al. (2005) for batch dissolution rate experiments.

Fig. 4. Element release stoichiometry of synthetic dawsonite. The solid line indicates stoichiometric dissolution, whereas the parallel dotted line indicates stoichiometric dissolution after a first rapid increase in the Na/Al ratio caused by the dissolution of the Na_2CO_3 impurity.

Fig. 5. Calculated reaction rates for the RD1 to 15 experiments. The cumulative error bars for the rates are set to 0.5 log units, whereas the error on pH measurements is set to 0.2 pH units.

Fig. 6. The equation $r_+ = k_1 a_{H^+}^{\nu} + k_2$ fitted to the experimental datapoints. The solid lines suggests that the best-fit is given by $\nu = 1$ for both temperatures, and k_1 and k_2 equal to $10^{-4.46}$ and $10^{-9.0}$ moles/m^{2}s at 22°C and $10^{-3.22}$ and $10^{-6.74}$ moles/m^{2}s At 77°C.

Fig. 7. A schematic illustration of the dawsonite structure projected down to a plane parallel to the *c-axis*. The carboaluminate chain $\left[Al(OH)_2CO_3\right]_n$ along the *c-axis* is the backbone of the dawsonite structure. Hydrogen bonds and Na-O and Na-OH bonds attach the chains together. Based on the pH dependences of the dissolution rates we propose that at pH < 4 substitution of H^+ for Na^+ is the dominant rate-controlling mechanism, whereas hydration of the surface dominates at higher pHs. We also propose that the additions of $Al(OH)_2^+$ to the chain together with the stabilization of the octahedral coordinated aluminium by the carbonate are controlling the precipitation rates.

Tables

Table 1. $CO_{2,aq}$ activities and corresponding molar concentrations of Na^+ and $Al(OH)_4^-$ at nahcolite and boehmite saturations respectively calculated at the vapour pressure of water at 100 and 175°C by the PHREEQC speciation code. The vapour press curve of water $P^v_{H_2O}$ was calculated by the SUPCRT92 code.

T°C	$P^v_{H_2O}$	$\log \mathbf{a}_{CO_{2,aq}}$	$c^{pH}_{Na^+}$	$c^{pH*}_{Al(OH)_4^-}$
100	1.013	-1.968	2.820	4.430 x 10^{-5}
175	8.918	-1.092	3.581	6.484 x 10^{-4}

Table 2. Experimental mixtures and conditions of the dawsonite synthesis experiments. Values of chemicals are grams added per 20 ml milliQ water. The dawsonite conversion is approximated percentage in the reacted sample based on SEM examinations. The Excess Na is calculated by equation (4) divided by the solution volume.

Exp #	$Al(OH)_3$ xH_2O (g)	$Al(OH)_3$ (g)	$NaHCO_3$ (g)	Na_2CO_3 (g)	NaOH (g)	pH[a]	pH[b]	T °C	Time (h)	Excess Na (mol/l)	%Conversion[c]	Comment
1-1	1.21	-	5.90	-	1.85	10.1	10.1	135	2h 30 min	5.19	0 %	Amorphous gel
1-2	1.21	-	7.51	-	1.87	9.82	10.2	135	2h 30 min	6.18	0 %	Amorphous gel
1-3	1.60	-	5.91	-	1.81	10.0	10.1	135	2h 30 min	4.95	0 %	Amorphous gel
1-4	1.60	-	7.52	-	1.88	9.82	-	135	2h 30 min	5.99	0 %	Amorphous gel
2-3	-	1.30	7.53	-	1.82	9.79	-	165	48	5.92	>90 %	Crystalline
3-1	1.59	-	1.33	3.80	-	10.1	-	175	3	1.76	50 %	Crystalline
3-2	1.40	-	1.70	3.82	-	10.0	-	175	3	2.09	50 %	Crystalline
3-3	1.41	-	1.30	4.80	-	10.2	-	175	3	2.30	50 %	Crystalline
3-4	1.40	-	1.70	4.84	-	10.1	-	175	3	2.57	1-2 %	Na-carb dominates
4-2	-	1.50	0.88	3.50	-	10.2	10.2	175	5	1.21	>95 %	Crystalline
5-1	-	1.30	5.90	-	1.80	10.0	-	165	12	2.68	>90 %	Crystalline
5-2	1.41	-	1.29	3.83	-	10.1	-	165	12	1.84	>90 %	Still some $Al(OH)_3$ left
6-1	-	1.50	0.88	3.50	-	10.2	-	175	1h 45 min	1.21	>95 %	Crystalline

[a]Calculated using PHREEQC v2. assuming total dissolution of the sodium carbonates and equilibrium with boehmite.

[b]Measured at 25°C.

[c]Approximated based on SEM examinations.

Table 3. SD series batch dissolution experiment to test the stoichiometric release of elements from the synthetic dawsonite.

Experiment	Na (mmol)	Al (mmol)	Time (min)	pH
SD1-1	1.261	0.566	1	2.1
SD1-2	1.261	0.489	3	2.1
SD1-3	1.609	0.800	5	2.1
SD1-4	1.783	0.966	8	2.2
SD1-5	2.175	1.342	15	2.3
SD1-6	2.436	1.652	30	2.4
SD1-7	2.784	1.959	60	2.7
SD1-8	3.001	2.024	120	2.8
SD1-9	3.306	2.331	240	3.7
SD1-10	3.349	2.620	1395	4.1
SD2-1	0.178	n.d.[a]	2	2.0
SD2-2	0.231	n.d.	4	2.0
SD2-3	0.231	n.d.	6	2.3
SD2-4	0.331	0.032	12	2.1
SD2-5	0.483	0.093	25	2.1
SD2-6	0.666	0.163	59	2.1
SD2-7	1.740	0.747	119	2.2
SD2-8	2.305	1.185	239	2.4
SD2-9	3.132	2.083	1395	2.9

[a]n.d. refers to not measurable at the detection limit of the atomic absorption spectrometer

Table 4. A summary of the batch dissolution rate experiments. The units of the rates are log(mol/m^{2}s). Both rates and affinities $\Omega = exp(\Delta G/RT)$ of the dawsonite dissociation reaction were interpolated according to equation (11).

Exp #	Temp °C	pH	*log(Ω)* Daws	log rate
1	77	2.7	-6.58	-5.72
2	77	2.2	-8.78	-5.41
3	77	4.3	-1.38	-6.74
4[a]	77	1.6	-10.87	-4.85
5	22	2.3	-10.28	-6.53
6	22	1.6	-13.24	-6.10
7	22	1.1	-15.49	-5.49
8	22	2.7	-9.31	-7.54
9	22	0.9	-16.17	-5.33
10[b]	22	4.2	-2.74	-8.69
11[b]	22	4.3	-2.85	-8.49
12	77	2.4	-7.61	-5.35
13	77	2.3	-8.48	-5.40
14	77	4.3	-1.37	-6.48
15	77	4.8	-0.46	-6.78

[a]Experiment 4 reached more than 50% dissolution prior to first sample. Rate is therefore calculated from the concentration at first sampling.

[b]Experiments 10 and 11 did not reach 50% dissolution . Rate is therefore calculated from the last two samples.

Table 5. 22 and 77°C batch dissolution rate experiments RD1 to 15. Rates *r*- (mol/m^{2}s) are calculated according to equation (9). The solubility indices $\Omega = exp(\Delta G/RT)$ of boehmite or gibbsite and dawsonite are estimated from the experimental solutions using the PHREEQC v2 code.

Exp #	Temp °C	Time (sec)	Na (mmol)	Al (mmol)	pH (22°C)	V (l)[a]	m/m0 (m0)	log r-	*log(Ω)*	
									$Al(OH)_3$	Daws
1-0	*77*	*0*	*0.00*	*0.00*	*2.1*	*0.51*	*1 (0.273g)*	-	*-inf*	*-inf*
1-1	77	60	1.78	1.11	2.4	0.51	0.63	-5.33	-0.72	-8.01
1-2	77	180	2.35	1.74	2.7	0.50	0.49	-5.77	0.32	-6.42
1-3	77	300	2.44	1.96	2.8	0.49	0.46	-6.56	0.66	-5.95
1-4	77	465	2.52	1.96	2.8	0.48	0.44	-6.69	0.66	-5.92
1-5	77	780	2.65	2.12	3.1	0.47	0.41	-6.77	1.55	-4.68
1-6	77	1160	2.78	2.18	3.3	0.46	0.38	-6.83	2.12	-3.87
1-7	77	1830	2.91	2.21	3.7	0.45	0.35	-7.05	3.18	-2.36
1-8	77	2680	3.09	2.28	3.9	0.44	0.31	-6.99	3.67	-1.62
2-0	*77*	*0*	*0.00*	*0.00*	*1.9*	*0.52*	*1 (0.225g)*	-	*-inf*	*-inf*
2-1	77	60	1.61	1.07	2.2	0.52	0.58	-5.24	-1.35	-8.97
2-2	77	155	2.09	1.58	2.2	0.51	0.42	-5.60	-1.22	-8.59
2-3	77	300	2.26	1.85	2.3	0.50	0.37	-6.12	-0.86	-8.06
2-4	77	460	2.35	1.91	2.3	0.49	0.34	-6.43	-0.85	-8.02
2-5	77	710	2.48	2.04	2.4	0.48	0.30	-6.41	-0.53	-7.54
2-6	77	1160	2.61	2.23	2.5	0.47	0.26	-6.62	-0.20	-7.07
2-7	77	1790	2.78	2.38	2.5	0.46	0.21	-6.57	-0.18	-6.99
2-8	77	2680	2.87	2.53	2.7	0.45	0.18	-6.95	0.44	-6.15
3-0	*77*	*0*	*0.00*	*0.00*	*2.4*	*0.49*	*1 (0.207g)*	-	*-inf*	*-inf*
3-1	77	50	0.78	0.33	2.7	0.49	0.83	-5.72	-0.25	-8.04
3-2	77	160	1.30	0.67	3.6	0.48	0.66	-5.78	2.52	-3.90
3-3	77	300	1.39	0.72	4.1	0.47	0.63	-6.61	3.66	-2.19
3-4	77	460	1.44	0.74	4.2	0.46	0.61	-6.97	3.85	-1.87
3-5	77	690	1.52	0.77	4.3	0.45	0.59	-6.82	4.03	-1.54

3-6	77	1080	1.70	0.79	4.3	0.44	0.53	-6.73	4.03	-1.42
3-7	77	1780	1.96	0.73	4.3	0.43	0.46	-6.76	4.00	-1.32
3-8	77	2700	2.22	0.75	4.3	0.42	0.38	-6.81	4.01	-1.20
4-0	*77*	*0*	*0.00*	*0.00*	*1.4*	*0.52*	*1 (0.232g)*	-	*-inf*	*-inf*
4-1	77	55	2.44	2.03	1.6	0.52	0.30	-4.85	-3.03	-10.87
4-2	77	117	2.70	-	1.6	0.51	0.21	-5.40	-	-
4-3	77	195	2.78	2.65	1.6	0.50	0.19	-5.88	-2.94	-10.66
4-4	77	312	2.91	2.74	1.6	0.49	0.15	-5.81	-2.93	-10.61
4-5	77	460	3.04	2.87	1.6	0.48	0.11	-5.80	-2.91	-10.55
4-6	77	600	3.13	2.90	1.6	0.47	0.08	-5.84	-2.91	-10.52
4-7	77	800	3.18	3.19	1.6	0.46	0.07	-6.21	-2.87	-10.48
4-8	77	950	3.22	3.09	1.6	0.45	0.06	-6.01	-2.88	-10.48
5-0	*22*	*0*	*0.00*	*0.00*	*1.8*	*0.49*	*1 (0.233g)*	-	*-inf*	*-inf*
5-1	22	60	0.52	0.07	2.0	0.49	0.93	-6.56	-6.37	-14.12
5-2	22	180	1.00	0.41	2.1	0.48	0.79	-5.97	-5.31	-12.28
5-3	22	360	1.35	0.80	2.2	0.47	0.69	-6.23	-4.74	-11.32
5-4	22	585	1.61	1.24	2.2	0.46	0.61	-6.41	-4.58	-11.00
5-5	22	885	1.91	1.58	2.3	0.45	0.53	-6.42	-4.19	-10.36
5-6	22	1480	2.17	1.88	2.3	0.44	0.46	-6.73	-4.13	-10.18
5-7	22	2685	2.39	2.04	2.4	0.43	0.40	-7.06	-3.80	-9.66
5-8	22	3600	2.52	2.24	2.4	0.42	0.36	-7.13	-3.77	-9.59

Table 5 continued

Exp #	Temp °C	Time (sec)	Na (mmol)	Al (mmol)	pH (22°C)	V (l)[a]	m/m0 (m0)	log r-	*log(Ω)*	
									$Al(OH)_3$	Daws
6-0	*22*	*0*	*0.00*	*0.00*	*1.4*	*0.49*	*1 (0.233g)*	-	*-inf*	*-inf*
6-1	22	60	0.78	0.23	1.6	0.49	0.87	-6.01	-7.18	-14.91
6-2	22	170	1.52	0.91	1.6	0.48	0.65	-5.69	-6.61	-13.70
6-3	22	285	1.78	1.19	1.6	0.47	0.57	-6.08	-6.51	-13.45
6-4	22	470	2.13	1.72	1.6	0.46	0.47	-6.10	-6.37	-13.15
6-5	22	710	2.44	2.03	1.6	0.45	0.39	-6.20	-6.31	-12.97
6-6	22	1020	2.70	2.37	1.7	0.44	0.32	-6.30	-5.93	-12.40
6-7	22	1500	2.91	2.66	1.7	0.43	0.26	-6.49	-5.89	-12.29
6-8	22	2400	3.22	2.96	1.7	0.42	0.18	-6.51	-5.85	-12.17
7-0	*22*	*0*	*0.00*	*0.00*	*0.9*	*0.49*	*1 (0.231g)*	-	*-inf*	*-inf*
7-1	22	55	1.48	0.91	1.1	0.49	0.66	-5.33	-8.29	-15.94
7-2	22	180	2.26	1.80	1.1	0.48	0.42	-5.57	-8.01	-15.26
7-3	22	300	2.48	2.26	1.1	0.47	0.36	-5.98	-7.91	-15.06
7-4	22	480	2.91	2.80	1.1	0.46	0.24	-5.75	-7.83	-14.83
7-5	22	670	3.00	2.99	1.1	0.45	0.21	-6.35	-7.80	-14.78
7-6	22	900	3.18	3.05	1.1	0.44	0.16	-6.07	-7.80	-14.72
8-0	*22*	*0*	*0.00*	*0.00*	*2.3*	*0.53*	*1 (0.151g)*	-	*-inf*	*-inf*
8-1	22	120	0.40	0.07	2.3	0.53	0.90	-6.62	-5.40	-13.28
8-2	22	480	0.65	0.31	2.3	0.52	0.78	-6.49	-4.79	-12.04
8-3	22	1200	0.91	0.54	2.5	0.51	0.65	-6.72	-3.95	-10.61
8-4	22	2400	1.04	0.74	2.6	0.50	0.59	-7.19	-3.53	-9.95
8-5	22	3600	1.13	0.80	2.7	0.49	0.55	-7.33	-3.19	-9.46
8-6	22	7200	1.26	1.00	2.7	0.48	0.49	-7.60	-3.12	-9.28
8-7	22	19500	1.39	1.20	2.9	0.47	0.43	-8.09	-2.45	-8.27
9-0	*22*	*0*	*0.00*	*0.00*	*0.8*	*0.49*	*1 (0.269g)*	-	*-inf*	*-inf*
9-1	22	45	2.04	1.51	0.9	0.49	0.55	-5.06	-8.76	-16.33

9-2	22	105	2.44	2.19	0.9	0.48	0.45	-5.59	-8.60	-16.00
9-3	22	185	2.91	2.92	0.9	0.47	0.33	-5.53	-8.49	-15.69
9-4	22	300	3.22	-	0.9	0.46	0.26	-5.77	-	-
9-5	22	490	3.52	3.70	0.9	0.45	0.18	-5.87	-8.39	-15.43
9-6	22	615	3.61	3.81	0.9	0.44	0.16	-6.14	-8.38	-15.40
10-0	*22*	*0*	*0.00*	*0.00*		*0.48*	*1 (0.202g)*	-	*-inf*	*-inf*
10-1	22	120	0.47	0.05	2.7	0.48	0.93	-6.92	-4.29	-11.44
10-2	22	435	0.73	0.21	2.8	0.47	0.83	-6.61	-3.39	-9.98
10-3	22	825	0.96	0.34	2.9	0.46	0.75	-6.73	-2.90	-9.16
10-4	22	1220	1.04	0.47	3.1	0.45	0.72	-7.13	-2.17	-8.11
10-5	22	2630	1.17	0.64	3.5	0.44	0.68	-7.49	-0.86	-6.30
10-6	22	5680	1.22	0.77	4.3	0.43	0.66	-8.30	1.50	-3.09
10-7	22	13650	1.26	0.79	4.3	0.42	0.65	-8.72	1.50	-3.06
10-8	22	19680	1.26	0.77	4.3	0.41	0.65	-	1.50	-3.06
10-9	22	26280	1.30	0.76	4.3	0.40	0.64	-8.65	1.49	-2.76
10-10	22	33480	1.35	0.73	4.3	0.39	0.63	-8.69	1.49	-2.74
11-0	*22*	*0*	*0.00*	*0.00*	*2.4*	*0.49*	*1 (0.178g)*	-	*-inf*	*-inf*
11-1	22	120	0.37	0.08	2.5	0.49	0.93	-6.67	-4.71	-12.30
11-2	22	385	0.69	0.31	2.6	0.48	0.79	-6.39	-3.85	-10.64
11-3	22	800	0.91	0.51	2.8	0.47	0.71	-6.67	-3.05	-9.40
11-4	22	1320	1.04	0.72	2.9	0.46	0.66	-6.98	-2.62	-8.72
11-5	22	2620	1.22	0.91	3.2	0.45	0.59	-7.22	-1.64	-7.29
11-6	22	5020	1.30	1.01	3.7	0.44	0.56	-7.77	-0.11	-5.20
11-7	22	7660	1.35	1.06	4.1	0.43	0.55	-8.10	1.09	-3.57
11-8	22	10710	1.39	1.07	4.3	0.42	0.53	-8.16	1.52	-2.91
11-9	22	16740	1.44	1.09	4.3	0.41	0.52	-8.46	1.52	-2.88
11-10	22	23280	1.48	1.14	4.3	0.40	0.51	-8.49	1.52	-2.85

Table 5 continued

Exp #	Temp °C	Time (sec)	Na (mmol)	Al (mmol)	pH (22°C)	V (l)[a]	m/m0 (m0)	log r-	*log(Ω)*	
									$Al(OH)_3$	Daws
12-0	*77*	*0*	*0.00*	*0.00*		*0.40*	*1 (0.198g)*	-	*-inf*	*-inf*
12-1	77	60	2.65	1.03	2.4	0.40	0.53	-5.34	-0.76	-7.82
12-2	77	180	3.61	1.38	2.8	0.39	0.25	-5.39	0.53	-5.84
12-3	77	300	3.74	1.48	2.9	0.38	0.22	-6.05	0.85	-5.39
12-4	77	480	3.83	1.59	3.0	0.37	0.19	-6.36	1.16	-4.95
12-5	77	720	3.87	1.70	3.2	0.36	0.18	-6.76	1.76	-4.15
12-6	77	1080	3.91	1.77	3.4	0.35	0.17	-6.92	2.32	-3.37
12-7	77	1500	3.96	1.83	3.6	0.34	0.16	-6.97	2.86	-2.62
12-8	77	2700	4.44	1.89	4.0	0.33	0.05	-6.20	3.81	-1.15
13-0	*77*	*0*	*0.00*	*0.00*		*0.40*	*1 (0.147g)*	-	*-inf*	*-inf*
13-1	77	60	2.22	0.68	2.3	0.40	0.51	-5.39	-1.21	-8.51
13-2	77	180	2.74	0.87	2.4	0.39	0.31	-5.55	-0.82	-7.89
13-3	77	300	3.00	1.04	2.4	0.38	0.22	-5.67	-0.76	-7.73
13-4	77	480	3.09	1.10	2.4	0.37	0.18	-6.22	-0.74	-7.68
13-5	77	720	3.13	1.21	2.5	0.36	0.17	-6.60	-0.40	-7.23
13-6	77	1080	3.22	1.26	2.6	0.35	0.14	-6.43	-0.09	-6.78
13-7	77	1500	3.26	1.30	2.6	0.34	0.12	-6.74	-0.08	-6.76
13-8	77	2700	3.35	1.36	2.6	0.33	0.10	-6.83	-0.06	-6.72
14-0	*77*	*0*	*0.00*	*0.00*	*2.4*	*0.51*	*1 (0.200g)*	-	*-inf*	*-inf*
14-1	77	60	0.87	0.60	3.6	0.51	0.74	-5.49	2.48	-4.22
14-2	77	225	1.13	0.70	4.3	0.50	0.63	-6.19	3.99	-1.82
14-3	77	300	1.17	0.75	4.3	0.49	0.61	-6.59	4.02	-1.76
14-4	77	600	1.39	0.88	4.3	0.48	0.54	-6.47	4.08	-1.53
14-5	77	1200	1.74	0.92	4.4	0.47	0.42	-6.50	4.24	-1.06
14-6	77	1800	2.09	0.95	4.4	0.46	0.30	-6.39	4.25	-0.89
14-7	77	2700	2.39	0.94	4.5	0.45	0.21	-6.48	4.37	-0.55

15-0	*77*	*0*	*0.00*	*0.00*	*2.7*	*0.48*	*1 (0.200g)*	*-*	*-inf*	*-inf*
15-1	77	60	0.74	0.37	3.8	0.48	0.83	-5.75	2.78	-3.95
15-2	77	180	0.87	0.41	4.3	0.47	0.78	-6.45	3.77	-2.29
15-3	77	300	0.91	0.44	4.3	0.46	0.77	-6.92	3.80	-2.22
15-4	77	600	1.17	0.48	4.4	0.45	0.68	-6.52	3.97	-1.70
15-5	77	1200	1.57	0.64	4.7	0.44	0.56	-6.59	4.40	-0.70
15-6	77	1840	1.78	0.65	4.8	0.43	0.49	-6.81	4.47	-0.42
15-7	77	2820	2.04	0.53	5	0.42	0.41	-6.86	4.46	-0.11

[a]Volume experimental solution before sampling

Figures

Fig. 1

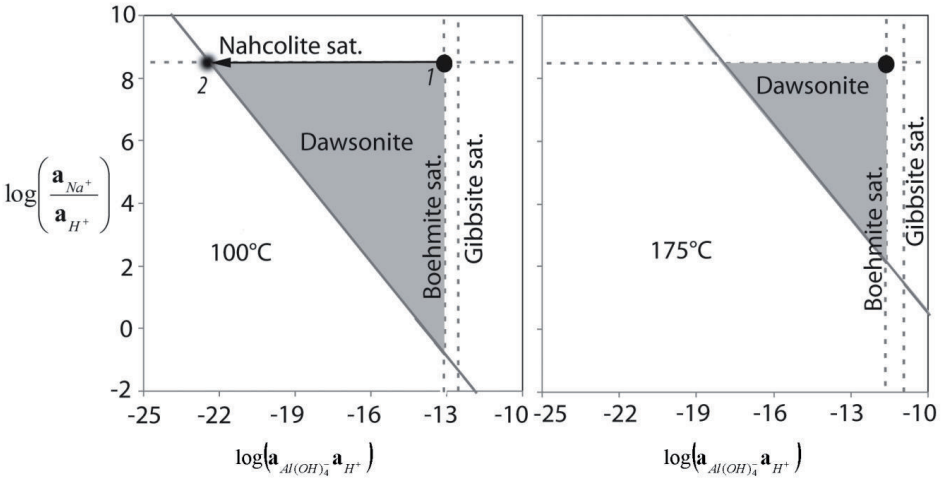

Fig, 2

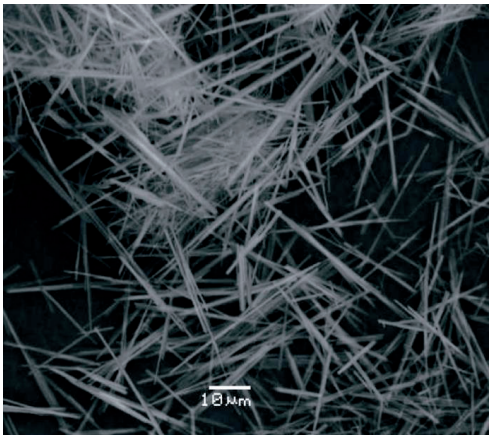

Fig.3

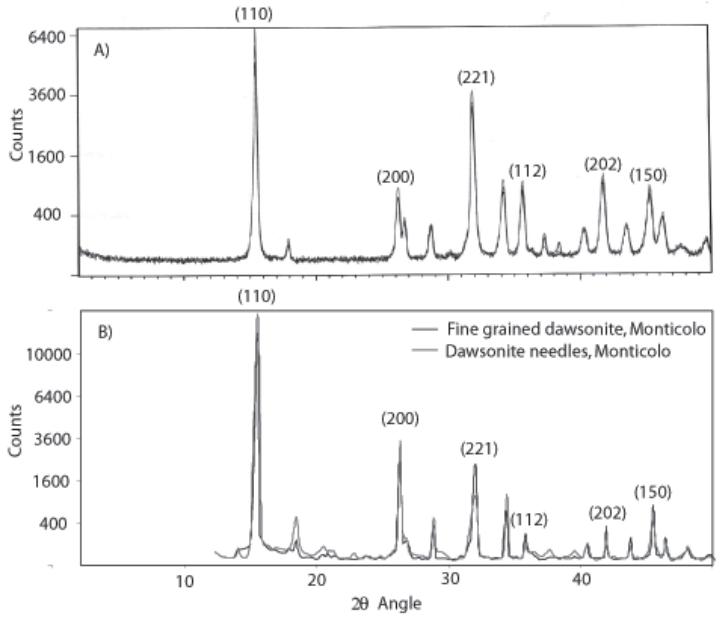
(110)
A)
6400
3600
1600
400
Counts
(221)
(200)
(112)
(202)
(150)
(110)
B)
Fine grained dawsonite, Monticolo
Dawsonite needles, Monticolo
10000
6400
3600
1600
400
Counts
(200)
(221)
(112)
(202)
(150)
10
20
30
40
2θ Angle

Fig. 4

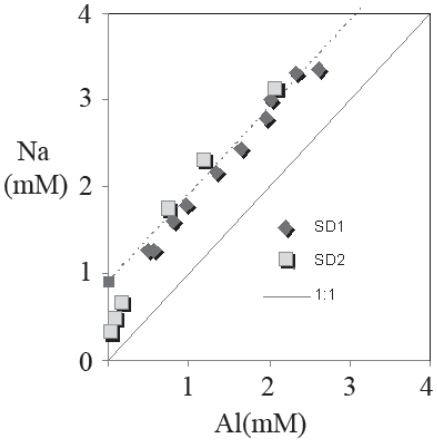
4
3
2
1
0
Na
(mM)
SD1
SD2
1:1
1
2
3
4
Al(mM)

Fig 5.

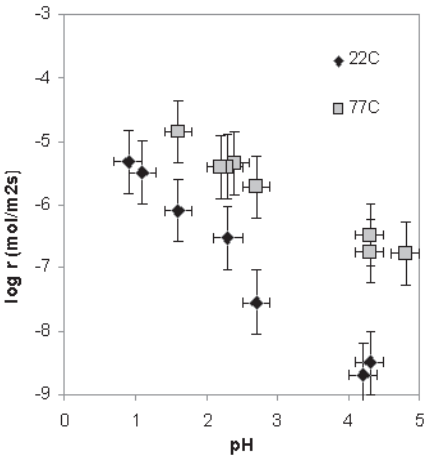

Fig. 6.

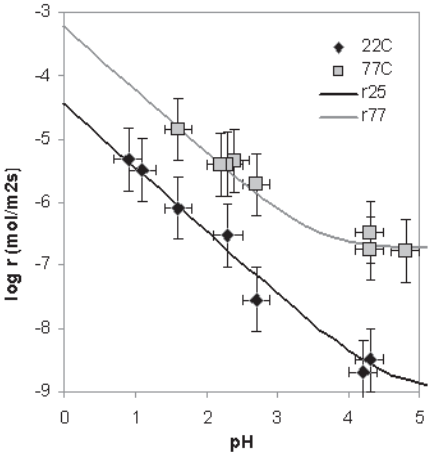

Fig. 7.

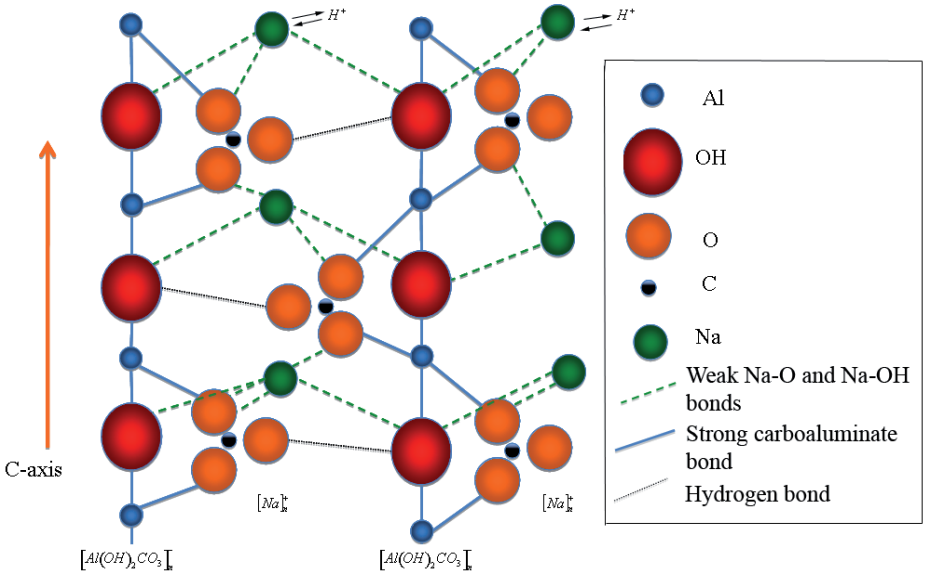
H+
H+
C-axis
[Na]+n
[Na]+n
[Al(OH)2CO3]n
[Al(OH)2CO3]n
Al
OH
O
C
Na
Weak Na-O and Na-OH bonds
Strong carboaluminate bond
Hydrogen bond

Appendix 1: Report on Dawsonite synthesis,

J. Declercq[1], Y. Jia[1], H. Hellevang[2], P. Aagaard[1]

[1]Department of Geosciences, University of Oslo, BP. 1047, Blindern, Oslo.

[2]Department of Earth Sciences, University of Bergen, Allégaten 41, 5007 Bergen.

1. Introduction

Green house gases such as CO_2 are responsible for a global temperature change. One way to reduce emissions to the atmosphere is to capture CO_2 from large anthropogenic point sources and inject it into geological formations. To understand the temporal and spatial behaviour of CO_2 in a reservoir with a long-term perspective (hundreds to thousands of years), it is important to study interactions between the CO_2, water and minerals. Dawsonite ($NaAl(OH)_2CO_3$) has been suggested to play an important role as a storage host for CO_2 (Johnson et al., 2004; Hellevang, 2006). Natural occurrences and numerical work suggest that dawsonite form from aqueous solutions containing sodium, aluminium, and sufficient dissolved CO_2 according to:

$$Na^+ + Al^{3+} + 2H_2CO_3 + H_2O \rightarrow NaAl(OH)_2CO_3 + CO_{2,aq} + 4H^+ \quad (1)$$

The stability of the dawsonite can be expressed as:

$$\Delta G = \Delta G^0 - RT \ln Q\,, \quad (2)$$

where ΔG^0 is the standard state Gibbs free energy of reaction (1), R is the gas constant, T is temperature, and Q is the activity product for reaction (1) given by:

$$Q = \frac{a_{H^+}^4 K_{CO_{2,g} \rightarrow CO_{2,aq}} f_{CO_2}}{a_{Na^+} a_{Al^{3+}} a_{H_2CO_3}^2 X_{H_2O}}, \quad (3)$$

where a is activity, f is fugacity, K is the pressure-corrected Henrys law constant for CO_2, and X is mole fraction. From expressions (2) and (3) it is evident that dawsonite will have an increased stability as the CO_2 fugacity increases at constant pH. This requires a buffering of the pH change as CO_2

dissolves. This is accomplished in most reservoirs by dissolution of carbonates like calcite or aragonite that are present prior to the CO_2 injection. Dawsonite is thus stable and expected to form in most saline aquifers (Hellevang, 2006).

To understand the significance of dawsonite during CO_2 storage, both the thermodynamic and kinetic stability must be known. The thermodynamic value is well established (ref), whereas little information is known about the reaction rate of dawsonite. The first data suggests that at 80°C and far-from-equilibrium conditions, the rate is constant with pH between 4 and 9 (Hellevang et al., 2005). To fully understand the reactivity and implement the reaction rates into numerical codes, the rate need to be examined over a larger pH range, at different temperatures, different salinities, and different affinities. In addition is the reaction order with respect to aqueous aluminium and sodium valuable. The experimental work by Hellevang et al., (2005) was performed on a very limited amount of natural dawsonite. To perform further comprehensive experiments more dawsonite is needed. Since pure natural dawsonite is hard to obtain in sufficient amounts, one option is to use synthetic material. The requirement for synthetic dawsonite is that it resembles the natural material to a close degree, i.e. similar crystal morphology and crystal size, and the same chemical composition. Several studies have reported chemistries, habit and crystal size of natural occurring dawsonite. One characteristic feature is the thin fibrous or needle shaped crystals that form in fractures and in pore space.

The objectives of this study are: (1) to produce synthetic dawsonite that resembles natural material; (2) to synthesize a homogeneous batch of material at a quantity sufficient to use it as a well-characterized standard-material for reaction rate studies; and (3) to perform extensive reaction rate studies to establish the role of dawsonite in a CO_2 storage setting. In addition, some work will be focused in understanding the mechanism of dawsonite precipitation and how factors like differences in solution chemistry can affect precipitation rate, habit, and crystal size.

2. Materials and Methods

2.1. Dawsonite synthesis

2.1.1 Chemicals

All the chemicals used were analytical grade and used as received. Sodium carbonate (Na_2CO_3), sodium bicarbonate ($NaHCO_3$), gibbsite ($Al(OH)_3$), citric acid ($C_6H_8O_7$), urea ($(NH_2)_2CO$), and amino-acids were purchased from Merck (Darmstadt, Germany). Water used in the synthesis is of Milli-Q quality deionised/demineralized H_2O.

2.1.2 Apparatus

50 ml Teflon liners with reactive solutions is placed inside an autoclave that is in turn placed within a heating oven on a rotating stage. The capacity of the oven is four simultaneous autoclaves. Temperature of the oven is specified and thermostatically controlled. A thermometer monitors the temperature. pH of reactive solutions are measured with a standard pH electrode. All reactants are weighted with an accuracy of four digits.

2.1.3. Experimental procedures

Preliminary studies have shown that a temperature of 160-175°C is required to completely convert the reactant solution to dawsonite. The preliminary study also suggests that $Al(OH)_3$ and the sodium carbonates provides a good source for the Dawsonite precipitation. Based on this dawsonite is synthesized following the present procedure:

1). The stock solution (S) was prepared by dissolving Na_2CO_3 and $NaHCO_3$ in Milli-Q water. The concentration was 0.33 M and 0.1 M for Na_2CO_3 and $NaHCO_3$, respectively. An exception of this is Series 11 (see section 2.1.5).

2). After 1.5 g $Al(OH)_3$ was added, 24 ml S was transferred into a liner. If additive for instance urea, citric acid, or amino acid was used, then these chemicals were supplied before the S was supplied. A detailed experiment set up is presented in Table 1, where the amount of additive is given.

3). The mixture in the liner from step 2) was mixed using an magnetic stirrer at room temperature for 10-15 min.

4). After weighing the liner with chemicals, the liner was put into an autoclave, and the autoclave was sealed to resist any pressure increases.

5). The autoclave was put into an oven with a rotating stage for some period (typically 5 hours, except in experiment to obtain time-dependence effects on synthesized dawsonite; see section 2.1.4), the experimental temperature and length of the experiment were presented in Table 1.

6). When the experiment was finished, the liner was taken out and cooled down in cold water. The weight of the liner with chemicals was measured again to ensure that no leakage occurred during the experiment.

7). The liner was then withdrawn from the autoclave and the chemical product (dawsonite) was filtered through 0,22μm micropore filters by a vacuum pump. Unless specified, the reaction temperature was 165 ^{o}C.

8). The dawsonite product was dried at 60^{o}C for 24 h.

9). The product was then ready for further analysis (see Section 2.1.6).

2.1.4. Time-dependence of crystallization (Series 10)

To get information about possible effects of time (time of synthesis in the oven) on the synthetic dawsonite, experiments with identical initial reactive solution (series 10) were run at different reaction times. The kinetics study for the series 10 was based on previous result from the preliminary studies (not included in the present study). In Series 10, the reaction time was chosen to be 1.75, 2.5, 3.25 and 4 h for No. 37, No. 36, No. 35, and No. 34, respectively. Detailed information for this series is presented in Table 1.

Table 1. Experiment setup for different purposes.

Series	No.	S (ml)	$Al(OH)_3$ (g)	Citric acid (mg)	Urea (g)	Reaction time (h)
10	34	24	1,50	-	-	4
10	35	24	1,50	-	-	3,25
10	36	24	1,50	-	-	2,5
10	37	24	1,50	-	-	1,75
11	38	20	0,50	-	-	5
11	39	20	0,50	33	-	5
11	40	20	0,50	66	0.66	5
12	41	24	1,50	-	-	5
12	42	24	1,50	50	-	5
12	43	24	1,50	100	-	5
12	44	24	1,50	250	-	5
13	45	24	1,50	-	-	5
13	46	24	1,50	-	1	5
13	47	24	1,50	-	2	5
13	48	24	1,50	-	4	5
14	49	24	1,50	50	2	5
14	50	24	1,50	50	1	5
14	51	24	1,50	100	2	5
14	52	24	1,50	100	1	5

2.1.5. Different additive effect

A preliminary test for the effect of different additives to the reactive solution on the synthesized dawsonite was done using citric acid and urea (Series 11) in according to US patent (5,078, 983) with some modification. In this Series, NaOH was used instead of Na_2CO_3. In the S, the concentration of NaOH and $NaHCO_3$ was 1.8 M and 1.6 M, respectively. Based on Series 11, separate series using citric acid (Series 12) and using urea (Series 13) as an additive was performed. To study the inter-reaction between different concentration of citric acid and urea, Series 14 was performed. More information for this Series is presented in Table 1.

2.1.6. Analysis

Physical characterization of dawsonite was performed using a JSM-6460LV scanning electron microscopy (SEM, JEOL, Japan) with an energy dispersive X-ray analysis system. This allows identification of changes in the particle morphology during the experiments. The SEM also allows semi-quantitative measurements of the chemistry of individual dawsonite crystals. To identify the mineral composition, analyses were performed using X-ray diffraction (XRD, X'Pert MPD, Philips, Netherlands) with X'Pert software (Version 6.1).

2.2. Reaction rate experiments

The dawsonite synthesis experiments have provided enough information to be able to start the reaction rate experiments. As will be presented under section 3, a simple mixture of $Al(OH)_3$, Na_2CO_3, $NaHCO_3$ and Milli-Q water heated to 165°C at the vapour pressure of the aqueous phase, produces dawsonite crystals that resembles natural material. We have enough of this material to start our reaction rate experiments, and will produce further identical material to make a standard solution. Two experimental setups are proposed for the reaction rate experiments. Details are given below.

2.1. Experimental Apparatus.

For the dawsonite far-from-equilibrium reaction rate experiments we have chosen two different types of reactors: (1) a titanium Parr™ mixed flow reactor with magnetic stirrer (Fig. 1); and (2) a shaker bath reactor setup for up to eight simultaneous experiments (Fig. 2).

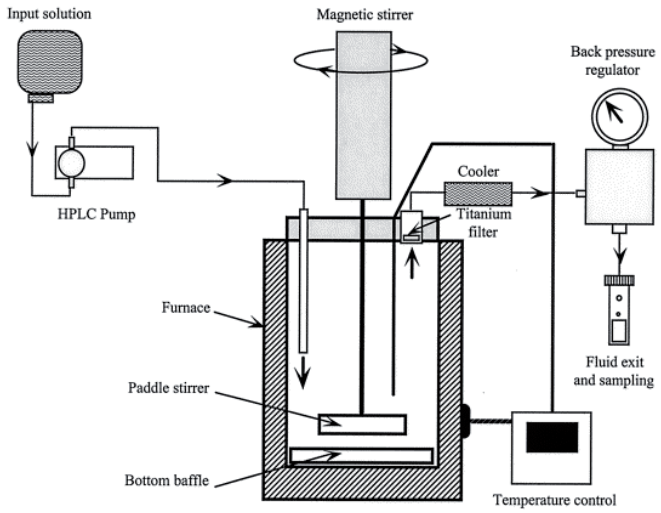

Fig. 1. Scheme of the mixed flow reactor (from Gautier et al., 2000)

For the titanium Parr™ reactor the temperature is controlled by a thermocouple linked to the oven and the inlet and outlet fluid rate are controlled by a Gilson minipulse pump and a backpressure regulator. The outlet rate is set to provide measurable concentration in the outlet solution.

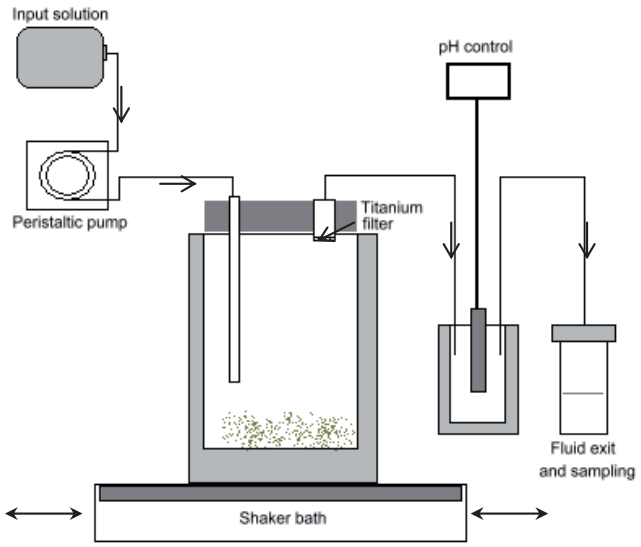

Fig. 2. Scheme of a shaker-flow reactor system.

The other experiment takes place in a shaker bath which ensures stirring of reactants without mechanical grinding, and provides adequate temperature up to 80°C. Eight experiments can be done simultaneously, with inlet fluids delivered from a Gilson peristaltic pump (Fig 3).

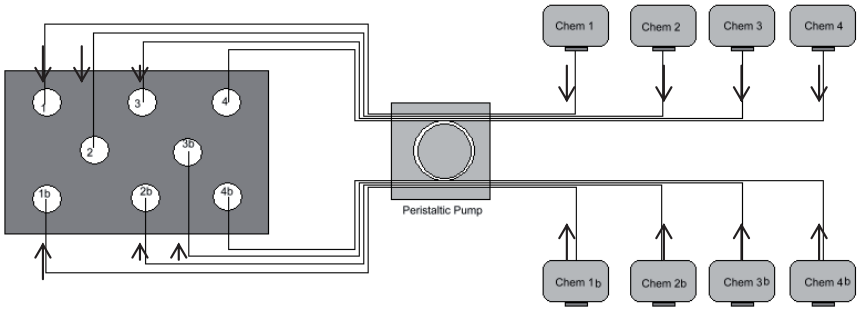

Fig. 3. Scheme of the experimental system (8 simultaneous shaker-flow reactors).

With that system we can modify for each individual reactor the chemical composition of the inlet solution and also the flow rate. We adjust this rate by changing the diameter of each tube. The temperature is the same for the whole bench.

3. Results

Table 2. Summary of XRD and SEM results for the different series.

Series	No.	XRD no.	XRD-result	SEM-result	Shape-SEM
10	34	4691B	Excellent	Excellent	Fibre
10	35	4692B	Excellent	Excellent	Fibre
10	36	4693B	Excellent	Excellent	Fibre
10	37	4694B	Excellent	Excellent	Fibre
11	38	4695B	Bad	Excellent	Fibre
11	39	4696B	Bad	Bad, with some aggregate	Particles
11	40	4697B	Bad	Bad, with some aggregate	Particles, with small fibre
12	41	4698B	Excellent	Excellent	Fibre
12	42	4699B	OK	Bad	Particles, with small fibre
12	43	4700B	OK	Bad	Particles, with small fibre
12	44	4701B	OK	Bad	Particles, with small fibre
13	45	4702B	Excellent	Excellent	Fibre
13	46	4703B	GOOD	Excellent	Fibre
13	47	4704B	Excellent	Excellent	Fibre
13	48	4705B	Excellent	Excellent	Fibre
14	49	4706B	Excellent	Bad	Particles
14	50	4707B	Excellent	Bad	Particles
14	51	4708B	Excellent	Bad	Particles
14	52	4709B	Excellent	Bad	Particles

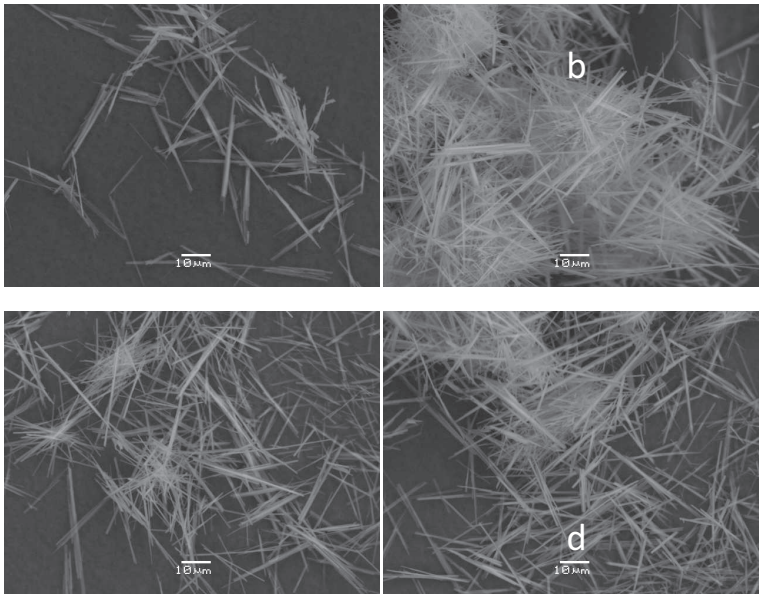

Fig. 4. SEM micrographs of produced dawsonite at different reaction time (Series 10). Reaction time was 4 hours (a), 3.25 hours (b), 2.5 hours (c) and 1.75 hours (d).

3.1. Dawsonite synthesis

3.1.1 Time dependence of synthesized dawsonite

Knowledge of the time-dependence of crystal structure and habit of synthesized dawsonite was examined by a series of experiments with identical initial chemical composition (series 10; table 2, Fig, 4). Experiments comprised 1.75, 2.5, 3.25 and 4 hours at 165C for the four respective experiments. Fig. 4 shows that dawsonite produced have a fibrous or needle-like habit with average crystal sizes (longest dimension) of 20-40 μm. Width of individual crystals is maximum 1-2 μm. At the present experimental times (from 1.75 to 4 hours) it is no obvious difference between the resultant crystal habit. Also XRD presented in Fig. 5. suggests that the main crystallographic features are close to identical for the four experiments.

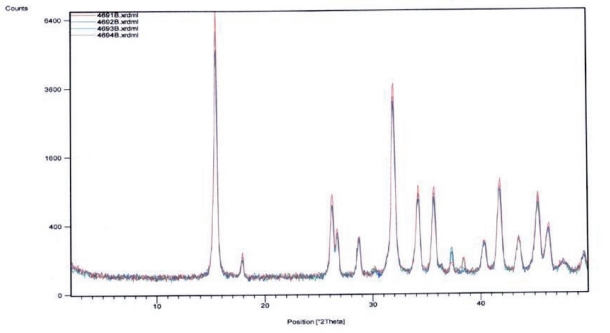

Fig. 5. XRD results for Series 10. In the figure, 4691B, 4692B, 4693B and 4694B represents No.34, 35, 36 and 37, respectively.

3.1.2 Effect of additives on synthetic dawsonite

The preliminary studies suggest that the amount of dawsonite that form and the crystal morphology show a strong dependence on the initial chemical composition. For example, changing source of aluminium from two different $Al(OH)_3$ powders (crystalline and amorphous) strongly affects how much dawsonite that forms. This is probably due to different rate of aluminium hydroxide dissolution. Also sodium source is expected to affect the precipitation of dawsonite. The experiments in this study use the aluminium source that provided the fastest dawsonite precipitation.

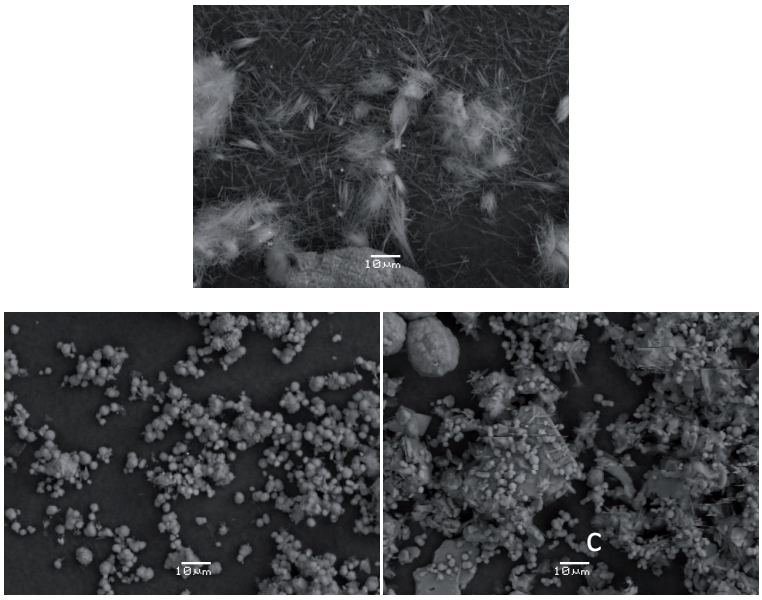

Fig. 6. SEM micrographs of produced dawsonite with different additive (Series 11). In the figure, a = control, b = citric acid, c = citric acid + urea.

One experimental series was devoted to examine the effect of partly replacing Na_2CO_3 and $NaHCO_3$ with NaOH as a sodium source. The result is illustrated in Fig. 6a. The figure suggests that the dawsonite habit change moderately. The experiment suggests formation of bigger aggregates of dawsonite crystals. XRD images of experiments using NaOH as a source suggest that some of the reactant minerals are still present in the final assemblage. In addition to changing the sodium source, the effect different additives have on the dawsonite precipitated have been examined. Fig. 6b and c shows results after adding citric acid (6b) and citric acid together with urea (6c). The latter two suggests that citric acid strongly inhibit growth of dawsonite. Adding urea to the mixture produces the same results as if only the citric acid was added. Natural dawsonite is needle shaped with a preferential growth in the crystallographic z-direction. Fig. 6 together with XRD data in Fig. 7 suggest that growth in the z-direction is inhibited, producing nearly spherical or irregular crystals. XRD data also suggests that the transformation from reactants to dawsonite may be incomplete in these experiments (Fig 7). The average size of the dawsonite particle is 1 µm when citric acid is present in the reagent. The XRD results show a big difference between different batches regarding the total number of mineral peaks and height.

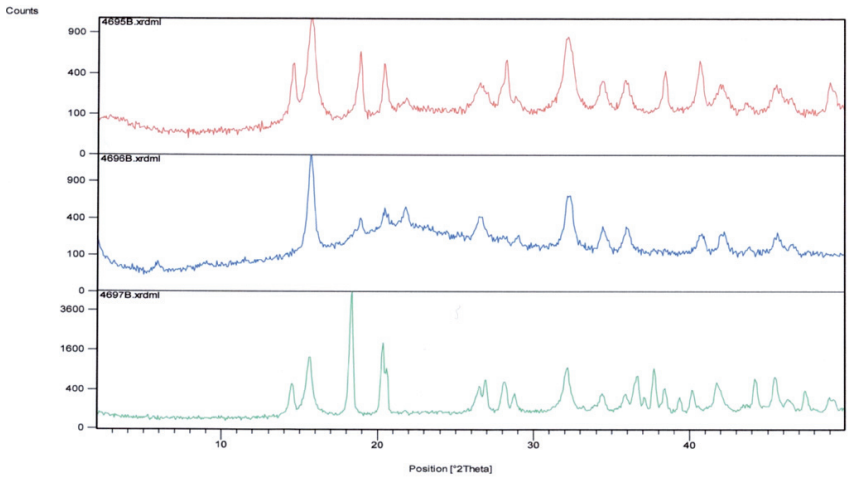

Fig. 7. XRD results for Series 11. In the figure, 4695B, 4696B, and 4697B represents No.38, 39, and 40, respectively.

Fig. 8 shows SEM images for series 12 with citric acid added to the standard assemblage. The figure suggests that dawsonite form needles, but at a much lower extent than experiments without citric acid. It is evident that the crystallographic z-direction is inhibited, and it is also expected that the other crystallographic growth directions are affected. XRD results show that there has some gibbsite left in the product for samples of No. 42, No. 43 and No. 44 (data not shown). This suggests that for the transformation of gibbsite and sodium carbonate to dawsonite the latter is the kinetically limiting factor, whereas the $Al(OH)_3$ source was suggested to be limiting in the preliminary studies.

Fig. 9 shows series 13 that is ran with different amounts of urea added. The figure suggests that the effect of urea on shape of dawsonite is minor. XRD results (data not shown) suggest that all the reactants are consumed and that dawsonite is the only product.

The effect of combining different amounts of different additives is demonstrated in Fig. 10. The two additives are urea and citric acid. In Fig. 10, urea effect is compared at low citric acid concentration (Fig. 10a versus 10b), and at high citric acid concentration (Fig. 10c versus 10d). Concerning citric acid effect isolated, comparison can be made by looking at Fig. 10a versus 10c or comparing Fig. 10b and 10d. The SEM results suggest that at high urea concentration, the higher the citric acid concentration, the smaller the crystal size. The XRD results show that there have some un-reacted gibbsite left in samples No. 49 and No. 51.

4. Discussion

4.1. Time dependence on dawsonite formation

The present study agrees very well with the previous preliminary study in dawsonite synthesis. It therefore suggests that the experimental method used in the present study is reproducible and reliable. The kinetics results show that the complete transformation from reactants to crystalline dawsonite (without adding additives) is less than 1.75 h.

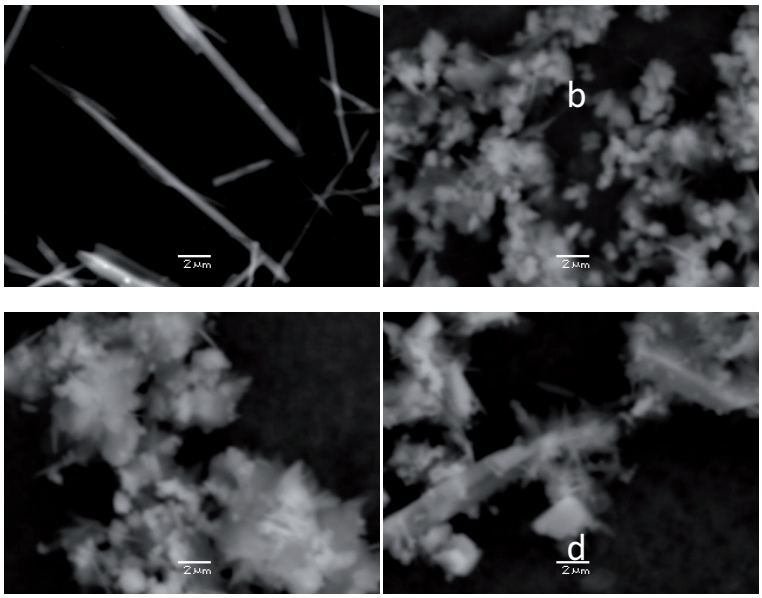

Fig. 8. SEM micrographs of produced dawsonite with additive citric acid at different concentration (Series 12). In the figure, a: 0 mM citric acid, b: 0.24 mM citric acid, c: 0.48 mM citric acid and d: 1.19 mM citric acid.

4.2. The effect of additives on the dawsonite formation

The use of NaOH decreases length of needles significantly in comparison with that of using Na_2CO_3. Nevertheless, both SEM and XRD suggest that the quality of dawsonite produced here were not of acceptable level since other minerals were recorded. It seems therefore that some chemicals were not

reacted, which is confirmed by XRD results that gibbsite was detected in the product (not shown). It might be due to that concentration of NaOH was too high. A dilution of concentration of reagent might be needed in the future experiment endeavour.

The results from Series 11 suggest that the proposition of reagents need to be taken into consideration. There might have some residue left in the liquid phase after the termination of the experiment. This is the case no matter if the additive is present in the reagents. Therefore, future study should continue on this topic to achieve an optimized ratio of the reagents.

The presence of additives might change the morphology of the dawsonite. For instance, the presence of citric acid slowed down the growth of crystal in all axes. It seems that citric acid is attached or covered on the surface of dawsonite, which inhibits the growth of crystal in any direction upon reaction. Therefore citric acid is not an ideal candidate for the application as an additive itself. In contrast to the presence of citric acid changes morphology significantly, the morphology of dawsonite has minor changes with respect to the presence of urea. Our results for Series 12 suggest that concentration of urea has a miner effect on crystallization, this holds for at least within the tested concentration range. However, inter-reaction between urea and citric acid shows more complicated phenomena, and more work needs to be performed in this regards.

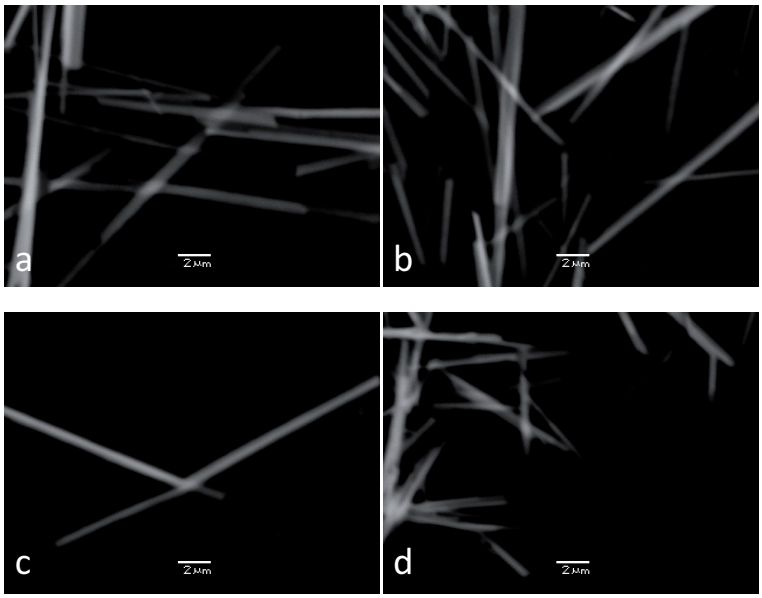

Fig. 9. SEM micrographs of produced dawsonite with urea at different concentration (Series 13). In the figure, a: 0 M urea, b: 0.69 M urea, c: 1.39 M urea and d: 2.78 M urea.

5. Conclusion

The present study presents detailed procedures for synthesis of dawsonite. The results suggest that the method used is reproducible and reliable. Dawsonite with crystal habit that resembles natural samples is easily produced. The presence of additives such as citric acid will change the morphology of dawsonite as it inhibits growth in the crystallographic z-direction. The present work is the basis for the next stage of experiments which comprise: (1) to achieve the reaction rate of dawsonite at different chemical conditions; and (2) further studies on the precipitation of dawsonite at various chemical conditions.

6. Future work

6.1. Dawsonite synthesis

Synthetic dawsonite has the same habit as found in nature, i.e. needle shaped highly elongated in the crystallographic z-direction. This study reports inhibiting effects of citric acid on growth of dawsonite. Further studies on possible inhibiting effects of additives are valuable to understand the formation of dawsonite in natural solutions. This work is ongoing. Some other effect not yet examined is the effect CO_2 pressure may have on dawsonite growth. It is well known that the affinity of reacting dawsonite is dictated by the CO_2 pressure, but the effect on growth mechanism is unknown. The present report focus on work performed at high pH. In the natural CO_2 storage setting the pH will be acidic. The possibility of precipitating dawsonite in acidic environments has immense importance in understanding the formation of dawsonite in a natural CO_2 storage setting. Thus, work should be done to understand precipitation of dawsonite in acidic environments.

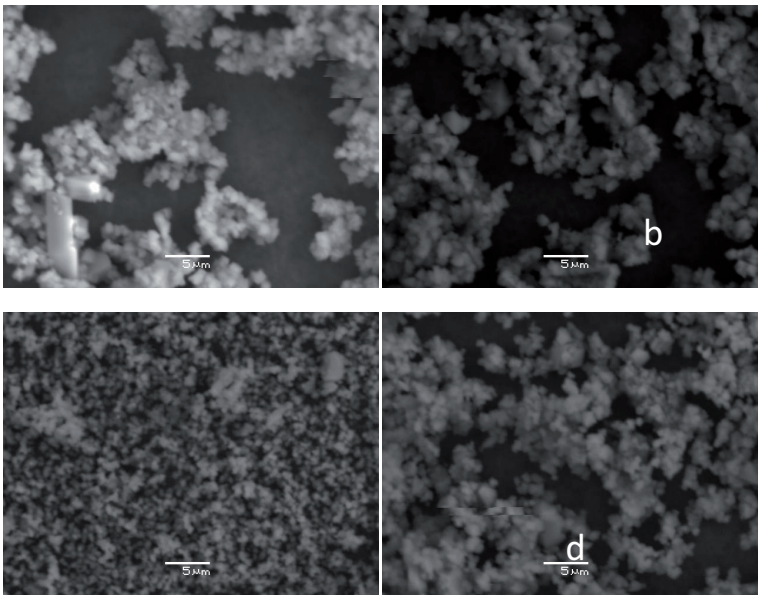

Fig. 10. SEM micrographs of produced dawsonite with additives citric acid and urea at different concentration (Series 14). In the figure, a: 0.24 mM citric acid + 1.39 M urea, b: 0.24 mM citric acid + 0.69 M urea, c: 0.48 mM citric acid + 1.39 M urea and d: 0.48 mM citric acid + 0.69 M urea.

6.2. Reaction rate experiments

The reason for making synthetic dawsonite is two-fold: (1) to understand at what conditions dawsonite form and the nature of precipitated dawsonite; and (2) to produce dawsonite that resembles natural material for the reaction rate experiments. The latter is important for numerical simulations to understand long-term reactivity of CO_2 in reservoirs. This study shows good growth of dawsonite crystals that resembles natural dawsonite habit, and it is easily reproduced by repeated experiments (e.g., series 10; table 2; Fig. 4). We have decided to use the procedure described for series 10 ran for 4 hours to produce a dawsonite standard for use in kinetic experiments. This standard will be used in the reaction rates studies in the laboratory at Institute of Geoscience at UoO, and will also be available for other laboratories if they would like to run alternative reaction rate experiments on the precise same precipitated dawsonite. As shown in section 2.2, two alternative setups are ready for performing reaction rate studies of dawsonite. The reaction rate studies will be started by end of November, 2006.

References

Gautier, J.-M., Oelkers, E.H., Schott, J., 2001. Are quartz dissolution rates proportional to BET surface areas? *Geochim. Cosmochim. Acta.*, **65**, 1059-1070.

Hellevang, H., Aagaard, P., Oelkers, E.H., Kvamme, B., 2005. Can dawsonite permanently trap CO2? *Environmental Science & Technology,* **39**, 8281-8287.

Hellevang, H., 2006. Interactions between CO_2, saline water and minerals during geological storage of CO_2. *PhD thesis, University of Bergen, Norway.*

Johnson, J.W., Nitao, J.J., and Knauss, K.G. (2004) Reactive transport modeling of CO2 storage in saline aquifers to elucidate fundamental processes, trapping mechanisms and sequestration partitioning. In: Baines, S.J., and Worden, R.H. (eds), Geological Storage of Carbon Dioxide. *Geological Society, London, Special Publications,* **233**, 107-128.

US Patent (5,078,983), 1992. Process for producing dawsonite. Pp7.

Appendix 2 : Posters

Goldschmidt 2007, August 2007, Cologne – Germany Reactivity of Rhyolitic Glass.
J.Declercq, E.H.Oelkers

Abstract - The steady-state dissolution rates of Öraefajökull rhyolitic glass were measured as a function of aqueous Si and Al concentration at temperatures from 40°C to 200°C and for pH from 2 to 10.4. Constant temperature and pH dissolution rates are independent of aqueous Si concentration but increase with decreasing aqueous aluminium concentration. All measured dissolution rates were found to be consistent with:

$$r_+ = k_+ . \exp\left(\frac{-E_A}{RT}\right) . \left[\frac{a_{H^+}^3}{a_{Al}^{3+}}\right]^{0.18}$$

where r_+ refers to the dissolution rate, k_+ represents a rate constant equal to 0.031 mol.cm^{-2}.s^{-1}, E_A denotes an Activation Energy equal to 77.3 kJ mol^{-1}, R designates the gas constant, T correspond to the absolute temperature and a_i defines the activity of the subscripted aqueous species. This rate behaviour is similar to that previously proposed for basaltic glass. This similarity suggests similar dissolution mechanism of all natural volcanic glasses consisting of the sequential removal of metals from the glass structure via proton exchange reaction. The overall dissolution rate, however, is controlled by the detachment of Si tetrahedral that have been partially liberated from the glass structure through the removal of adjoining Al.

Reactivity of a Ryolitic Glass

J. Declercq and E. H. Oelkers
julien.declercq@geo.uio.no
Laboratoire des Mécanismes et Transferts en Géologie

Introduction

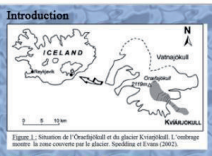

Figure 1 : Situation de l'Öraefajökull et du glacier Kviarjökull. L'ombrage montre la zone couverte par le glacier. Spedding et Evans (2002).

The dissolution of volcanic glass had a major role in natural process. There is about 1 km3 of glass produced every year, mostly along the ocean volcanic ridges. The weathering of the oceanic floor, mostly formed of basalts influence the global ammount of CO2 in the atmosphere and so the climate on a long term. This study follow the one from Oelkers and Gislason where the dissolution mecanism of the basaltic glass was defined.
Our goal in this study is to is to demonstrate that the dissolution mecanism of basalt can be extended to the rhyolite.

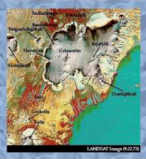

The glass sample came from the Oraefajokull, one of the most active volcanoes in Iceland. Thes samples used in this study are from the 1367 eruption. It was the biggest historical eruption of Iceland, a plinnian eruption with a VEI of 5.

SiO_2	TiO_2	Al_2O_3	Fe_2O_3	FeO	MnO	MgO	CaO	Na_2O	K_2O	P_2O_5
70.6	0.24	13	2.4	1.18	0.1	0.02	0.97	5.45	3.41	0.02

The composition of the glass shows a high silica content (>60 wt% SiO2) and a (Na2O +K2O) content of 8.86. According to the TAS classification it is a rhyolite.

Dissolution Mechanism of Basaltic glass

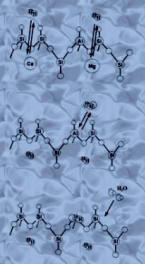

The dissolution mecanism of basaltic glass as been extensively studied and is now well known.
The dissolution mechanism of the basaltic glass begin with a metal – proton exchange reaction where monovalent and divalent cations are exchanged. These permutations are followed with the partial removal of trivalent cations in a reaction of proton exchange.
The final and slowest step of the dissolution process is the departure of the silica atoms from the glass structure (Oelkers and Gislason, 2001). In this mechanism the activated complex is formed by the silica thetraedral bounded to one of the of the aluminium site. This site is replaced by oxygen. We can calculate the concentration of the activated complex with a law of mass action of the reaction.

$$r_+ = Ae^{-\left(\frac{E_a}{RT}\right)}\left(\frac{a_{H^+}^3}{a_{Al^{3+}}}\right)^{1/n}$$

This equationdescribe the dissolution of the basaltic glass with respect to the composition of the aqueous solution.
With, r+ the dissolution rate
A a constant
Ea the activation energy
T the absolute temperature

Material and Method

The experiment was conducted in a Titanium Parr1M mixed flow reactor. The outlet flow was set in order to give measurable Si and Al concentration in the outlet flow (0.5 to 5mol/min).
The inlet solution was prepared using HCl ultrapur and Merck analytical grande for NH3 and NH4Cl. The concentrations were calculated using PHREEQC 2.6.

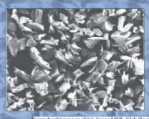

Verre rhyolitique non altéré. Image MEB. L'échelle est indiquée au centre de chaque vignette

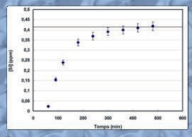

The experimental conditions were maintained until we reached a steady state,as it is shown here for a solution pH2 and 120°C.

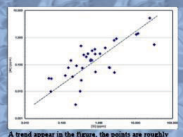

A trend appear in the figure, the points are roughly aligned over a line with a slope of 0.16. This slope corresponds to the ratio Al/Si of the glass. Some points are unaligned, due to the loss of Al during the precipitation of Al rich secondary phases.

In order to explain the results given by the dissolution rate, probably due to secondary phases precipitation, we have observed the samples with a SEM. The SEM pictures from unaltered samples show acicular glass shards. After the experiment the angles are rounded but the average morphology is unchanged. Some small deposit appeared on the shards. Their density seemed to be a function of the length of the experiment (up, after a day of weathering, down, after three days).

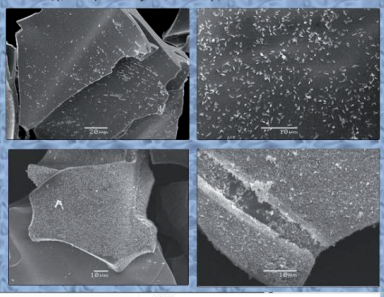

Rhyolite Dissolution mecanism

$$r_+ = Ae^{-\left(\frac{E_a}{RT}\right)}\left(\frac{a_{H^+}^3}{a_{Al^{3+}}}\right)^{1/n}$$

To define the dissolution mecanism of the Ryolite we have determined each unknown of this equation, then we have confront it to the real data.

In order to define the 1/n values we have measured the dissolution rate of the rhyolitic glass at a constant pH, in function of the aluminium concentration in the solution.
The data regression gives us a slope of -0.18, wich is consistent with 1/n=0.18.

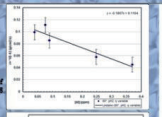

To confirm the values of 1/n we calculated this ratio for all the experiment made at 80°.
The line had a slope of 0.18.
Despite the noise in the dataset the curve is mostly consistent with the rates measured.

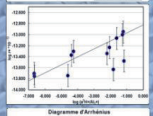

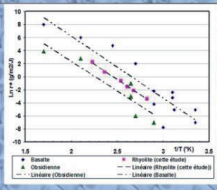

The evolution of the weathering rate with the invert of temperature is shown on the figure. the rates obtained in that study are consistant with the previous studies. The logarithm of r+ decrease with temperature for the three kind of glasses. This decrease is not constant for the whole scale in the obsidian from the previous studies ; in fact around 100°C a break of the slope show a variation in the mecanism, before and after this change. Our data didn't show this pattern.

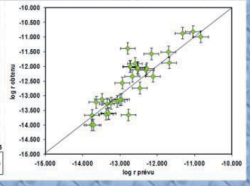

The figure shows a comparison between the measured data and those estimated with the general equation. The predicted and computed values are aligned on a line with a slope of 1.
It shows that predicted and computed values are consistant, annd that the general equation can be used to predict the dissolution rate of rhyolitic glass.

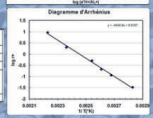

The shape of the curve is totally controlled by the dissociation constant of the aluminium hydroxides complex (Oelkers, 2000). These rates decrease until they reach a minimum around neutrality, then they increase with the pH in a basic environment. This behaviour is consistant with the dissolution rate of the whole aluminosilicates, including basaltic glass (Gislason et Oelkers, 2003).

Minéraux	pH	E_a (kj/mole)	Reference*
Olivine	3-5	35	Grandstaff (1986)
Quartz	4-6	75	Manghi (1985)
	9-10	105	Kazmi et Walsey (1988)
Verre basaltique	3	69	Guy et Schott (1989)
	7	75	
	8	75	
Verre rhyolitique	2	77	Cette étude

The Arhenius diagram shows the influence of the temperature (40° to 200°C). The slope is consistent with an Ea of 77.3 kJ/mol, value compared with those of other minerals in the table. The value obtained for the rhyolitic glass is closed to the one of the basaltic glass, confirming that the dissolution mechanism for the two glasses is the same.

$$r_+ = 0.031.exp\left(\frac{-77300}{RT}\right)\left[\frac{a_{H^+}^3}{a_{Al^{3+}}}\right]^{-0.18}$$

The same dissolution mechanism applies for the two most extreme types of natural glasses. Therefore it is conceivable to develop a general equation of the dissolution of natural glasses.

CMS, June 2007, Santa Fe – New Mexico – USA Alteration of synthetic impact crater glass. J.Declercq, H.Dypvick, J.Jahren

GSA, November 2007, Denver – Colorado – USA EXPERIMENTAL ALTERATION OF IMPACT GLASSES FROM THE CHESAPEAKE BAY IMPACT — EYREVILLE AND CAPE CHARLES CORES. J.Declercq, H.Dypvik, P.Aagaard, J.Jahren, R.E.Ferrel, J.W.Horton

Abstract – Impact melt can be found as e.g. spherules, tektites, fragments and clasts in suevite breccias. The possible alteration or transformation of impact-melt to clay minerals, particularly smectite, has been recognized in several impact structures (e.g. Ries, Chicxulub, Mjølnir). We have studied the alteration of two natural impact melt rocks from clasts in suevites of the CBIS and two synthetic glasses. These experiments were conducted at hydrothermal temperature (265°C) in order to reproduce the condition found in melt-sheets deposit in the first thousand years after deposition. The results of the experiments was then compared to a geochemical (PHREEQC) model of the same alteration and to mineral assemblages in the CBIS drill cores.

In the alteration experiments clay minerals were formed on the surfaces of the melt particles in addition to fine-grained suspended material. Authigenetic expanding clay minerals (saponite and Ca-smectite) and vermiculite/chlorite (clinochlore) have been identified in addition to analcime. Ferripyrophyllite was formed in all experiments. Comparable minerals were predicted in the PHREEQC modelling and have been identified in stratigraphical clay mineralogical studies of the Eyreville cores. The comparison between the phases formed in our experiments and in the cores suggest that the alteration happened at hydrothermal temperatures i.e. >250°C

Experimental alteration of impact glasses from the Cheaseapeak Bay Impact Structure

J.Declercq, H. Dypvik, P.Aagaard, J.Jahren, R.E.Ferrel and J.W.Horton
Department of Geoscience,
University of Oslo, P.B. 1047 Blindern, NO-0316 Oslo (julien.declercq@geo.uio.no)

Introduction.

The Chesapeake Bay Crater was formed by a marine impact 35 My ago. During meteoritic impact, glass and melt are commonly produced. The melt is oftenly in suevite and meltsheets.

Alteration products such as clays (smectite) have been recognized in the Chesapeak Bay Crater. We will study the alteration of synthetic and natural impact glass in order to understand its alteration to clays and clay minerals.

Several samples of the natural glass were collected in the Eyreville core. They were sampled at depth ranging from 735.9 m to 1398 m.

The natural samples came from the same clast of suevite that yielded sample ST2453.3C of Lee et al. (2006), wich is confirmed to be impact melt rock with a meteoritic component.

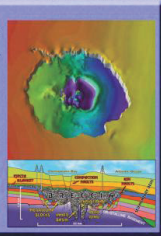

Glass dissolution mechanism

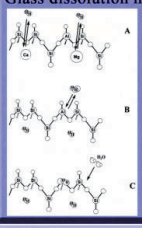

The picture shows the possible glass dissolution mechanism (from Oelkers and Gislason, 2001).
The dissolution process is limited by the slowest step of this mechanism, the liberation of the silica atom.

Samples description

Artificial glass

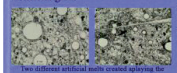

Two different artificial melts created applying the Table 1 composition.

Table 1:

Drammens Granite	84%
Glauconite sand (L. Cretac. Bornholm)	6%
Garnet Amphibolite	7%
Black Shale (Jurassic Svalbard)	3%

The glass was formed at 1200°C for 45min by a composition of lithologies comparable to those in the target area of Chesapeak Bay, see Table 1.

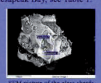

SEM picture of the glass shards

Natural glass

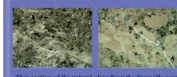

Thin section of the natural glass from the Eyreville core.

SiO2	Al2O3	Fe2o3	MnO	MgO	CaO	Na2O	K2O	TiO2	P2O5
42.33	13.89	11.06	0.21	11.8	9.87	1.35	0.11	0.52	0.35

Table 2: Major elements analysis (XRF - %oxyde) on the natural glass.

The natural glass shows a composition (XRF - %oxides) close to those to the typical basaltic glass.

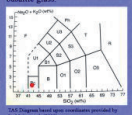

TAS Diagram based upon coordinates provided by Le Maitre et al. (2002).
The glass has a picritic composition.

Results

SEM

Artificial glass / Natural glass

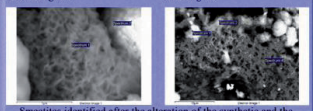

Smectites identified after the alteration of the synthetic and the natural glass.

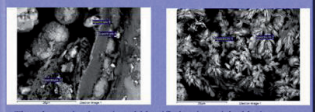

The other main clay mineral identified as iron-rich chlorite

XRD

Artificial glass / Natural glass

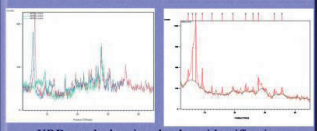

XRD graph showing the three identification treatment runs.
The bulk run in blue,
the ethylene glycol saturation in red
and the heated (55°C) in green.

Modelling

The modelisation of the dissolution of the impact glass and the precipitation processus was done using the software PHREEQC.

Ca	Mg	Sr	Na	K	Cl	HCO3-	SO4	Br	TDS
7400	230	200	14200	150	23400	60	1800	137	59000

Table 3: Pore water composition.

List of the presumably precipitating minerals and their saturation index.

Mineral	SI
Calcite	0,8
Chlorite	3,75
Gibbsite	2,72
Kaolinite	6,49
Illite	7,74
Montmorillonite-Ca	5,98
Montmorillonite-K	5,74
Montmorillonite-Na	5,89
Montmorillonite-Mg	6,1

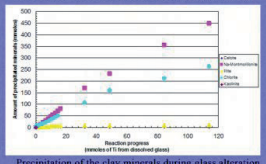

Precipitation of the clay minerals during glass alteration

Experimental setup

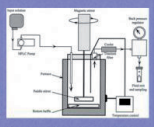

The artificial melt was crushed in an opal mortar and then processed in a 450ml ParrTM reactor.
The reactor was then half-filled with artificial seawater and the samples were altered for one week.
The temperature used was 200°C to 300°C.

Conclusion

The weathering of artificial glass as well as the alteration of the original CBIC glass results in the formation of smectite and Fe-rich chlorite.

The modelling predict the precipitation of those clay minerals and illite. Illite was not detected.

The model shows also that almost 20% of the glass is transformed into clays.

For more information: julien.declercq@geo.uio.no

EGU, April 2008, Vienna – Austria Dawsonite Dissolution Rates. J.Declercq, H.Hellevang, P.Aagaard

Abstract - One of the major difficulties surrounding the mineralogical storage of CO2 is obtaining metals required to make stable carbonate minerals. Most mineralogical storage scenarios are based on creation of carbonate minerals using divalent metals such as Ca, Mg, and Fe originating from silicate dissolution. Within sedimentary basins, however, much of the divalent metal cations have already been transformed into carbonates, limiting the potential for such storage. In contrast the carbonate mineral dawsonite ($NaAlCO_3(OH)_2$) offers the potential to mineralogically store CO_2 in the absence of potentially unavailable divalent metal cations.

Thermodynamic calculation indicate that precipitation of dawsonite occur in alkaline environment (pH > 8) in presence of CO_2, Na and an aluminium source such as gibbsite. Calculation performed upon natural composition and mineralogical assemblage shows that at a pH of 7.5 determined by the carbonate buffer the dawsonite still precipitate.

To assess the potential use of dawsonite for the mineralogical storage of CO_2, the precipitation rates of dawsonite were measured in $4 < pH < 8$ and temperature ranging from 20 to 80°C. Experiments were performed in closed system reactor using different reactant from gibbsite and NaOH to the Utsira sand composition (Chadwick et al (2004)), increasing the likeliness to a natural system.

Reference:

Geological reservoir characterization of a CO_2 storage site: The Utsira Sand, Sleipner, northern North Sea. **R. A. Chadwick**, P. Zweigel, U. Gregersen, G. A. Kirby, S. Holloway and P. N. Johannessen, Energy, 29, Issues 9-10, pp. 1371-1381, July-August 2004.

Experimental determination of dawsonite precipitation rates and their application to CO_2 sequestration

J.Declercq, E.H. Oelkers and P. Aagaard.
University of Oslo, Norway, LMTG, Toulouse, France

Introduction

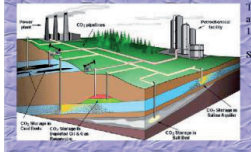

The successful underground storage of CO_2 should at a minimum sequester CO_2 for at least for 1000 to 10000 years.

Such storage is possible via mineral trapping.

The successful underground storage of CO_2 can include:
+ Dissolution of the gas in aqueous solution
+ Creation of carbonic acid
+ Increased acidity of the aqueous fluid induces dissolution of primary minerals
+ Following neutralization of this fluid precipitation of secondary phases, including carbonates occurs
+ Secondary carbonates are commonly viewed as permanent host for injected CO_2.

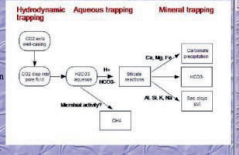

+ Dawsonite may be an ideal carbonate host for mineralogical storage of CO_2 for numerous reasons.

Dawsonite?

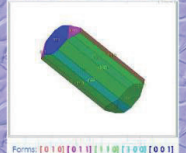

Forms: [0 1 0] [0 1 1] [1 1 0] [1 0 0] [0 0 1]

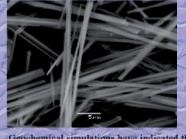

+ It is a natural forming carbonate mineral.
+ It commonly forms as needles in an acicular or fibrous habit.
+ It was discovered in 1874 on the campus of McGill University on the Island of Montreal (Canada).
+ It is named after the Canadian geologist Sir John William Dawson.

The most common dawsonite as the formula:

$NaAl(OH_2)CO_3$

Natural dawsonite has been found in volcanic environments near CO_2 rich discharges, and in the oil Green River shales due to CO_2 seepage into groundwater.
All these occurences are linked to highly alkaline fluids.

Geochemical simulations have indicated that dawsonite will form under reservoir conditions, but this is based on unknown kinetic data.

If it can be proved that dawsonite really can form under reservoir conditions, the mineral trapping of CO2 will be considerably increased, specially because, Na, K, Al-containing feldspars is a normal mineral constituent in most reservoirs.

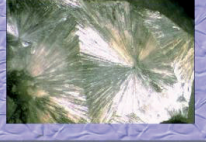

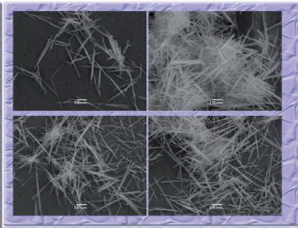

Dawsonite synthesis

Making dawsonite is mixing gibbsite and Na2CO3+NaHCO3 solution.

+ Stock solution with Na2CO3 and NaHCO3 dissolved in MQ water

+ Add Al(OH)3

+ Autoclave at 175°C for 4 hours.

$$Na^+ + Al^{3+} + 2H_2CO_3 + H_2O \rightarrow$$
$$NaAl(OH)_2CO_3 \downarrow + CO_{2,aq} \uparrow + 4H^+$$

Dawsonite is easily formed when gibbsite is combined with a concentrated NaHCO3 solution.

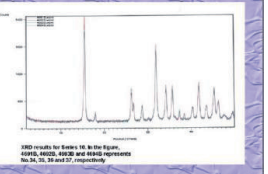

XRD results for Series 16. In the figure, 4918B, 4902B, 4903B and 4904B represents No.34, 35, 36 and 37, respectively

Dissolution

Experimental setup

Shaker bath

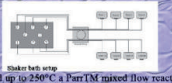

Shaker bath setup

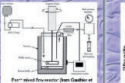

Above 80 and up to 250°C a ParrTM mixed flow reactor was used.
Between 25 and 80°C we used a shaker bath flow through system.
Reaction temperatures overlap at 80°C for the two reactor systems used, to allow a control of consistency of the calculated rates.

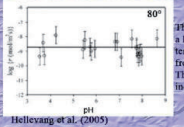

The previous studies used a limited range of pH and temperature (80°C, pH from 4 to 9).
The rate appears to be pH independant.

Hellevang et al. (2005)

$$r_i = \frac{q([i]_s - [i]_f)}{S.m.v_i}$$

The dissolution rate was calculated from steady state Na concentrations.
r_i refers to the dissolution rate,
q is the output flow,
$[Na]_f$ and $[Na]_s$ are the amount of sodium in respectively the input and output solution.
S is the specific BET surface area of the initial dawsonite powder.
v_{Na} is the stochiometric number of moles of sodium in one mole of dawsonite(in this case =1)
m is the mass of dawsonite present in the reactor.

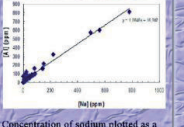

Concentration of sodium plotted as a function of the aluminum concentration in all gibbsite undersaturated reactive solutions.

The line corresponds to a 1:1 slope consistent with stochiometric dawsonite dissolution.

Analytical uncertainty for sodium and aluminum are 2% and 5% respectively.

The dissolution rate is strongly pH dependant

There is three distinct mechanisms characterised by the pH of the alteration solution.

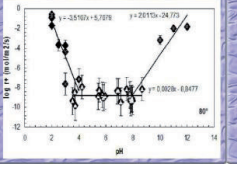

Precipitation

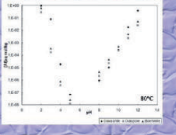

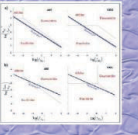

pH	$[C]_{ini}$ mol	$[Na]_{ini}$ mol	$[Al]_{ini}$ mol
8	3,00E-01	3,04E-01	9,02E-07
8	6,00E-01	6,09E-01	3,99E-07
9	3,00E-01	3,65E-01	1,01E-05
9	6,00E-01	6,20E-01	4,50E-05
10	3,00E-01	3,34E-01	2,65E-04
10	6,00E-01	3,95E-01	1,18E-04

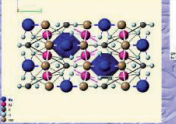

The dawsonite structure shows layers of Al(OH)+2 and NaCO3

During acid dissolution H+ may replace the other cations

The diffusion in solution is fast so complexes must be formed on the surface.

Conclusion

mineral	vol %	r	A (m²/mol)	k_+ (mol/m²/s)	E_a (kJ/mol)	ref.
dawsonite	85.7	0.3	2252.9	3.97×10^{-11}	67.00	29
albite	10.0	0.3	49.8	7.66×10^{-13}	57.55	30
kaolinite	3.3	0.085	725.6	2.45×10^{-11}	33.76	31
diaspore	0.3	0.07	9.8	1.88×10^{-9}	72.36	this study
calcite	0.7	0.3	24.9	6.31×10^{-10}	41.87	32
corundum	[illegible]					

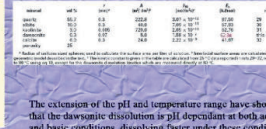

The extension of the pH and temperature range have shown that the dawsonite dissolution is pH dependant at both acidic and basic conditions, dissolving faster under these conditions.

The dissolution mechanism of Dawsonite is surface reaction controlled comparable to the dissolution mechanism of Magnesite (Pokrovsky et al, 1999)

Dawsonite may form in response to the high PCO2 during injection/post injection.

However, reduction of PCO2 and competing reactions may destabilize dawsonite.

Rencontres Scientifiques de l'IFP, May 2009, Rueil-Malmaison – France Dawsonite dissolution rate and mechanism at neutral and basic pH ; implication for CO_2 storage. J.Declercq, H.Hellevang, P.Aagaard.

Dawsonite dissolution rate and mechanism at acidic and basic pH ; implication for CO_2 sequestration.

Declercq J., Hellevang H., Aagaard P.
University of Oslo, Norway

Introduction

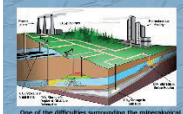

One of the difficulties surrounding the mineralogical storage of CO_2 is obtaining metals required to make stable minerals.
Within sedimentary basins much of the divalent cations have already been transformed into carbonates, limiting the potential for such storage.

In order to sustain the experiments we need large amount of chemically homogeneous Dawsonite.

It is not possible to have it from natural samples
So we synthesized our own Dawsonite

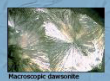

Macroscopic dawsonite

Injection of CO_2

Dissolution in the aqueous solution
Gets carbonic acid
Increased acidity induces dissolution of primary minerals,
The following neutralization leads to precipitation of secondary phases, including carbonates
Such secondary carbonates are commonly viewed as a permanent host for injected CO_2

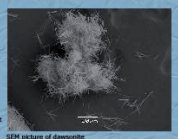

SEM picture of dawsonite

Dawsonite structure

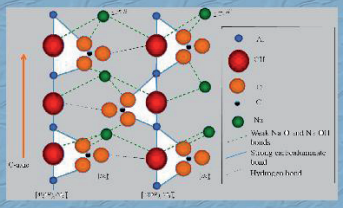

Dawsonite structure is built by carboaluminate chains. These chains are bound together by Na.

Dissolution progresses by breaking apart the carboaluminate chains

The high dissolution rate of dawsonite can be explained by the fast removal of Na resulting in a separation of the carboaluminate chains.

Material and method

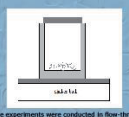

Initially the experiments were conducted in flow-thru reactors but the light dawsonite material clogged the filters. So we went for a simpler system.

The experiments were conducted in at 25 and 80°C in batch reactors immersed in a shaker bath

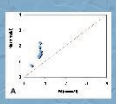

Effect of gibbsite precipitation during the dawsonite dissolution at low temperature and high pH.
A: Gibbsite precipitation.
B: Temporal dissolution of dawsonite, gibbsite precipitation has no effect on the calculated dissolution rates.

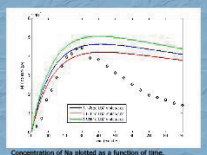

Concentration of Na plotted as a function of time.
The concentration of sodium rise sharply due to the dissolution of fine particles. Then the concentration decreases has a result of the diminishing specific surface area.

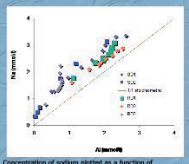

Concentration of sodium plotted as a function of aluminium concentration. Distance from the stoechiometric line is due to the quick dissolution of the Na_2CO_3 impurities.

Dawsonite synthesis

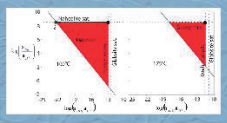

It's basically mixing gibbsite with Na_2CO_3 solution.

Our method:

Prepare a stock solution by dissolving Na_2CO_3 and $NaHCO_3$ in Milli-Q Water
We add $Al(OH)_3$
The liner containing the solution is then put in an autoclave at 175°C for 4 hours.

pH around 10 (25°C)

Stoichiometric dissolution
Impurities:
Boehmite (extra Al dissolving – seen on XRD)
Na_2CO_3 up to 5%
Gibbsite precipitation

We can easily correct the equation for these impurities

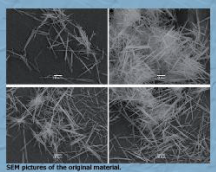

SEM pictures of the original material.

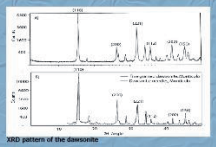

XRD pattern of the dawsonite

Dawsonite kinetics

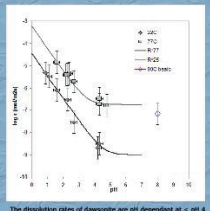

The dissolution rates of dawsonite are pH dependant at < pH 4 they become then pH independant around neutrality.
At pH > 8 the rates appear to decrease.

At low pH the rates show a first order dependance on proton activity.
Above pH 4 the rates are dominated by surface hydration.

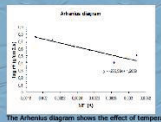

The Arhenius diagram shows the effect of temperature on the dissolution rate, the slope is consitent with an Ea of 80,58 +/- 8,1 kJ/mol.

Calculation of the reaction rate.
where V is volume aqueous solution, C is concentration, m is mass and t is time. Subscripts t and t-1 denotes time of sampling and time at previous sampling respectively

$$r_i = \frac{2V_{t-1}}{(m_t + m_{t-1})S_{BET}} \cdot \frac{\Delta C_{diss}}{\Delta t}$$

$$r_{CO_3H^+} = k_{CO_3H^+} \frac{a_{H^+}^n}{a_{H_2CO_3}^m}$$

The rate-controlling step is the disintegration of the surface complex with a rate proportional to the H+ activity and inversely proportional to the activity of carbonic acid.

Comparison withs other carbonates

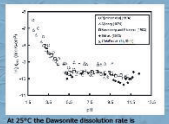

At 25°C the Dawsonite dissolution rate is slower than the calcite dissolution rate.

The dissolution mecanism appears to be comparable to the Magnesite dissolution mecanism where the process is surface controlled (Pokrovsky and Schott (1999)).

Assuming that the shorter bonds observed within the carboaluminate chain are stronger than the Na-O and Na-OH bonds, we propose that the first-order dependence of the rates with respect to proton activity at pH < 4 can be explained by surface protonation of surface carbonate complexes where Na+ is exchanged by H

$>CO_3Na_s + H+ = >CO_3H_s + Na+$

This is followed by a disintegration of the surface CO_3 group from the carboaluminate chain.

$>CO_3H_s + H+ = H_2CO_3^*$
which results in destabilization of the aluminate chain and a collapse of the dawsonite structure.

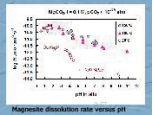

Magnesite dissolution rate versus pH

Conclusion

In acid condition dawsonite dissolution rates are comparable to magnesite.

There is a first order dependance on proton activity at pH < 4.

At pH < 4 the dissolution mechanism of dawsonite appear to be the same as calcite and magnesite.

At pH > 4 the rates are dominated by surface hydration.

Corresponding author: Julien Declercq
julien.declercq@geo.uio.no

Reykjavik – Iceland Dawsonite Dissolution Mechanism. J.Declercq, H.Hellevang, P.Aagaard

Dawsonite dissolution mechanism

J. Declercq, H. Hellevang, P.Aagaard
University of Oslo

Introduction

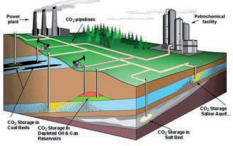

One of the difficulties surrounding the mineralogical storage of CO_2 is obtaining metals required to make stable minerals.
Within sedimentary basins much of the divalent cations have already been transformed into carbonates, limiting the potential for such storage.

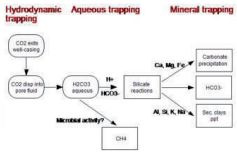

Injection of CO_2

Dissolution in the aqueous solution
Gets carbonic acid
Increased acidity induces dissolution of primary minerals,
The following neutralization leads to precipitation of secondary phases, including carbonates
Such secondary carbonates are commonly viewed as a permanent host for injected CO_2

Material and Methods

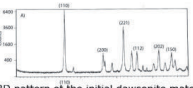

XRD pattern of the initial dawsonite material.

Synthesis

It is basically mixing gibbsite and a Na_2CO_3 solution.

Method

Prepare a stock solution by dissolving Na_2CO_3 and $NaHCO_3$ in Milli-Q water
Add $Al(OH)_3$
Put the liner containing the mixture in an autoclave at 175°C for 4 hours.

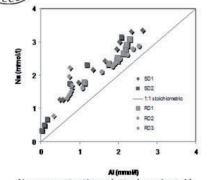

Na concentration plotted against Al concentration for all batch experiments

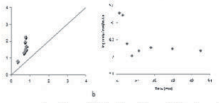

a, concentration of Al in function of Na showing the former diminishing drastically due to the precipitation of secundary phases (boehmite or gibbsite) and b, the logarithm of the dissolution versus time for the same experiment as in a (RB86 see table 1) showing the lack of effect of the secundary precipitation.

Results

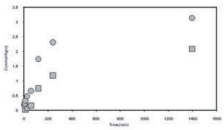

The slope is consistent with an activation energy of 80,5 kJ/mol at neutral conditions and 44,6 kJ/mol at acid conditions

Concentration of Na plotted against time at 25°C (squares) and 85°C (rounds)

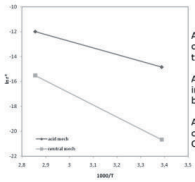

At acidic pH (<4) the slope is consistent with a pH dependance of the rate.

Around neutrality the rate is pH independant and probably dominated by the hydration of the surface.

At pH superior to 8 the rate controlling step is probably OH- adsorption.

Arhenius diagram for the acidic and neutral pH domains.

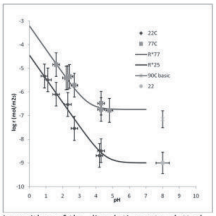

Logarithm of the dissolution rate plotted against pH for experiement at 22C and 77C.

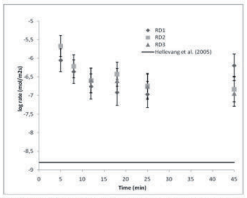

Logarithm of the dissolution rate depicted in function of time for three experiments (RD1, RD2 and RD3) at 25°C showing the constant decrease of the rates over time. The solid line represents the value obtained by Hellevang et al. in 2005 on a very limited amount of powder.

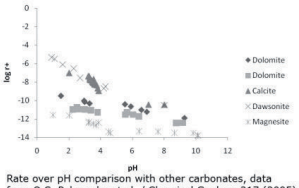

Rate over pH comparison with other carbonates, data from O.S. Pokrovsky et al. / Chemical Geology 217 (2005) 239–255 and Magnesite from Pokrovsky and Schott 1999. Dawsonite data at pH 8 is an estimation based on the rate at 90°C.

The rate of dissolution of dawsonite is compared to the dissolution rates of calcite, dolomite and magnesite at 25°C. It can be seen that dawsonite rates are comparable to those of calcite at neutral and basic conditions and slightly faster in acidic conditions.
Dawsonite behaves like a one-component carbonate as described by Chou et al. (1989). So despite being a two components carbonate like dolomite, dawsonite requires only one step to dissolve.

Dawsonite dissolution mechanism

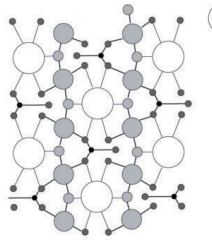

Dawsonite structure modified from Frost and Bouzaid, 2007. A schematic illustration of the dawsonite structure projected down to a plane parallel to the c-axis. The carboaluminate chain $[Al(OH)_2CO_3]_\infty$ along the c-axis is the backbone of the dawsonite structure. Hydrogen bonds and Na-O and Na-OH bonds attach the chains together.

The dawsonite structure can be described by a chain of Al(O)2(OH)4 octahedra bond together by common hydroxyl ions along the c-axis crystallographic direction. This chain is stabilized by carbonate groups forming the carboaluminate chain [Al(OH)2CO3]n - the backbone of the dawsonite structure. These chains are bond together by shared hydrogen bonds around the sodium

The one component behaviour of dawsonite suggests that only one step is necessary to accomplish dissolution.
From the structure one can see that removing Na will in fact break apart the carboaluminate chains holding dawsonite together.

At acidic pH (pH<4) the first order dependence of the dissolution rate on pH suggests that Na is removed through a protonation reaction of the surface carbonate complexes. Na+ being replaced by H+.

>CO3Na0 + H+ <-> >CO3H0 + Na+
This is followed by a disintegration of the surface CO3 group from the carboaluminate chain.

>CO3H0 + H+ <-> H2CO3*
which results in destabilization of the aluminate chain and a collapse of the dawsonite structure.

Between pH 4 and 8 the rates are pH independent and are probably dominated by the hydration of the surface.

>CO3Na0 + H2O <-> >CO3H0 + Na++OH-
Which is also followed by a the disintegration of the surface CO3 group from the carboaluminate chain.

$Al(OH)2CO3H0 + H2O <-> Al(OH)3+H2CO3^*$

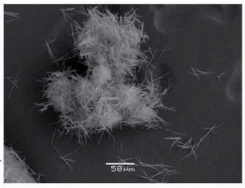

SEM picture of dawsonite

Conclusion

Dissolution experiments on dawsonite showed that the dissolution rate at pH 4 and 22°C is comparable with that of magnesite. At pH < 4 the rates are first-order dependent on the proton activity, whereas around neutrality the rate approach a pH-independent region which is strongly supported by the earlier reported rate data by Hellevang et al. (2005), at pH above 8 the rate decrease. Based on the similarity in activation energies between dawsonite, calcite and magnesite over the proton promoted rate region we propose that a similar mechanism is responsible for the dissolution rate at these conditions for all three.

The dawsonite formation requires breaking of Al-OH bounds, then the formqtion of new ones and is hindered by the high activation energy. Thus it will be very difficult to form.
Even if dawsonite forms, as soon as it becomes undersaturated it will dissolve at once due to its high dissolution rate. Releasing the mineralized CO2 in the process.

Corresponding author: Julien Declercq
julien.declercq@geo.uio.no